JAMES | Journal of Advances in Modeling Earth Systems®

RESEARCH ARTICLE
10.1029/2024MS004697

Addressing Challenges in Simulating Inter–Annual Variability of Gross Primary Production

Ranit De[1,2], Shanning Bao[1,3], Sujan Koirala[1], Alexander Brenning[2,4], Markus Reichstein[1,4], Torbern Tagesson[5], Michael Liddell[6], Andreas Ibrom[7], Sebastian Wolf[8], Ladislav Šigut[9], Lukas Hörtnagl[8], William Woodgate[10,11], Mika Korkiakoski[12], Lutz Merbold[13], T. Andrew Black[14], Marilyn Roland[15], Anne Klosterhalfen[16], Peter D. Blanken[17], Sara Knox[18,19], Simone Sabbatini[20], Bert Gielen[15], Leonardo Montagnani[21], Rasmus Fensholt[22], Georg Wohlfahrt[23], Ankur R. Desai[24], Eugénie Paul-Limoges[25], Marta Galvagno[26], Albin Hammerle[23], Georg Jocher[9,27], Borja Ruiz Reverter[28], David Holl[29], Jiquan Chen[30], Luca Vitale[31], M. Altaf Arain[32], and Nuno Carvalhais[1,4,33]

[1]Department for Biogeochemical Integration, Max Planck Institute for Biogeochemistry, Jena, Germany, [2]Department of Geography, Friedrich Schiller University Jena, Jena, Germany, [3]National Space Science Center, Chinese Academy of Sciences, Beijing, China, [4]ELLIS Unit Jena, Jena, Germany, [5]Department of Physical Geography and Ecosystem Science, Lund University, Lund, Sweden, [6]Centre for Tropical, Environmental, and Sustainability Sciences, James Cook University, Cairns, QLD, Australia, [7]Department of Environment and Resource Engineering, Technical University of Denmark (DTU), Lyngby, Denmark, [8]Department of Environmental Systems Science, ETH Zürich, Zürich, Switzerland, [9]Global Change Research Institute of the Czech Academy of Sciences, Brno, Czech Republic, [10]School of the Environment, The University of Queensland, St Lucia, QLD, Australia, [11]CSIRO, Space and Astronomy, Kensington, WA, Australia, [12]Finnish Meteorological Institute, Climate System Research Unit, Helsinki, Finland, [13]Integrative Agroecology Group, Agroscope, Zürich, Switzerland, [14]Faculty of Land and Food Systems, University of British Columbia, Vancouver, BC, Canada, [15]Plants and Ecosystems (PLECO), Department of Biology, University of Antwerp, Wilrijk, Belgium, [16]Bioclimatology, University of Göttingen, Göttingen, Germany, [17]Department of Geography, University of Colorado Boulder, Boulder, CO, USA, [18]Department of Geography, McGill University, Montreal, QC, Canada, [19]Department of Geography, The University of British Columbia, Vancouver, BC, Canada, [20]CMCC Foundation - Euro-Mediterranean Center on Climate Change, Lecce, Italy, [21]Faculty of Agricultural, Environmental and Food Sciences, Free University of Bozen-Bolzano, Bolzano, Italy, [22]Department of Geosciences and Natural Resource Management, University of Copenhagen, Copenhagen, Denmark, [23]Institut für Ökologie, Universität Innsbruck, Innsbruck, Austria, [24]Department of Atmospheric and Oceanic Sciences, University of Wisconsin-Madison, Madison, WI, USA, [25]Swiss Federal Institute for Forest, Snow and Landscape Research (WSL), Birmensdorf, Switzerland, [26]Environmental Protection Agency of Aosta Valley, Climate Change Unit, (ARPA Valle d'Aosta), Saint-Christophe AO, Italy, [27]Thünen Institute of Climate-Smart Agriculture, Braunschweig, Germany, [28]Departamento de Química e Física, Universidade Federal da Paraíba - Campus II, Areia, Brazil, [29]Institute of Soil Science, University of Hamburg, Hamburg, Germany, [30]Department of Geography, Environment, and Spatial Sciences, Michigan State University, East Lansing, MI, USA, [31]Institute for Agriculture and Forestry Systems in the Mediterranean (ISAFoM), Portici, Italy, [32]School of Earth, Environment and Society, McMaster University, Hamilton, ON, Canada, [33]CENSE, Departamento de Ciências e Engenharia do Ambiente, Faculdade de Ciências e Tecnologia, Universidade NOVA de Lisboa, Caparica, Portugal

Key Points:

- We investigated the limitations of biogeochemical models in simulating inter–annual variability (IAV) of gross primary production (GPP)
- Capturing IAV of model parameters and diurnal GPP peaks can be key to understanding IAV of GPP
- Variability in model performance is jointly influenced by model types, parameterization strategies, and site characteristics

Supporting Information:

Supporting Information may be found in the online version of this article.

Correspondence to:

R. De and N. Carvalhais,
rde@bgc-jena.mpg.de;
de.ranit19@gmail.com;
ncarvalhais@bgc-jena.mpg.de

Citation:

De, R., Bao, S., Koirala, S., Brenning, A., Reichstein, M., Tagesson, T., et al. (2025). Addressing challenges in simulating inter–annual variability of gross primary production. *Journal of Advances in Modeling Earth Systems*, *17*, e2024MS004697. https://doi.org/10.1029/2024MS004697

Received 11 SEP 2024
Accepted 18 FEB 2025

Author Contributions:

Conceptualization: Ranit De, Shanning Bao, Sujan Koirala, Nuno Carvalhais
Data curation: Ranit De, Sujan Koirala, Torbern Tagesson, Michael Liddell, Andreas Ibrom, Sebastian Wolf, Ladislav Šigut, Lukas Hörtnagl, William Woodgate, Mika Korkiakoski, Lutz Merbold, T. Andrew Black, Marilyn Roland, Peter D. Blanken, Sara Knox, Simone Sabbatini, Bert Gielen, Leonardo Montagnani, Rasmus Fensholt,

Abstract A long-standing challenge in studying the global carbon cycle has been understanding the factors controlling inter–annual variation (IAV) of carbon fluxes, and improving their representations in existing biogeochemical models. Here, we compared an optimality-based model and a semi-empirical light use efficiency model to understand how current models can be improved to simulate IAV of gross primary production (GPP). Both models simulated hourly GPP and were parameterized for (a) each site–year, (b) each site with an additional constraint on IAV ($Cost^{IAV}$), (c) each site, (d) each plant–functional type, and (e) globally. This was followed by forward runs using calibrated parameters, and model evaluations using Nash–Sutcliffe efficiency (NSE) as a model-fitness measure at different temporal scales across 198 eddy-covariance sites representing diverse climate–vegetation types. Both models simulated hourly GPP better (median normalized NSE: 0.83 and 0.85) than annual GPP (median normalized NSE: 0.54 and 0.63) for most sites. Specifically, the optimality-based model substantially improved from NSE of −1.39 to 0.92 when drought stress was explicitly included. Most of the variability in model performances was due to model types and parameterization strategies. The semi-empirical model produced statistically better hourly simulations than the optimality-based model, and site–year parameterization yielded better annual model performance. Annual

Georg Wohlfahrt, Ankur R. Desai, Eugénie Paul-Limoges, Marta Galvagno, Albin Hammerle, Georg Jocher, Borja Ruiz Reverter, David Holl, Jiquan Chen, Luca Vitale, M. Altaf Arain
Formal analysis: Ranit De
Methodology: Ranit De, Shanning Bao, Sujan Koirala, Nuno Carvalhais
Resources: Markus Reichstein, Nuno Carvalhais
Software: Ranit De
Supervision: Sujan Koirala, Alexander Brenning, Markus Reichstein, Nuno Carvalhais
Validation: Ranit De
Visualization: Ranit De
Writing – original draft: Ranit De
Writing – review & editing: Ranit De, Shanning Bao, Sujan Koirala, Alexander Brenning, Markus Reichstein, Torbern Tagesson, Michael Liddell, Andreas Ibrom, Sebastian Wolf, Ladislav Šigut, Lukas Hörtnagl, William Woodgate, Mika Korkiakoski, Lutz Merbold, T. Andrew Black, Marilyn Roland, Anne Klosterhalfen, Peter D. Blanken, Sara Knox, Simone Sabbatini, Bert Gielen, Leonardo Montagnani, Rasmus Fensholt, Georg Wohlfahrt, Ankur R. Desai, Eugénie Paul-Limoges, Marta Galvagno, Albin Hammerle, Georg Jocher, Borja Ruiz Reverter, David Holl, Jiquan Chen, Luca Vitale, M. Altaf Arain, Nuno Carvalhais

model performance did not improve even when parameterized using $Cost^{IAV}$. Furthermore, both models underestimated the peaks of diurnal GPP, suggesting that improving predictions of peaks could produce better annual model performance. Our findings reveal current modeling deficiencies in representing IAV of carbon fluxes and guide improvements in further model development.

Plain Language Summary Terrestrial vegetation assimilates and releases carbon dioxide through photosynthesis and respiration, respectively, and their net magnitude determines if vegetation can be a sink or source of carbon dioxide. We are interested in understanding what controls the inter–annual variability (IAV) of gross primary production (GPP) which represents photosynthesis, and how their representations can be improved in models simulating GPP. Here, we considered an optimality-based model that can be applied equally well globally, and a data-driven semi-empirical model. We found both models better simulated diurnal and seasonal cycles than the IAV of GPP. Such differences probably stem from model parameters, as critical ecosystem functions they represent may not be well-constrained or model structures may lack critical representations via inaccurate simulation of peak diurnal GPP and drought stress. The IAV of GPP was comparatively better simulated if model parameters were fine-tuned with data from specific years. Another challenge is that IAV of GPP can also be observed due to disturbances, such as forest fire, and human management besides natural causes, which were also not represented in models. Our results suggest that learning the variability of model parameters over the years can be key to better simulation of the IAV of GPP.

1. Introduction

The global carbon cycle is an important biogeochemical cycle, which affects the climate on Earth (Schimel, 2001). Terrestrial vegetation, which covers a large part of the land area, assimilates atmospheric carbon dioxide (CO_2) through photosynthesis. Simultaneously, CO_2 of similar magnitude is released into the atmosphere through terrestrial ecosystem respiration (TER). The net balance of these two fluxes determines if terrestrial ecosystem acts as a sink or source of carbon (Ruehr et al., 2023). Terrestrial gross primary production (GPP) can be defined as "apparent" photosynthesis, that is, the rate at which the vegetation assimilates carbon through photosynthesis minus the loss of carbon only through photorespiration (Plummer, 2006; Wohlfahrt & Gu, 2015). GPP can be estimated directly using gas exchange measurements at the leaf and canopy scales (Jez et al., 2021), and indirectly through measurements of net ecosystem exchange (NEE) using the eddy covariance (EC) method at the ecosystem or landscape scale (D. D. Baldocchi, 2003). Though the GPP estimated using the EC method represents "apparent" photosynthesis, its magnitude can be closer to "true" photosynthesis which is the actual amount of carbon assimilated due to overestimation of daytime mitochondrial respiration in flux–partitioning algorithm (Reichstein et al., 2005; Wohlfahrt & Gu, 2015). Furthermore, a large variety of biogeochemical models have been developed to simulate and upscale carbon fluxes from local to regional or global scales to better describe the global carbon cycle (Burton et al., 2023; Dannenberg et al., 2023; Nelson et al., 2024; Xiao et al., 2014).

Biogeochemical models that simulate GPP can be of different types and complexities. On the one hand, process-based models, such as the models used in the Trends in Net Land-Atmosphere Carbon Exchange (TRENDY) project, mechanistically describe the physiological processes involved in photosynthesis or plant respiration (Sitch et al., 2015). Their ability to capture a certain process largely depends on the underlying model structure and calibration of model parameters (Anav et al., 2015). Similar, but simpler than fully mechanistic approaches are the models constructed on the concept of light use efficiency (LUE), which treat a canopy usually as one big leaf, but where the GPP is calculated as the product of the absorbed photosynthetically active radiation (aPAR) and LUE (Monteith, 1972). These models are semi-empirical as they combine both the simplicity of empirical models and the theoretical mechanisms that underpin process-based models (J. Chen, 2021; Running et al., 2000; Yuan et al., 2007). On the other hand, data–driven empirical models (Jung et al., 2011, 2020) are largely based on learning regression functions to establish a general relation between input data, such as meteorology and ecosystem properties, and the desired output, such as GPP. These models' performance largely relies on good quality training data and generally lacks comprehensive representations of long-term forcing functions.

Considering the methodological diversity and differences in GPP estimates, various model benchmarking and model–data integration experiments have been designed to compare approaches and to unveil drivers of ecosystem functioning for various climate–vegetation types, across spatial and temporal scales. A long-standing

challenge, and still a key area of interest, lies in understanding the factors controlling inter–annual variability (IAV) of the various carbon fluxes (D. Baldocchi et al., 2018). The challenge presents itself from the mechanistic to the more data–driven approaches and contests the dominant role of meteorology in determining the IAV of ecosystem fluxes (Richardson et al., 2007). At the local ecosystem level, J. Wu et al. (2012) looked at the IAV of net ecosystem fluxes by fitting the parameters of a semi-empirical model at shorter timescales to capture the seasonality, but also annual variability of model parameters. The approach allows testing the role of changes in ecosystem functioning in the IAV of carbon fluxes (Richardson et al., 2007). They concluded that climate and parametric variability control IAV of ecosystem fluxes at shorter and longer timescales, respectively.

Simultaneously, Fatichi and Ivanov (2014) highlighted the role of climate when using 200 years of hourly synthetic meteorological data to force an ecohydrological model to find that the random occurrence of favorable weather conditions at certain hours of the day can be a major predictor of IAV of net primary production (NPP). This statistical relationship was corroborated by Zscheischler et al. (2016) using actual flux data from EC sites from forested areas in North America, where the 91st percentile values of hourly GPP flux, that is, peak GPP values, substantially contributed to the IAV of GPP flux. These studies highlight the correlation between the distribution tails and the IAV in EC fluxes. However, there is no robust pattern across sites nor do they challenge there is no variability in ecosystem function.

More recently, a model selection study compared an ensemble of 5600 possible semi-empirical LUE model structures to find a global best model structure (Bao, Wutzler, et al., 2022). The best LUE model was calibrated at a daily timescale per site and simulated GPP fluxes across the FLUXNET EC tower sites (Pastorello et al., 2020), considering the effect of various environmental conditions on maximum LUE through partial sensitivity functions. Though the best global model performed similarly to the best model selected for each site at the daily resolution, it failed to represent the variability of annually aggregated GPP fluxes for 74% of sites, that is, the Nash-Sutcliffe efficiency (NSE) of model performance (Nash & Sutcliffe, 1970) was below or equal to 0.5. This may be attributed to (a) the use of daily data in the study, as the model had no information on the favorable conditions that occurred in a diurnal cycle and failed to simulate the diurnal GPP peaks which had a major influence on IAV (Bao, Wutzler, et al., 2022; Fatichi & Ivanov, 2014; Zscheischler et al., 2016), (b) the assumption of invariance in ecosystem function, that is, values of model parameters remain constant for all site–years in a site, and (c) the need to explicitly consider different timescales in the cost function (Desai, 2010).

In contrast, Mengoli et al. (2022) proposed an optimality-based framework (Stocker et al., 2020; Wang et al., 2017), that is, optimality-based P-model which simulates GPP following optimality principle and differentiates between instantaneous and acclimated photosynthetic responses. This model demonstrated its capability in simulating half-hourly GPP dynamics at 10 EC sites, covering four vegetation classes for limited time periods. Whereas, the performance of this modeling framework across sites representing diverse climate–vegetation features and various temporal resolutions were not evaluated. Though this modeling framework considers the effect of temperature, vapor pressure deficit (VPD), atmospheric CO_2 concentration, solar radiation, and the fraction of absorbed photosynthetically active radiation (fAPAR), it does not explicitly consider the effect of drought stress on GPP variability at sub-daily scale. However, numerous studies (Anderegg et al., 2015; Assal et al., 2016; Kannenberg et al., 2019; Reichstein et al., 2013; C. Wu & Wang, 2022) in the past highlighted the effect of climatic extremes, such as drought on the reduction of GPP through observations and simulations, as well as ecosystems can temporarily act as a carbon sink during drought (Ciais et al., 2005). Moreover, various studies (Müller & Bahn, 2022; Orth et al., 2020; Seneviratne et al., 2012; X. Yu et al., 2022) also found that the drought can also impose a prolonged legacy effect on seasonal and annual dynamics of GPP and recovery days can vary between ecosystems (Z. Yu et al., 2017). Recently, Mengoli et al. (2023) proposed an improved version of this model by incorporating climatic aridity and calculating a scaling factor for GPP. However, in the improved model, the scaling factor could only be applied to improve the simulation of daily GPP.

The challenge to correctly reproduce IAV is also apparent on a global scale as Anav et al. (2015) found a high level of disagreement in annual GPP estimates from diverse global GPP modeling frameworks. These discrepancies highlight that site-level limitations in simulating IAV propagate to larger scales where additional mechanisms play a role, such as natural or anthropogenic disturbances and land–use land cover change (Bultan et al., 2022; McGuire et al., 2001).

As highlighted above, the major persistent drawbacks in most of the past studies were the limited implementation of either model structures or parameterization approaches and the evaluation of models for limited sites and

timescales. To address this, here we explore ecosystem-level estimations of GPP flux to systematically investigate how various factors can be linked to describing the IAV of GPP flux, such as peak values of diurnal GPP, climatic conditions, and variables represented by model parameters, which are usually hard to measure directly and can be difficult to interpret even when various modeling approaches are adopted. We tested the impact of the constant or time–varying parameterizations and evaluated their performances in capturing GPP variability at various temporal aggregation scales, especially at the annual scale. We also tested the hypothesis that observational constraints complement and enhance theoretically grounded process formulations and that improving the model simulations at the sub-daily scale improves the prediction of IAV of GPP. Additional analysis on parameter inversion approaches and cost functions, as well as on parametric variability are treated in a companion paper (De, Brenning, et al., 2025). In this study, we aim to answer:

1. How well does an optimality-based model perform compared to a semi-empirical model across various temporal scales with different model parameterization approaches?
2. What factors influence the variability of model performance at different temporal scales?
3. Can the performance of an optimality-based model be improved if drought stress is included?
4. How much are the differences in model performance between an optimality-based and a semi-empirical model related to variations across plant–functional types (PFT) and climate–vegetation types?
5. Does improved simulations of peak diurnal GPP lead to improved simulations of IAV of GPP?

2. Methods and Data

In this study, we focused on parameterization of both a semi-empirical model, at daily and sub-daily scales, and an optimality-based model at a sub-daily scale using various parameterization strategies consisting of different subsets of data and cost functions (Figure 1). Thereafter, we performed forward runs of models with calibrated parameters at the temporal resolution of model parameterization data and evaluated model performances at different temporal aggregations (Figure 1). The following sections describe each methodological step in a detailed manner.

2.1. Models

2.1.1. Optimality-Based Model: P-Model of Mengoli

Stocker et al. (2020) proposed the first version of the P-model based on theories formulated by Wang et al. (2017), which unified the classic Farquhar–von Caemmerer–Berry model (Farquhar et al., 1980) with the simplified formation of big leaf LUE models (Monteith, 1972). The probable reasons behind using the "P" in the P-model are (a) "P" stands for photosynthesis, (b) classically, GPP used to be denoted by "P" (Monteith, 1972), and (c) the initial of the lead author (Prentice et al., 2014) who formulated the theories behind the model starts with "P" (B. D. Stocker, personal communication, 06 May 2024). The underlying equations of the P-model were formulated based on the optimality principle (Prentice et al., 2014) and the coordination principle (J.-L. Chen et al., 1993; Maire et al., 2012). According to the optimality principle, plants aim to optimize the cost of transpiring water to assimilate CO_2 through the stomata. In the P-model, the ratio of leaf internal and ambient CO_2 concentration ($\chi = C_i/C_a$) is calculated for which the above-described cost is minimal, and the sensitivity (ξ) of χ to VPD is predicted. The coordination principle describes the achievement of equilibrium between the maximum rate of carboxylation ($V_{c_{\max}}$) and electron transport ($J_{\max}$) by the plants.

Mengoli et al. (2022) adapted the first version of the P-model to simulate half-hourly GPP dynamics. Here, we applied this same model at an hourly scale and called it the P_{hr} model. The major improvement in this version was defining an explicit differentiation between instantaneous (such as RuBisCo and light-limited carbon assimilation), and photosynthetic responses ($V_{c_{\max}}$, $J_{\max}$, and ξ) which acclimate over time in response to environmental conditions. One of the important aspects of this P_{hr} model is that the parameters associated with cellular biochemistry acclimate to favorable conditions during the day over a period of time or acclimation time (A_t). In this study, we considered the favorable condition as the average of three hourly input data points in the middle of the day from 11:00 (hh:mm) LT, 12:00 (hh:mm) LT, and 13:00 (hh:mm) LT. A rolling mean of the average condition from mid-day was taken over the A_t, which was used to calculate optimal values of the model parameters, as described in Mengoli et al. (2022). The value of A_t was calibrated as a parameter in our study

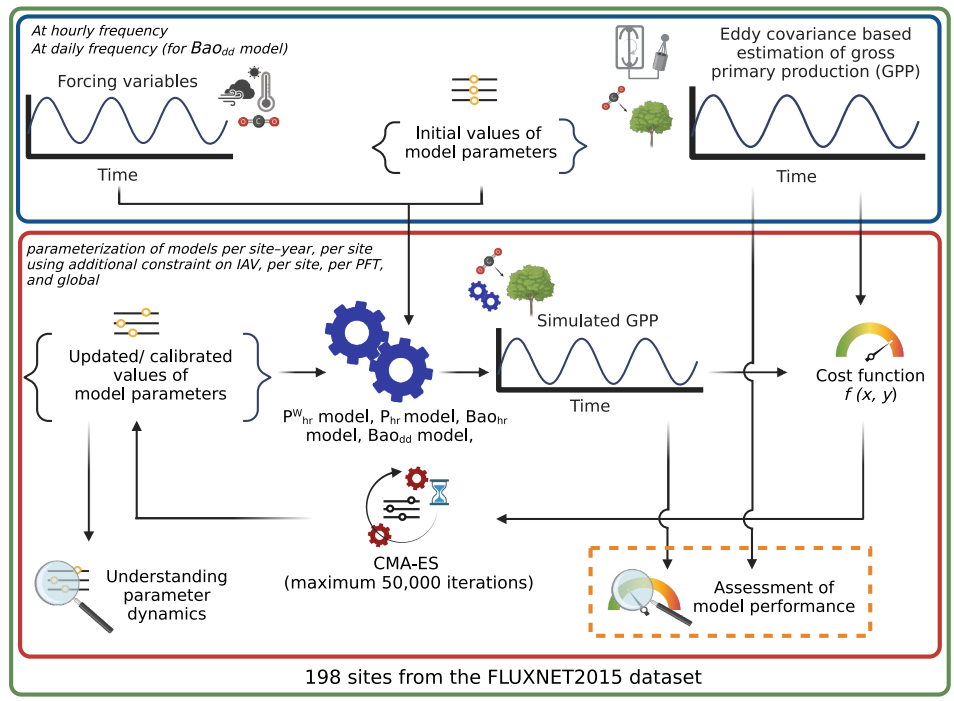

Figure 1. Graphical representation of the model–data–integration workflow adopted in this study. The blue box indicates the preparation of forcing and observation data at hourly and daily scales for each site, as well as defines the initial value of parameters and their range by surveying literature. Then five different model parameterization tasks were performed for the light use efficiency (LUE) model from Bao, Wutzler, et al. (2022) at hourly scale (Bao$_{hr}$ model) and at daily scale (Bao$_{dd}$ model), P-model from Mengoli et al. (2022) at hourly scale (P$_{hr}$ model), and P$_{hr}$ model with an explicit drought stress function (P$^{W}_{hr}$ model) using the Covariance Matrix Adaptation Evolution Strategy (CMA-ES) (Hansen & Kern, 2004), which is indicated by the red box. The cost function (f) is a function of observed (y) and simulated (x) gross primary production. The green box denotes that the whole workflow was applied for the 198 sites from the FLUXNET2015 data set (Pastorello et al., 2020). The dotted orange box highlights the focus of this study. The parameter dynamics is explored in detail in a companion paper (De, Brenning, et al., 2025). The figure was created in BioRender. R. De (2025).

(Table 1). We chose the mid-day and rolling mean approach from Mengoli et al. (2022) as it produced the best results in their evaluations of the P$_{hr}$ model at the half-hourly scale.

One of the known limitations of the P$_{hr}$ model is its tendency to overestimate GPP fluxes in water–limited ecosystems, as no explicit representation of soil moisture conditions was included (Mengoli et al., 2022, 2023). In order to relax such drawbacks here we used the water availability index (*WAI*) as a proxy of soil moisture (Bao, Wutzler, et al., 2022; Boese et al., 2019; Tramontana et al., 2016). The *WAI* represents the spatial and temporal dynamics in plant available water based on a simple hydrological model where storage is controlled by precipitation and evapotranspiration. We further introduced a drought stress function that additionally scaled the GPP estimates of the P$_{hr}$ model, and we denoted this new version as the P$^{W}_{hr}$ model. We calibrated 10 parameters in the P$^{W}_{hr}$ model in which nine parameters were in the hydrological model and the drought stress function (Table 1). Further details on the implementation of the P$^{W}_{hr}$ model, along with the drought stress function can be found in Text S1 and S2, Figures S1 and S2 of Supporting Information S1.

2.1.2. Semi-Empirical Model: Bao Model

Vegetation stores energy from absorbed solar radiation in the form of biochemical energy through photosynthesis. The efficiency of the photosynthetic apparatus in performing this energy conversion is termed as light use efficiency (ε). In a LUE model, GPP is calculated as the product of instantaneous ε, photosynthetic photon flux density (*PPFD*), and the fraction of incident photosynthetically active radiation that is absorbed by vegetation (*fAPAR*). Instantaneous ε reaches its maximum, that is, ε_{max}, when all environmental factors are optimal for photosynthesis.

Table 1
Description, Range, Initial Values, and Units of Calibrated Model Parameters

fX/model name	Symbol	Definition	Initial value	Lower bound	Upper bound	Units	Reference
P_{hr}^{W}, P_{hr} models	A_t	Length of acclimation time	18	1	100	Days	after Mengoli et al. (2022)
Bao_{hr}, Bao_{dd} models	ε_{max}	Maximum light use efficiency	0.04	0	0.13	$\mu molCO_2 \cdot \mu mol\ photons^{-1}$	Skillman (2008)
fT (Bao_{hr}, Bao_{dd} models)	T_{opt}	Optimal temperature	10	5	35	°C	Bao, Wutzler, et al. (2022)
	k_T	Sensitivity to temperature changes	2	1	20	$°C^{-1}$	Bao, Wutzler, et al. (2022)
	α_{fT}	Lag parameter for temperature effect	0.29	0	0.9	–	Bao, Wutzler, et al. (2022)
$fVPD$ (Bao_{hr}, Bao_{dd} models)	κ	Sensitivity to VPD changes	-5×10^{-5}	−0.01	-1×10^{-5}	Pa^{-1}	Bao, Wutzler, et al. (2022)
	C_κ	Sensitivity to atmospheric CO_2 concentration changes	0.4	0	10	–	Bao, Wutzler, et al. (2022)
	C_{a0}	Minimum optimal atmospheric CO_2 concentration	380	340	390	ppm	Bao, Wutzler, et al. (2022)
	C_m	CO_2 fertilization intensity indicator	2000	100	4,000	ppm	Bao, Wutzler, et al. (2022)
fL (Bao_{hr}, Bao_{dd} models)	γ	Light saturation curvature indicator	2×10^{-3}	0	0.05	$\mu mol\ photons^{-1} \cdot m^2 \cdot s$	Bao, Wutzler, et al. (2022)
fCI (Bao_{hr}, Bao_{dd} models)	μ	Sensitivity to cloudiness index changes	0.5	10^{-3}	1	–	Bao, Wutzler, et al. (2022)
fW (P_{hr}^{W}, P_{hr}, Bao_{hr}, Bao_{dd} models)	W_I	Optimal soil moisture	0.26	0.01	0.99	$mm \cdot mm^{-1}$	Bao, Wutzler, et al. (2022)
	k_W	Sensitivity to soil moisture changes	−11	−5	−30	–	Bao, Wutzler, et al. (2022)
	α	Lag parameter for soil moisture effect	0.98	0	1	–	Bao, Wutzler, et al. (2022)
WAI (P_{hr}^{W}, P_{hr}, Bao_{hr}, Bao_{dd} models)	AWC	Available water capacity	100	1	1,000	mm	Bao, Wutzler, et al. (2022)
	θ	Rate of evapotranspiration	0.05	10^{-4}	0.1	$mm \cdot h^{-1}$	Bao, Wutzler, et al. (2022)
	PET_{scalar}	Multiplicative scalar for potential evapotranspiration	1.2	0	5	–	Trautmann et al. (2018)
	MR_{tair}	Snow melt rate for temperature	0.125	0	0.5	$mm \cdot °C^{-1} \cdot h^{-1}$	Trautmann et al. (2018)
	MR_{netrad}	Snow melt rate for net radiation	0.0375	0	0.125	$mm \cdot MJ^{-1} \cdot h^{-1}$	Trautmann et al. (2018)
	sn_a	Sublimation resistance	0.44	0	3	–	Bao, Wutzler, et al. (2022)

Instantaneous ε is determined as the product between ε_{max} and the partial sensitivity functions (fX) for the different environmental factors controlling GPP, such as air temperature (T), VPD, available soil water supply (W), absorbed photosynthetic photon flux ($L = PPFD \times fAPAR$), the cloudiness index (CI, Table A1), and atmospheric CO_2 concentration (Bao, Wutzler, et al., 2022; Horn & Schulz, 2011; Mäkelä et al., 2008).

$$GPP_{sim} = (\boldsymbol{\varepsilon}_{max} \cdot fT \cdot fVPD \cdot fL \cdot fCI \cdot fW) \cdot PPFD \cdot fAPAR \quad (1)$$

$$fT = \frac{2 \cdot \exp\left(-\frac{T_f - \boldsymbol{T_{opt}}}{\boldsymbol{k_T}}\right)}{1 + \left(\exp\left(-\frac{T_f - \boldsymbol{T_{opt}}}{\boldsymbol{k_T}}\right)\right)^2} \quad (2)$$

$$T_f(t) = \left(1 - \boldsymbol{\alpha_{fT}}\right) \cdot T(t) + \boldsymbol{\alpha_{fT}} \cdot T_f(t-1) \quad (3)$$

$$fVPD = \exp\left(\boldsymbol{\kappa} \cdot \left(\frac{\boldsymbol{C_{a0}}}{CO_2}\right)^{\boldsymbol{C_\kappa}} \cdot VPD\right) \cdot \left(1 + \frac{CO_2 - \boldsymbol{C_{a0}}}{CO_2 - \boldsymbol{C_{a0}} + \boldsymbol{C_m}}\right) \quad (4)$$

$$fL = \frac{1}{\gamma(PPFD \cdot fAPAR) + 1} \tag{5}$$

$$fCI = CI^{\mu} \tag{6}$$

$$fW = \frac{1}{1 + \exp(k_W(W_{ft} - W_1))} \tag{7}$$

$$W_{ft} = (1 - \alpha) \cdot W_t + \alpha \cdot W_{ft-1} \tag{8}$$

In this study, we used the LUE model of Bao, Wutzler, et al. (2022), Bao et al. (2023) since it emerged as a robust representation from the systematic comparison across the large diversity of LUE formulations in the literature. The model selection followed a Bayesian approach that leveraged on the evaluation of modeling performance across FLUXNET EC sites (Pastorello et al., 2020) when forced and calibrated with daily data for each site. We denoted this model as the Bao_{hr} model when we parameterized at hourly scale, and as the Bao_{dd} model when we parameterized at daily scale. The model is described in Equations 1–8, where fT, $fVPD$, fW, fL, and fCI are partial sensitivity functions for T, VPD, W, L, and CI, respectively. In this case, W and fW were calculated similar to the implementation in $\text{P}^{\text{W}}_{\text{hr}}$ model, that is, with a simple hydrological model (Text S1 and Figure S1 of Supporting Information S1) and drought stress function (Equations 7 and 8 are same as Equations S1 and S2 of Supporting Information S1), respectively. Bold terms in the Equations 1–8 are model parameters, and their initial values, units, and ranges are described in Table 1. The physical ranges for most of the parameters were based on Bao, Wutzler, et al. (2022), Bao et al. (2023), and Trautmann et al. (2018). The $fVPD$ term, viz. Equation 4, also accounts for atmospheric CO_2 concentration. The partial sensitivity functions range from zero to one (except the 2nd part of Equation 4 which can be greater than one), where a value of zero completely diminishes, and of one completely favors GPP. In this study, we changed the denominator of Equation 2 in comparison to the original exponential function $\exp\left(-\frac{T_f - T_{opt}}{k_T}\right)^2$ of Bao, Wutzler, et al. (2022), Bao et al. (2023), as the revised version produced a more realistic range of fT (Figure S3 of Supporting Information S1). Sensitivity functions fT and fW also consider a lag effect of T and W. The lag effect of temperature was considered for Temperate, Boreal, and Polar regions where the first letter of the Köppen–Geiger (KG) climate class is "C," "D," "E," and that of soil water supply was considered for arid regions where the first letter of the KG climate class is "B" (Beck et al., 2018; Rubel et al., 2017).

2.2. Data Used

We selected 198 eddy covariance sites, for which the required forcing and observation or derived data for model parameterization were available from the FLUXNET2015 data set (Pastorello et al., 2020; FLUXNET.org, 2024a). A list of these sites is provided in Table S8 of Supporting Information S1 and their spatial distributions are plotted in Figure S4 of Supporting Information S1. The variables which were used to force, and parameterize models as well as data processing steps such as gap–filling, and quality control are described in detail in Table A1, Appendix B and Appendix C. We prepared these data in both hourly and daily resolutions.

In our study, a total of 13 different PFTs (as defined in FLUXNET.org, 2024b) were represented: croplands (CRO; 19 sites), deciduous broadleaf forests (DBF; 25 sites), deciduous needle leaf forest (DNF; one site), evergreen broadleaf forests (EBF; 13 sites), evergreen needle leaf forests (ENF; 47 sites), grasslands (GRA; 35 sites), mixed forests (MF; nine sites), closed shrublands (CSH; three sites), open shrublands (OSH; 13 sites), savannas (SAV; six sites), permanent wetlands (WET; 20 sites), woody savannas (WSA; six sites), and land cover under snow for most of the year (SNO; one site). The major KG climate classes (Rubel et al., 2017; Beck et al., 2018; FLUXNET.org, 2024c) are represented by 12 tropical sites, 18 arid sites, 87 temperate sites, 71 boreal sites, and 10 polar sites. We also classified sites into nine climate–vegetation types, similar to Bao, Wutzler, et al. (2022), in which seven sites are tropical forests (TropicalF), five sites are tropical grassland (TropicalG), six sites are arid forest (AridF), 12 sites are arid grassland (AridG), 51 sites are temperate forest (TemperateF), 36 sites are temperate grassland (TemperateG), 52 sites are boreal forest (BorealF), 19 sites are boreal grassland (BorealG), and 10 sites have polar vegetation.

Table 2
Description of Models and Tasks Accomplished With Each Specific Model

Models	Description	Parameterization strategies				
		Per site–year	Per site using $Cost^{IAV}$	Per site	Per PFT	Global
P_{hr}	P-model of Mengoli et al. (2022) parameterized using hourly data	a, d	a, d	a, d	a, d	a, d
P_{hr}^{W}	P-model of Mengoli et al. (2022) with an additional constraint on drought stress and parameterized using hourly data	a, b, d, e	a, b, d, e	a, b, d, e	a, b, d, e	a, b, d, e
Bao_{hr}	LUE model of Bao, Wutzler, et al. (2022) parameterized using hourly data	a, c, d, e	a, c, d, e	a, c, d, e	a, c, d, e	a, c, d, e
Bao_{dd}	LUE model of Bao, Wutzler, et al. (2022) parameterized using daily data	a, c, d	a, c, d	a, c, d	a, c, d	a, c, d

Note. The tasks are described in the footnote of the table. [a]Evaluation of model performance across timescale with different model types, parameterization strategies, and cost functions. [b]Evaluation of an optimality-based model with an explicit drought stress function. [c]Evaluation of a semi-empirical model with different temporal resolutions of data used for model parameterization. [d]Factors behind variability of model performance across timescales. [e]Variability of annual model performance with model performance in simulating diurnal gross primary productivity (GPP) peaks.

2.3. Model Parameterization

We primarily defined four different parameterization strategies consisting of various subsets of data to calibrate the model parameters controlling hourly GPP dynamics. These parameterization strategies were used to determine a vector of calibrated parameter values (a) for each site–year, (b) for each site, (c) for each PFT, and (d) for all sites at once (global parameterization). We also performed another parameterization per site using a modified cost function which used an additional constraint on the IAV of GPP ($Cost^{IAV}$). We chose various parameterization strategies ranging from more flexible to rigid to evaluate how good or bad the model performs with changing parameterization. We parameterized and forced the Bao_{hr} model, and the Bao_{dd} model using hourly and daily data, respectively to perform a comparative analysis (Table 2). The P_{hr}^{W} model and the P_{hr} model were only parameterized and forced using hourly data (Table 2).

We used Python (Python Core Team, 2021) implementation (pycma v3.3.0.1) of the Covariance Matrix Adaptation Evolution Strategy (CMA-ES) (Hansen & Kern, 2004; Hansen et al., 2019) as our global search algorithm to find the values of model parameters for which cost function reached its minimum. This is a derivative-free, evolutionary algorithm, which is designed to find global minima in a rugged parameter space.

$$Cost_{i_P} = (1 - GPP_{NNSE_i}) + (1 - ET_{NNSE_i}) \tag{9}$$

$$Cost_{i_{Bao}} = (1 - GPP_{NNSE_i}) + (1 - ET_{NNSE_i}) + Cost_{ideal} + Cost_{non\_ideal} \tag{10}$$

A robust cost function is a necessity for the numerical optimizer to find the global minimum. The cost functions for P_{hr}^{W}, P_{hr} models ($Cost_{i_P}$) and the Bao_{hr}, Bao_{dd} models ($Cost_{i_{Bao}}$) were calculated as Equations 9 and 10, respectively, in case of per site–year and per–site parameterization. Here, i is either a site or site–year based on parameterization type. For PFT-specific model parameterization, the cost functions were $\sum_{i=1}^{N_{PFT}} Cost_{i_P}$ and $\sum_{i=1}^{N_{PFT}} Cost_{i_{Bao}}$ for P_{hr}^{W}, P_{hr} models and Bao_{hr}, Bao_{dd} models, respectively. i denotes a site and N_{PFT} denotes the total number of sites in a specific PFT. In the case of global model parameterization, the cost functions were $\sum_{i=1}^{N} Cost_{i_P}$ and $\sum_{i=1}^{N} Cost_{i_{Bao}}$ for the P_{hr}^{W} model and Bao_{hr}, Bao_{dd} models, respectively. i denotes a site and N denotes the total number of sites used in this study.

$$NNSE_i = \frac{1}{2 - NSE_i} \tag{11}$$

$$NSE_i = 1 - \frac{\sum_{t=1}^{N_{t,i}} (\sigma_{weight_{t,i}} \cdot (EC_{t,i} - sim_{t,i}))^2}{\sum_{t=1}^{N_{t,i}} (\sigma_{weight_{t,i}} \cdot (EC_{t,i} - \overline{EC_{t,i}}))^2} \quad (12)$$

$$\sigma_{weight_{t,i}} = 1 - \frac{\sigma_{t,i} - \min(\sigma_i)}{\max(\sigma_i) - \min(\sigma_i)} \quad (13)$$

GPP_{NNSE_i} and ET_{NNSE_i} were calculated (Equation 11) as a weighted normalized NSE, viz. NNSE (Hundecha & Merz, 2012) between the time series of good quality data points (see Appendix B for the selection criteria) of EC derived and simulated GPP and ET, respectively. The GPP and ET derived from EC measurements are denoted as GPP_{EC} and ET_{LE}, respectively. The simulated GPP and ET are denoted as GPP_{sim} and ET_{sim} (see Figure S1 of Supporting Information S1 for calculation of ET_{sim}), respectively. We considered ET as well in our cost function to better constrain the parameters of the simple hydrological model used in this study. The NNSE values (Nash & Sutcliffe, 1970) are between zero and one, where one is the best, and zero is the worst agreement between observed and simulated data. Here, we used these normalized values so that minimizing $(1 - NNSE)$ always results in better model performance in comparison to using $(1 - NSE)$, where NSE can have values between $-\infty$ (worst agreement) and one (best agreement). In Equation 12, $N_{t,i}$ is the total number of good quality data points from each timestep t for a site–year or site i. $\sigma_{t,i}$ in Equation 13 is random uncertainty (standard deviation of fluxes in a sliding window of ±5 days and ±1 hr of the time-of-day of the current timestamp) of NEE or ET from each timestep t for a site–year or site i (Table A1). Similarly, σ_i in Equation 13 is random uncertainty of full NEE and ET time series for a site–year or site i. The normalized random uncertainty in Equation 13 was used in the cost function to allocate higher and lower weight to EC–derived values with lower and higher uncertainties, respectively.

$$Cost_{ideal} = ((1 - \max(fT_r)) + (1 - \max(fVPD_r)) + (1 - \max(fW_r)) + (1 - \max(fL_r))) \cdot 10^3 \quad (14)$$

$$\begin{aligned} Cost_{non\_ideal} = & \sum_r \left((fT_r - \theta_{fT}) \left(T < 0°C \ \& \ fT_r > \theta_{fT} \right) \right) \\ & + \sum_r \left((fVPD_r - \theta_{fVPD}) \left(VPD > 2000Pa \ \& \ fVPD_r > \theta_{fVPD} \right) \right) \\ & + \sum_r \left((fW_r - \theta_{fW}) \left(W < 0.01 \ \& \ fW_r > \theta_{fW} \right) \right) \end{aligned} \quad (15)$$

The $Cost_{ideal}$ and $Cost_{non\_ideal}$ were introduced as regularizers in $Cost_{i_{Bao}}$ to avoid over-fitting of the sensitivity functions (Bao et al., 2023; Bao, Wutzler, et al., 2022). These cost function components ensure that values of partial sensitivity functions were not penalized and favored under ideal and non-ideal conditions, respectively. The ideal and non-ideal conditions were determined by certain constant thresholds for all sites. Equation 14 ensured that the partial sensitivity functions, fT (Equation 2), only left part of the $fVPD$ (Equation 4), fW (Equation 7) and fL (Equation 5) approaches one, when certain ideal environmental conditions ($PPFD \in$ [0 to 600 µmol photons $\cdot m^{-2} \cdot s^{-1}$], $fAPAR \in$ [0 to 1], $T \in$ [−5 to 40 °C], $VPD \in$ [0–4,500 Pa], $W \in$ [0 to 1]) occur (these ranges are denoted by subscript r), so that the ε_{max} in Equation 1 reaches its maximum potential. The factor 10^3 in Equation 14 was included to match the ranges of all other components in the cost function for the Bao_{hr}, Bao_{dd} models ($Cost_{i_{Bao}}$) so that all the components had equal weight. Equation 15 penalized the cases when the values of fT (Equation 2), only left part of $fVPD$ (Equation 4), and fW (Equation 7), were greater than a certain threshold ($\theta_{fT} = 0.2$, $\theta_{fVPD} = 0.9$, $\theta_{fW} = 0.2$) under non-ideal conditions ($T < 0$ °C, $VPD >$ 2,000 Pa, $W < 0.01$) for photosynthesis.

$$Cost_{i_P}^{IAV} = (1 - GPP_{NNSE_i}) + (1 - GPP_{NNSE_i}^{y}) + (1 - ET_{NNSE_i}) \quad (16)$$

$$Cost_{i_{Bao}}^{IAV} = (1 - GPP_{NNSE_i}) + (1 - GPP_{NNSE_i}^{y}) + (1 - ET_{NNSE_i}) + Cost_{ideal} + Cost_{non\_ideal} \quad (17)$$

$$GPP^{y}_{NNSE_i} = \frac{1}{2 - GPP^{y}_{NSE_i}} \tag{18}$$

$$GPP^{y}_{NSE_i} = 1 - \frac{\sum_{t=1}^{N_{t,i}} (\sigma^{y}_{weight_{t,i}} \cdot (EC^{y}_{t,i} - sim^{y}_{t,i}))^2}{\sum_{t=1}^{N_{t,i}} (\sigma^{y}_{weight_{t,i}} \cdot (EC^{y}_{t,i} - \overline{EC^{y}_{t,i}}))^2} \tag{19}$$

$$\sigma^{y}_{weight_{t,i}} = 1 - \frac{\sigma^{y}_{t,i} - \min(\sigma^{y}_{i})}{\max(\sigma^{y}_{i}) - \min(\sigma^{y}_{i})} \tag{20}$$

$$EC^{y}_{t,i} = \sum_{t=1}^{t} EC_{t,y,i};\ sim^{y}_{t,i} = \sum_{t=1}^{t} sim_{t,y,i};\ \sigma^{y}_{t,i} = \sum_{t=1}^{t} \sigma_{t,y,i} \tag{21}$$

In the case of per–site–year parameterization using cost functions in Equations 9 and 10, we fitted the model so that the annual average of GPP can be captured well for each site–year. Whereas, in the case of per–site parameterization using cost functions in Equations 9 and 10, the model was parameterized for each site. We performed another experiment as a balance between these two experiments using the $Cost^{IAV}$, which is similar to Desai (2010) to put an additional constraint on IAV, and parameterized P^{W}_{hr}, P_{hr}, Bao_{hr}, and Bao_{dd} models for each of the EC sites. The cost functions, $Cost^{IAV}_{i_P}$ for P^{W}_{hr}, P_{hr} models (Equation 16) and $Cost^{IAV}_{i_{Bao}}$ for Bao_{hr}, and Bao_{dd} models (Equation 17) now include an additional term $(1 - GPP_{NNSE_i}{}^{y})$ to constrain the annual cumulative sum of GPP flux from each site i. $EC^{y}_{t,i}$, $sim^{y}_{t,i}$, and $\sigma^{y}_{t,i}$ (Equation 21) are cumulative sums of GPP_{EC}, GPP_{sim}, and σ_{NEE} from start of each year y to timestep t for each site i, respectively.

2.4. Simulating and Evaluating GPP Estimates

2.4.1. Forward Runs

In the case of the site–year parameterization, we performed a forward run for each site–year using the respective set of calibrated parameter values and forcing data for that year. Afterward, we concatenated GPP_{sim} from all the years for a given site to assess model performance. For per–site parameterization using $Cost^{IAV}$, and per–site parameterization, we used site-specific values of calibrated parameters to perform site-level model evaluation. We also applied calibrated model parameters for a certain PFT to simulate GPP at all the sites which belong to a certain PFT. Similarly, for the global parameterization, a single set of calibrated parameter values was used to simulate GPP for each site.

2.4.2. Model Performances Metric

We performed forward runs at an hourly scale and averaged the hourly simulations to daily, weekly, monthly, and annual temporal frequencies to calculate model performance measures at different temporal aggregations. Model performance was only evaluated for temporal aggregations from daily to annual for the Bao_{dd} model. We applied a data screening procedure (Appendix C) before calculating model performance measures.

$$\mathrm{NSE}(y, \hat{y}) = 1 - \frac{\sum_{t=1}^{N} (y_t - \hat{y}_t)^2}{\sum_{t=1}^{N} (y_t - \bar{y})^2} \tag{22}$$

We evaluated how well a model can simulate the IAV of GPP based on how well a model simulated the annual average GPP for a site. In this study, we performed most of our analysis using NSE (Nash & Sutcliffe, 1970) and normalized NSE, viz. NNSE (which is $\frac{1}{2-\mathrm{NSE}}$) as NSE indicates the degree to which scatter between observed and simulated data fits to the 1:1 line. We used Equation 22 to calculate NSE between a reference (y) and a predicted ($\hat{y}$) variable, where N is the total number of time-steps, and y_t, $\hat{y}_t$ are the values of reference and predicted variables, at timestep t. In addition, we calculated the square of the Pearson correlation coefficient (R^2) (Kirch, 2008) which explains whether the dispersion of observed and simulated data matches and in the case of an unbiased model, values of NSE will be closer to values of R^2. Whereas, if a model is systematically biased, it will result in higher R^2 values, but bad NSE values (Krause et al., 2005). We also calculated Root Mean Squared Error

(Chai & Draxler, 2014) to quantify how closely the mean of simulated data matches with the mean of the observed data.

$$NSE = 2 \cdot \alpha_{NSE} \cdot r - \alpha_{NSE}^2 - \beta_n^2 \tag{23}$$

$$\alpha_{NSE} = \frac{\sigma_{sim}}{\sigma_{EC}} \tag{24}$$

$$\beta_n = \frac{\mu_{sim} - \mu_{EC}}{\sigma_{EC}} \tag{25}$$

Moreover, using Equations 23–25, we decomposed NSE values to linear correlation (r), relative variability (α_{NSE}), and bias (β_n) in some cases to investigate which of these were improved or diminished between different model parameterization strategies (Gupta et al., 2009). In Equations 24 and 25, σ_{sim} and σ_{EC} are standard deviations of GPP_{sim} and GPP_{EC}, respectively, μ_{sim} and μ_{EC} are mean GPP_{sim} and GPP_{EC}, respectively. We calculated these metrics using the Python (Python Core Team, 2021) package Permetrics v1.5.0 (Van Thieu, 2023; Van Thieu & Mirjalili, 2023), and the definition of each of the model performance metrics can be found in the package documentation.

2.4.3. Estimating Uncertainties in Annual GPP

GPP is not directly measured using the EC technique (Foken et al., 2011; Montgomery, 1948; Swinbank, 1951). Rather, GPP is derived from NEE using a flux partitioning method (Lasslop et al., 2010; Reichstein et al., 2005). The measurement of NEE is affected by low turbulence conditions when the EC system misses the carbon flux due to advection transport (Aubinet et al., 2010). The low turbulence conditions were identified by friction velocity threshold (u_*), and NEE measurements during these conditions were discarded and gap-filled (Papale et al., 2006). 200 values of u_* thresholds were estimated using a bootstrap approach for each site–year, and finally 40 different values (chosen from percentile 1.25 to percentile 98.75 with a step of 2.5) of u_* was used to produce 40 different realizations of NEE data. These u_* thresholds were either estimated per year using variable u_* threshold (VUT) method where the u_* threshold of a year depends on data from a given year and its neighboring years or estimated using data from all years, and remains constant across years, which is known as constant u_* threshold (CUT) method (Pastorello et al., 2020). Thereafter, seven different representative NEE data were produced as percentiles (XX) 5, 16, 25, 50, 75, 84, and 95 of the 40 different NEE values for each VUT and CUT method. These seven NEE data were further partitioned to estimate GPP using daytime (DT) and night-time (NT) partitioning methods (Lasslop et al., 2010; Reichstein et al., 2005).

Here, we used GPP_NT_VUT_USTAR50 from the FLUXNET2015 data set (Pastorello et al., 2020) as our reference GPP or GPP_{EC} for model calibration and evaluation (see Section 2.2 and Appendix A). These GPP values were derived using night-time partitioning from NEE data (NEE_VUT_USTAR50) where the VUT method was considered, and the 50 percentile value of u_* thresholds was applied. However, the GPP data disseminated in the FLUXNET2015 data set has a systematic uncertainty on the choice of NEE data (depending on percentile XX), and partitioning methods. This uncertainty can be large when the fluxes are aggregated to annual scale. We annually aggregated four other GPP variables (GPP_NT_VUT_05, GPP_NT_VUT_95, GPP_DT_VUT_05, GPP_DT_VUT_95) derived using either daytime or night-time partitioning method, and derived from 5 (NEE_VUT_05) and 95 (NEE_VUT_95) percentile NEE values, and screened for good site–years with their respective quality control flags (see Appendix C). We quantified the uncertainty range of annual GPP_{EC} for a site–year as the minimum of annual GPP_NT_VUT_05 and GPP_DT_VUT_05 to the maximum of annual GPP_DT_VUT_95 and GPP_NT_VUT_95. Thereafter, we also quantified the fraction of site years in a site for which annual GPP_{sim} estimated from different experiments were within the uncertainty range of GPP_{EC}. The values of GPP_{EC} were also affected by random uncertainties in NEE flux. We used hourly random uncertainties in NEE flux to weigh the contribution of a GPP value from a given hour in the cost function (Section 2.3). However, the random uncertainty at annual scale was not considered as they greatly reduce with aggregation (Hollinger & Richardson, 2005; Tramontana et al., 2016).

2.4.4. Factors Influencing Model Performance

We selected potential factors that can affect model performance at different temporal resolutions. These factors can be of two types. There were factors which we determined based on our experiment design, which included model types (P^{W}_{hr} model, P_{hr} model, Bao_{hr} model, and Bao_{dd} model), parameterization strategies (per site–year, per site using $Cost^{IAV}$, per site, per PFT, and global parameterization), number of years with good quality data (Appendix C) in a site. Whereas, other factors represent site-specific characteristics, including PFT, KG climate class, and climate–vegetation types.

First, we conducted Levene's test (Levene, 1960) to determine if the assumption of homoscedasticity was fulfilled across groups in the controlling factors. Then, we performed an N-way Analysis of Variance (ANOVA) (Kaufmann & Schering, 2014) with the potential controlling factors to determine which of them played a major role in determining model performance at hourly and annual temporal scales. For analysis at an hourly scale, the Bao_{dd} model was not included as this model produced simulations at a daily scale. We performed two N-way ANOVA analyses once including the performance of the P_{hr} model, and then excluding the performance of the P_{hr} model. The Levene's test and N-way ANOVA analyses were implemented using SciPy v1.11.3 (Virtanen et al., 2020) and statsmodels v0.14.0 (Seabold & Perktold, 2010), respectively.

2.4.5. Evaluating GPP Estimates in Water–Limited Ecosystems

We investigated to determine whether explicit accounting of the drought stress function in the P^{W}_{hr} model had improved its performance at arid sites. For this purpose, we chose the aridity index (AI) to determine which sites were arid or semi-arid, as this index provided a numerical representation of moisture availability (Zomer et al., 2022) at a location. The AI values were calculated by dividing the average precipitation (P) per hour by the average potential evapotranspiration (PET) per hour for the whole observation period at a site.

We drew examples from a few site-specific results to highlight different aspects of the behaviour of P^{W}_{hr} and P_{hr} models for ecosystems with contrasting soil moisture controls on GPP and with a larger availability of good–quality measurements. For this purpose, we chose a water–limited semi-arid site (annual average precipitation of 318 mm) in central Australia (Alice Springs, AU-ASM). This site also features a complex mixture of Mulga woodland and savanna (Cleverly et al., 2013; Pastorello et al., 2020). In contrast, we also highlighted the behaviours of P^{W}_{hr} and P_{hr} models in an irrigated cropland (Mead - irrigated continuous maize site, US-Ne1) in the mid-western U.S.A (Amos et al., 2005; Pastorello et al., 2020).

2.4.6. Effect of Temporal Resolution of Data on Model Performance

We parameterized the LUE model of Bao, Wutzler, et al. (2022) with hourly and daily data for Bao_{hr} model and Bao_{dd} model, respectively. We performed a comparison between these two versions of the model to highlight whether the resolution of data used for model parameterization can substantially affect the prediction of the annual average or IAV of GPP fluxes. Here, we also drew a site-specific example from an energy–limited deciduous forest in central Germany (Hainich, DE-Hai) as this site had a very long observation period (Knohl et al., 2003).

2.4.7. Evaluating Modeling Experiments of Various Complexities

We formulated our experiments using models and parameterization strategies consisting of varying numbers of model parameters to be calibrated. The number of parameters calibrated for a detailed parameterization strategy, such as per site–year parameterization was substantially higher than a generic parameterization strategy, such as global parameterization. We used Akaike's Information Criterion (AIC) to investigate whether a complex modeling experiment with a higher number of parameters can better simulate GPP (Burnham & Anderson, 2004).

$$AIC = n \log\left(\frac{\sum (EC_i - sim_i)^2}{n}\right) + 2K \tag{26}$$

$$AIC_c = n \log\left(\frac{\sum (EC_i - sim_i)^2}{n}\right) + 2K + \frac{2K(K+1)}{n-K-1} \tag{27}$$

Following recommendations of Burnham and Anderson (2004), we used Equation 26 to calculate AIC when $n/K > 40$, where n is the total number of observations and K is the total number of parameters. Otherwise, we used a corrected version of AIC (AIC_c, Equation 27). Though the values of AIC or AIC_c can be in any range, the lowest value of AIC or AIC_c determines the preferred modeling experiments. EC_i and sim_i are i^{th} observations of EC-derived GPP and simulated GPP, respectively in Equations 26 and 27. We considered GPP_{sim} from all the four variations of models, that is, P^W_{hr} model, P_{hr} model, Bao_{hr} model, and Bao_{dd} model for calculation of AIC or AIC_c. We calculated AIC at hourly and daily aggregations by concatenating good quality (Appendix C) hourly or daily data, and daily averages GPP_{EC} and GPP_{sim} from all the days from all sites. Similarly, we used monthly and annual aggregations for calculating AIC_c at monthly and annual scales, respectively. AIC_c was calculated at monthly and annual aggregation, as n was usually smaller than K in these cases. The value of K was the total number of model parameters calibrated for all the site–years, for all the sites, for all the PFT, and for a specific model in case of per site–year parameterization, per site parameterization using $Cost^{IAV}$, per site parameterization, per PFT parameterization, and global parameterization, respectively.

2.4.8. Difference in Model Performances Between PFTs

We studied the distribution of model performances of the P^W_{hr} model and the Bao_{hr} model for different parameterization strategies across PFTs and climate–vegetation types (Section 2.2). We performed non-parametric statistical significance testing using a two-sample Kolmogorov-Smirnov (K-S) test (Hodges, 1958) between a given pair of parameterization strategies for a given model and PFT to test if model performance obtained from a parameterization strategy is significantly different from another for a PFT and a model. Similarly, we performed the K-S test between model performances of the P^W_{hr} model and the Bao_{hr} model for a given parameterization strategy and a PFT to test if model performances were significantly different between two models. We performed the K-S test using SciPy v1.14.1 (Virtanen et al., 2020).

2.4.9. Simulating GPP Peaks

We assessed model performance in predicting peak GPP_{EC}. We defined peak GPP_{EC} and peak GPP_{sim} as the 90th percentiles of hourly GPP_{EC} ($P90_{GPP_{EC}}$) and GPP_{sim} ($P90_{GPP_{sim}}$), respectively, following the concept of good hours by Zscheischler et al. (2016) and Fatichi and Ivanov (2014). We calculated $P90_{GPP_{EC}}$ and $P90_{GPP_{sim}}$ for each site–year considering only good quality hourly data (Appendix B). We compared the ratios of peak GPP_{sim} from P^W_{hr} model and Bao_{hr} model to GPP_{EC} for each parameterization strategy in order to identify possible biases.

$$\Delta NNSE_{P90} = NNSE^{j1}_{P90} - NNSE^{j2}_{P90} \quad (28)$$

$$\Delta NNSE_{y} = NNSE^{j1}_{y} - NNSE^{j2}_{y} \quad (29)$$

We furthermore investigated whether improving the simulation of peaks of GPP_{EC} improved the simulation of IAV of GPP. We calculated NNSE between $P90_{GPP_{EC}}$ and $P90_{GPP_{sim}}$ ($NNSE^j_{P90}$) from all the site–years in a site considering only good site–years and only for sites with more than 3 years of good quality data (Appendix C) for a parameterization strategy j. Similarly, we calculated NNSE between the annual average of GPP_{EC} and GPP_{sim} ($NNSE^j_y$) for sites with more than 3 years of good quality data (Appendix C) for a parameterization strategy j. Then, differences between $NNSE^{j1}_{P90}$ and $NNSE^{j2}_y$ were calculated for a pair of parameterization strategies where $j1$ and $j2$ are two different parameterization experiments, for both P^W_{hr} model and Bao_{hr} model (Equations 28 and 29). Correlation between $\Delta NNSE_{P90}$ and $\Delta NNSE_y$ were then investigated to study whether a certain parameterization strategy for a given model better captured the GPP_{EC} peaks, and thus contributed to higher annual model performance.

3. Results

3.1. Overall Model Performance

All four models, that is, P^W_{hr}, P_{hr}, Bao_{hr}, and Bao_{dd} models performed significantly better at the hourly scale than the annual scale (Figure 2). The use of an additional constraint on IAV, that is, $Cost^{IAV}$ did not contribute to better

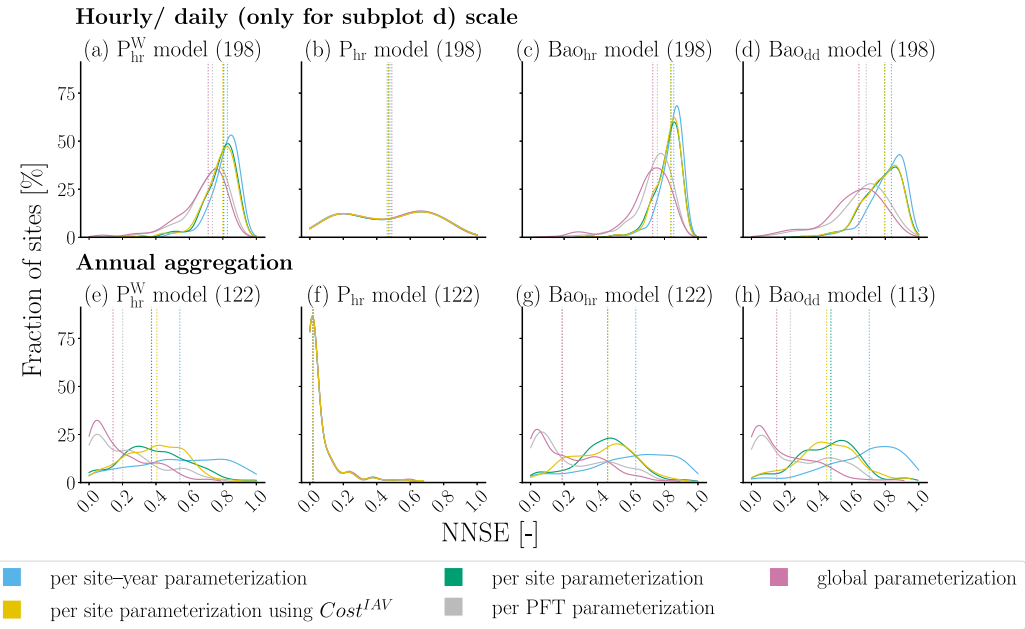

Figure 2. Distributions of model performance measure (normalized Nash-Sutcliffe efficiency, viz. NNSE) at hourly/daily scale (first row) and at annual timescale (second row) from P-model of Mengoli et al. (2022) with drought stress, parameterized at hourly scale (P^{W}_{hr}), P-model of Mengoli et al. (2022) without drought stress, parameterized at hourly scale (P_{hr}), the global best model of Bao, Wutzler et al. (2022) parameterized at hourly scale (Bao_{hr}), and global best model of Bao, Wutzler, et al. (2022) parameterized at daily scale (Bao_{dd}). For the Bao_{dd} model, subplot (d) shows model performance at daily scale as this model was parameterized at daily scale. $Cost^{IAV}$ denotes the usage of an additional constraint on annual gross primary production flux during per–site parameterization. The dotted vertical lines represent the median model performances, which are summarized in Table D1. The numbers in parentheses beside the model name on top of each of the sub-figures represent the total number of sites. The model performance at an annual scale was calculated for fewer sites as some sites have a very low measurement period (Appendix C).

model performance across sites at an annual scale and performed closer to parameterization per site and poorer than site–year parameterization (Figure 2). The median model performance was highest for the model parameterization per site–year among all model parameterization strategies (per site–year, per site using $Cost^{IAV}$, per site, per PFT, and global parameterization) for all four models (Table D1). Model parameterization per site–year also produced the best model performance at all temporal aggregation levels including annual aggregation (Figures 2, S5, and Table S2 of Supporting Information S1). P^{W}_{hr} model performed substantially better for the majority of the sites compared to P_{hr} model at all temporal aggregation levels as it explicitly considered site-specific water availability (Figures 2, S5, and Table S2 of Supporting Information S1). Comparison of model performances at different temporal aggregations also revealed that Bao_{hr} and Bao_{dd} models performed slightly better than the P^{W}_{hr} model across all timescales (hourly, daily, weekly, monthly, and annual), as the Bao_{hr} and Bao_{dd} models were more flexible than the P^{W}_{hr} model and captured ecosystem response with a broad range of parameters (Figure 2, Table D1, Figure S5 and Table S2 of Supporting Information S1). For example, the median NNSE(s) at the hourly resolution were 0.827 and 0.855 for the P^{W}_{hr} model and the Bao_{hr} model, respectively. Conversely, at the annual resolution, the median NNSE(s) were 0.543 and 0.628 for the P^{W}_{hr} model and Bao_{hr} model, respectively.

The annual average of GPP_{sim} was within the uncertainty range of GPP_{EC} (as defined in Section 2.4.3) for most site–years in most of the sites when P^{W}_{hr} (mean fraction of site–years per site: 0.87), Bao_{hr} (mean fraction of site–years per site: 0.93), and Bao_{dd} (mean fraction of site–years per site: 0.94) models were parameterized per site–year (Figure 3 and Table E1). P_{hr} model overestimated annual GPP_{sim} beyond the uncertainty range of GPP_{EC} in most cases for all parameterization methods, where the mean fraction of site–years per site within the uncertainty range of GPP_{EC} was $\leq$0.13 (Figure 3 and Table E1). Mean fractions of the site–years per site for which GPP_{sim} was within the uncertainty range were also similar for site-specific parameterization compared to site–year specific parameterization for P^{W}_{hr}, Bao_{hr}, and Bao_{dd} models (Table E1). However, for PFT-specific

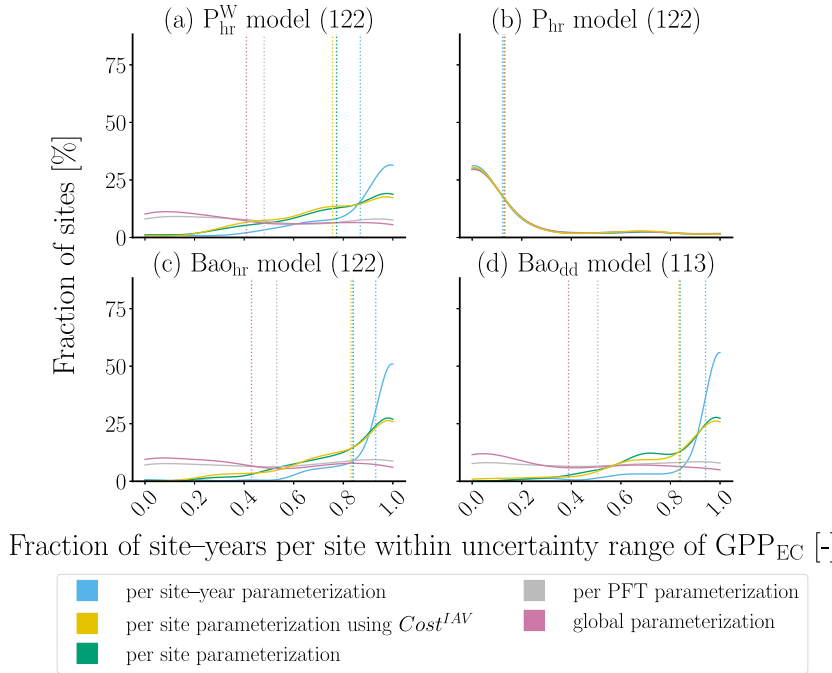

Figure 3. Distributions of fractions of site–years of a site for which annual average of simulated gross primary production (GPP_{sim}) was within the uncertainty range of eddy-covariance derived GPP (GPP_{EC}). The GPP_{sim} were estimated using (a) P-model of Mengoli et al. (2022) with drought stress, parameterized at hourly scale (P_{hr}^{W} model), (b) P-model of Mengoli et al. (2022) without drought stress, parameterized at hourly scale (P_{hr} model), (c) global best model of Bao, Wutzler, et al. (2022) parameterized at hourly scale (Bao_{hr} model), and (d) global best model of Bao, Wutzler, et al. (2022) parameterized at daily scale (Bao_{dd} model). $Cost^{IAV}$ in the legend denotes the usage of an additional constraint on annual gross primary production flux during per–site parameterization. The dotted vertical lines represent the mean fractions of site–years of a site for which the annual average of GPP_{sim} was within the uncertainty range of GPP_{EC}. The mean values are summarized in Table E1. The numbers in parentheses beside the model name on top of each of the sub-figures represent the total number of sites. The model performance at an annual scale was calculated for fewer sites as some sites have a very low measurement period (Appendix C).

parameterization and global model parameterization, the annual average of GPP_{sim} was unreliable and went beyond the uncertainty range of GPP_{EC} for most cases (Figure 3).

3.2. Factors Influencing Variability in Model Performance

We summarized the percentage contributions of factors which influenced model performance at hourly and annual scales and found that most of the variability in model performance came from how we designed our modeling experiments (Figure 4). Model types was a crucial factor when the P_{hr} model was included in N-way ANOVA analysis, as this model had comparatively poor performance at both hourly and annual scales and resulted in greater variability in the NNSE values (70.1% and 63.5% contribution to the sum of squares of the regression, viz. SSR in hourly and annual scale, respectively). We then excluded the P_{hr} model from further analysis to uncover the other factors behind the model performance and found that for the hourly scale, the model performance varied the most across the groups of KG classes (33.9% contribution to the SSR), followed by parameterization type (31.0% to the SSR) and climate–vegetation type (25.4% contribution to the SSR) (Figure 4). However, at an annual scale, the parameterization strategy strongly affected (62.3% contribution to the SSR) the model performance, as per–site–year parameterization usually better simulated the annual GPP_{obs} compared to other parameterization strategies. The number of good years (Appendix C) used for calculating annual NNSE also exerted a small influence (4.9% contribution to the SSR) on the annual model performance. In general, there were only slight performance differences between models when the P_{hr} model was not considered, and model parameterization played a bigger role in the variability of model performance.

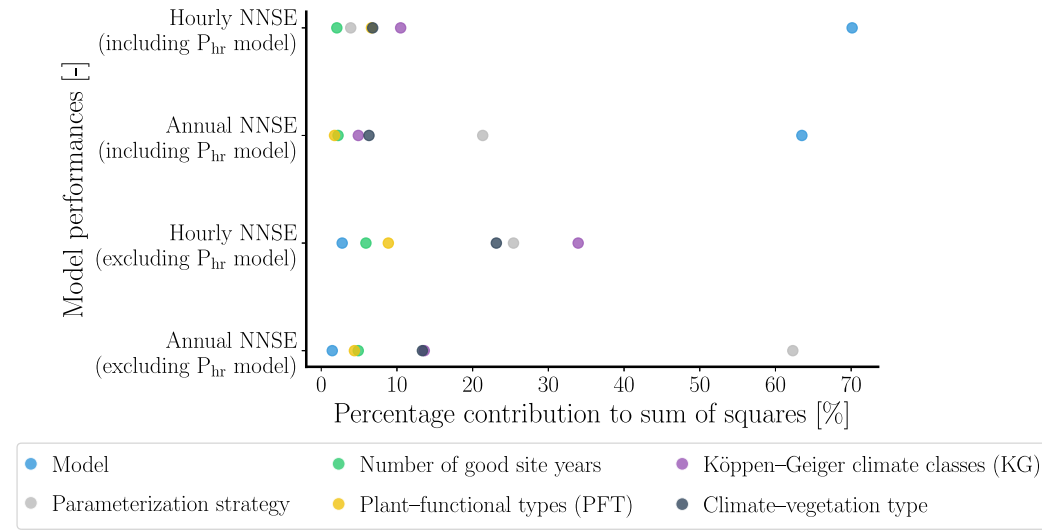

Figure 4. Percentage contributions of factors influencing variability in model performance (normalized Nash-Sutcliffe efficiency, viz. NNSE) in the sum of squares in N-way Analysis of Variance (ANOVA). The percentage contributions show the influence of various factors on hourly and annual model performance when the P-model (Mengoli et al., 2022) without any explicit drought stress function, parameterized at hourly scale (P_{hr} model) was considered in the analysis, as well as on hourly and annual model performance excluding the P_{hr} model. The sum of squares of residual was removed before plotting the percentage contributions of the factors and only the explained variance is shown.

3.3. Effect of Drought Stress on Model Performance

The performance of the P_{hr}^{W} model to predict the annual average of GPP_{EC} from each of the site–years substantially improved in comparison to P_{hr} model (from an NSE of −1.39 to 0.92) after explicit consideration of soil water supply in the model (Figure 5). Most of this improvement came from the better prediction of the annual average of GPP_{EC} at the arid and semi-arid sites (with AI values lower than 0.5). For the semi-arid site (AU-ASM) the predicting performance of the P_{hr}^{W} model for all the parameterization strategies largely benefited from the explicit inclusion of soil water supply constraints (Figure 6). The systematic bias in model simulations was also improved after the inclusion of a drought stress constraint, as well as the modeling bias also improved from a generalized to a detailed parameterization strategy. Although the coupling of a simple hydrological model which calculated water–availability based on precipitation and evapotranspiration and inclusion of drought stress function generally improved the P_{hr}^{W} model for most of the site–years at an arid site, the model failed to capture the GPP_{EC} (Text S3, Figure S6 of Supporting Information S1) at an irrigated cropland site (US-Ne1), as the simple hydrological model which we used to calculate water–availability lacked representation of human management.

3.4. Effect of Temporal Resolution of the Data on Model Performance

The use of hourly data to constrain Bao_{hr} model parameters and aggregating hourly values of GPP_{sim} to annual scale did not have a significant effect on the Bao_{hr} model performance in comparison to parameterization of the same model with daily data, that is, Bao_{dd} model, in simulating the annual average of GPP_{EC} (Figure 7) for each site–year. The value of NSE decreased from 0.961 to 0.891 for the Bao_{hr} model compared to the Bao_{dd} model, and both models performed mostly similarly. Here, for the Bao_{hr} model, we also focus on a site-specific example at a site (DE-Hai) in central Germany with a deciduous broadleaf forest where the Bao_{hr} model proved to be capable of simulating annual average of GPP_{EC} flux relatively well when the model was parameterized for each site–year and each site (Figure 8). However, GPP_{EC} was underestimated in cases of PFT-specific and global parameterization. For this specific site, the Bao_{hr} model performed relatively better in comparison to Bao_{dd} model (Figures 8 and S7 of Supporting Information S1).

3.5. Role of Parameterization Strategies on Model Performance

Model performances at an annual scale generally increased with a more detailed parameterization strategy (Figure 9). For the P_{hr}^{W} model, the median differences in annual model performance between the most detailed

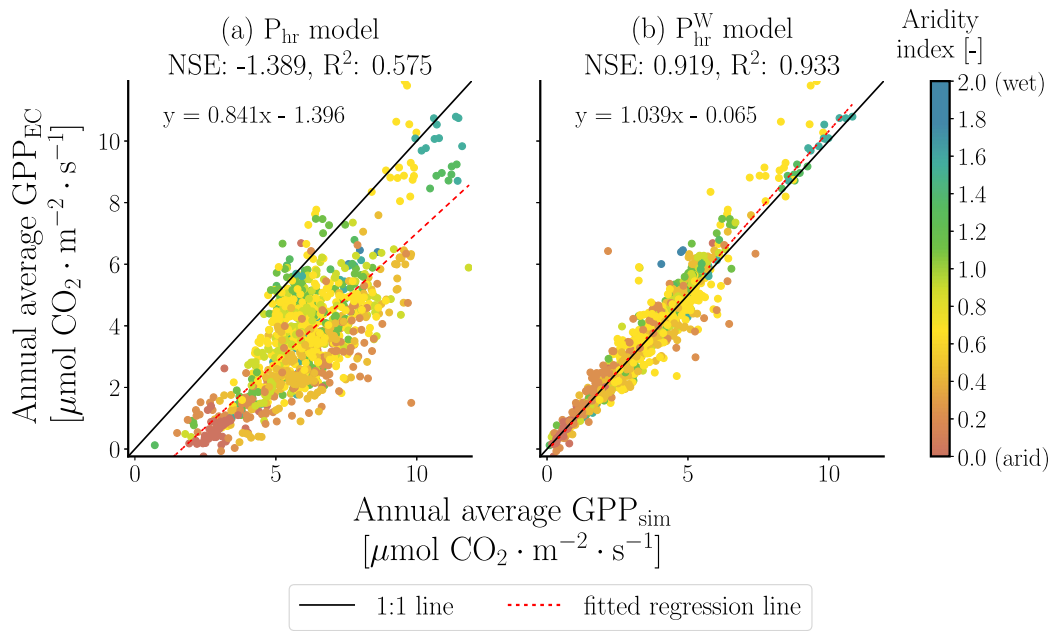

Figure 5. Scatter plot of the annual average (from good quality site–years, see Appendix C) of eddy covariance measurements derived gross primary production (GPP_{EC}) versus simulated gross primary production (GPP_{sim}) from P-model of Mengoli et al. (2022) parameterized at hourly scale (a) without drought stress (P_{hr} model) and (b) with drought stress (P^W_{hr} model). The results in this plot are from parameterization for each site–year. We only used good–quality site–years in this figure (Appendix C). The dots in the scatter represent a site–year and are colored by the aridity index (AI) of the site. The model performance metrics (Nash-Sutcliffe efficiency, viz. NSE) are shown at the top of each subplot. The equations of fitted regression lines are shown in respective subplots.

parameterization strategy, that is, site–year parameterization, and other detailed parameterization strategies, that is, per site parameterization using $Cost^{IAV}$ and per site parameterization were small, which were 0.12, and 0.11, respectively. In contrast, the median differences in annual model performance between the most detailed parameterization strategy, that is, site–year parameterization, and other generalized parameterization strategies, that is, PFT-specific parameterization, and global parameterization were quite large, which were 0.28, and 0.37, respectively. Similarly, for the Bao_{hr} model, the median differences in annual model performance between the most detailed parameterization strategy, that is, site–year parameterization, and other detailed parameterization strategies, that is, per site parameterization using $Cost^{IAV}$ and per site parameterization were 0.16, and 0.15, respectively. In contrast, the median differences in annual model performance between the most detailed parameterization strategy, that is, site–year parameterization, and other generalized parameterization strategies, that is, PFT-specific parameterization, and global parameterization were 0.34, and 0.39, respectively. The positive values of median annual model performance confirm the highest median performance of site–year parameterization compared to the other four parameterization strategies.

At an hourly scale, differences in model performance between a pair of similar parameterization strategies, such as a pair of detailed parameterization (i.e., between site–year-specific and site-specific) or a pair of generalized parameterization (i.e., between per PFT and global) approaches for both models were small (Figure S8 of Supporting Information S1). However, this difference can be higher between a detailed and a generalized model parameterization strategy. The median differences in hourly NNSE between site–year-specific and site-specific model parameterization were 0.02 and 0.01 for the P^W_{hr} model and Bao_{hr} model, respectively. In contrast, the median differences in hourly NNSE between site–year-specific and global model parameterization were 0.11 for both P^W_{hr} and Bao_{hr} models.

The median differences in annual model performance between per–site parameterization using $Cost^{IAV}$ and per–site parameterization were relatively small, which were 0.01 and 0.00 for P^W_{hr} model and Bao_{hr} model, respectively, and it shows the additional constraint on IAV of GPP flux in the cost function did not substantially improve annual model performance. At hourly scale, median differences in model performance between per–site

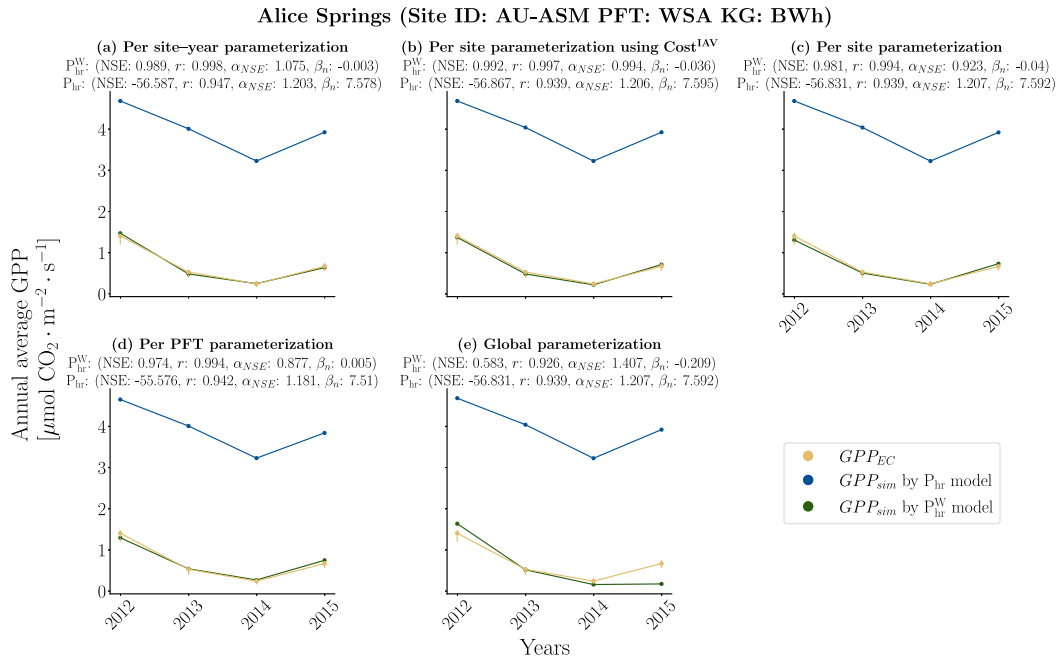

Figure 6. Comparison of annual average of gross primary production (GPP) derived by eddy covariance measurements (GPP_{EC}), and GPP simulated (GPP_{sim}) by the P-model of Mengoli et al. (2022) parameterized at hourly scale without drought stress (P_{hr} model) and with drought stress (P_{hr}^{W} model). The five subplots show simulated GPP from (a) site–year specific parameterization, (b) site-specific parameterization using an additional constraint on inter–annual variability in the cost function ($Cost^{IAV}$), (c) site-specific parameterization, (d) plant–functional types (PFT) specific parameterization, and (e) global parameterization. The values of model performance measures (Nash-Sutcliffe efficiency, viz. NSE, correlation coefficient, viz. r, relative variability, viz. α_{NSE}, and bias, viz. β_n) are shown on top of respective subplots. This site is dominated by Mulga (*Acacia aneura*), and had an annual average temperature of ≈22 °C, and an annual average precipitation of ≈318 mm during the observation period (Cleverly et al., 2013; Pastorello et al., 2020). The vertical error bars represent the uncertainty range (see Section 2.4.3) of the annual average of GPP_{EC} for the corresponding years (the uncertainty range is relatively small for this specific site). The site ID, PFT, and Köppen–Geiger climate class (KG) of the site are provided on top of the figure in bold.

parameterization using $Cost^{IAV}$ and per–site parameterization were also non-existent, which were 0.00 for both P_{hr}^{W} and Bao_{hr} models. Though the per–site parameterization using $Cost^{IAV}$ did not improve the annual model performance, it also did not degrade the hourly model performance.

3.6. Differences Between Modeling Experiments of Various Complexities

The lowest AIC values were obtained for per site–year parameterization for all the models at hourly and daily scales or aggregations, suggesting the sum of squares errors (*SSE*) was substantially reduced even when a comparatively complex parameterization strategy with a large number of model parameters was chosen (Table 3). The AIC values gradually increased from per site–year, per site, per PFT to global parameterization at hourly and daily scales or aggregations for all three models which are P_{hr}^{W} model, Bao_{hr} model, and Bao_{dd} model (Table 3). Semi-empirical models, that is, Bao_{hr} model and Bao_{dd} model also had mostly lower values of AIC compared to optimality-based P_{hr}^{W} model even though more parameters were parameterized for these models (Table 3). At the daily scale, the Bao_{dd} model had the lowest AIC for all the parameterization experiments due to the parameterization at daily scale. Whereas, for the other two models, parameterization and forward runs were performed at an hourly scale and then simulations were aggregated to daily resolution. The P_{hr} model was not included in AIC or AIC_c analysis as previous results proved this model significantly underperformed compared to the other models, and this will always result in higher AIC or AIC_c values.

At monthly and annual scales, we show the differences in AIC_c values between P_{hr}^{W}, Bao_{hr}, and Bao_{dd} models for the same parameterization strategy, and not between parameterization strategies in a same model. The reason behind this is AIC_c values largely depend on the relationship between sample size, that is, n, and the total number of parameters which were parameterized, that is, K. The values of AIC_c became very large even when a

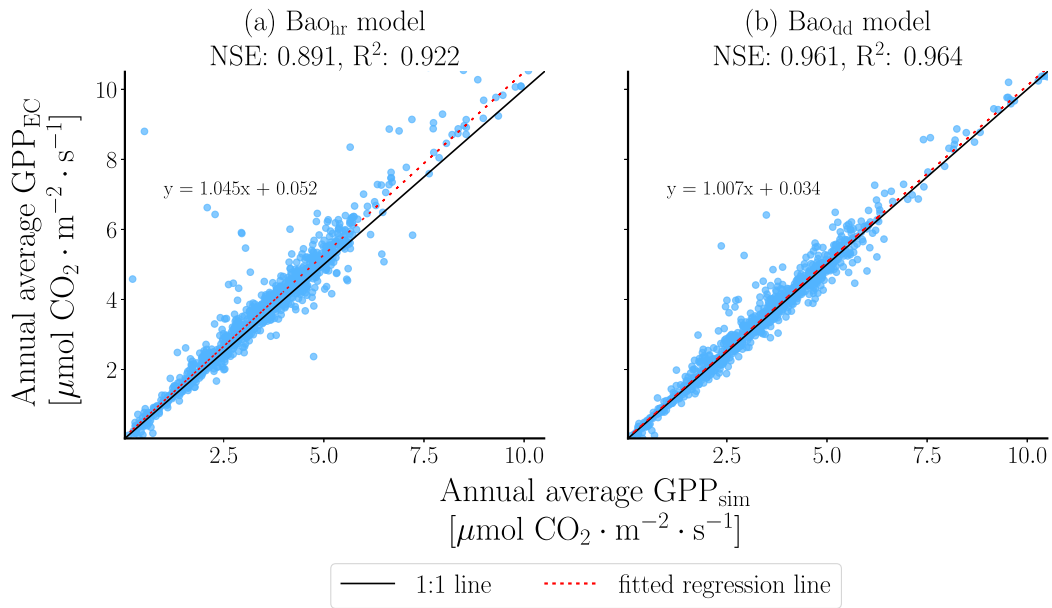

Figure 7. Scatter plot of annual average (from good quality site–years, see Appendix C) eddy covariance derived gross primary production (GPP_{EC}) versus simulated gross primary production (GPP_{sim}) by the light use efficiency model of Bao, Wutzler, et al. (2022) parameterized at hourly (Bao$_{hr}$ model) and daily scale (Bao$_{dd}$ model) for each site–year. The plots show the performance of the (a) Bao$_{hr}$ model, and (b) Bao$_{dd}$ model. The dots in the scatter represent a site–year. The model performance metrics (Nash-Sutcliffe efficiency, viz. NSE) are shown on the top of each subplot. The equations of fitted regression lines are shown in respective subplots.

significantly smaller *SSE* was obtained, and they became unreliable when the value of n was closer to K. For example, at monthly aggregation, per site–year parameterization of the P^W_{hr} model had a very high AIC_c value of 1.30×10^6 even when it had the lowest *SSE* among all the five parameterization strategies (Tables S3, S4, and S5 of Supporting Information S1). The Bao$_{dd}$ model proved to be better able to capture the seasonal cycle, that is, monthly GPP estimates compared to the other two models for most of the parameterization experiments considering the number of parameters parameterized (Table 3). However, the P^W_{hr} model had the lowest AIC_c value in the case of per site parameterization using $Cost^{IAV}$ and per site parameterization at monthly aggregation. In contrast, at an annual scale, the P^W_{hr} model had mostly the lowest AIC_c values, and some of the experiments also suffered from the above-described unreliable AIC_c estimates, where n and K had similar values (Tables 3, S3, S4, and S5 of Supporting Information S1).

3.7. Model Performances Across Different Plant–Functional Types

Generally better model performances were achieved with both the P^W_{hr} model and the Bao$_{hr}$ model when parameterized detailed model parameterization strategies were used (Figure 10). In this analysis, we removed the per–site parameterization experiment using $Cost^{IAV}$ as it performed very similar to per–site parameterization, and also we did not consider the P_{hr} model as it produced poor performance across all the PFTs.

The highest median NNSEs were obtained with per–site–year parameterization for almost all the PFTs for both models. The only exception is WSA for which the median model performance (median NNSE: 0.85) was marginally higher for per–site parameterization experiment using $Cost^{IAV}$ compared to per–site–year parameterization (median NNSE: 0.84) of Bao$_{hr}$ model. For the P^W_{hr} model parameterization experiments, the highest median value of NNSE was found for CSH for per–site–year parameterization (median NNSE: 0.88), DBF for per–site parameterization (median NNSE: 0.85), CSH and DBF for per-PFT parameterization (median NNSE: 0.81), and CSH for global parameterization (median NNSE: 0.80). However, CSH had only three sites and highest median model performance for CSH should be interpreted with caution. For the Bao$_{hr}$ model parameterization experiments, the highest median value of NNSE was found for DBF for per–site–year parameterization (median NNSE: 0.89), DBF and MF for per–site parameterization (median NNSE: 0.87), DBF for per-PFT

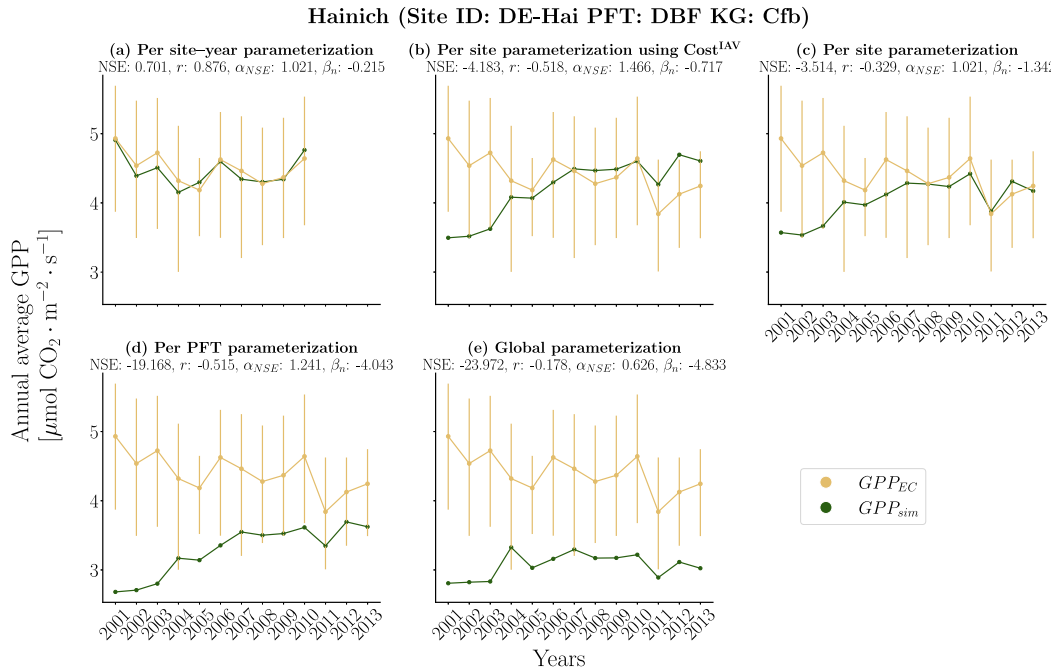

Figure 8. Comparison of annual average of gross primary production (GPP) derived by eddy covariance measurements (GPP_{EC}), and GPP simulated (GPP_{sim}) by the light use efficiency model of Bao, Wutzler, et al. (2022), which was parameterized with hourly data (Bao_{hr} model). The five subplots show simulated GPP from (a) site–year specific parameterization, (b) site-specific parameterization using an additional constraint on inter–annual variability in the cost function ($Cost^{IAV}$), (c) site-specific parameterization, (d) plant–functional types (PFT) specific parameterization, and (e) global parameterization. The years 2010–2012 could not be parameterized in the case of site–year parameterization, as there were no good quality evapotranspiration estimates from latent heat flux measurements for those years. The values of model performance measures (Nash-Sutcliffe efficiency, viz. NSE, correlation coefficient, viz. r, relative variability, viz. α_{NSE}, and bias, viz. β_n) are shown on top of respective subplots. This site represents an average 140-year-old deciduous forest (Tamrakar et al., 2018) with a distinct seasonal cycle and an annual average temperature of ≈8.3 °C, and an annual average precipitation of 750–800 mm during the observation period (Knohl et al., 2003a; Pastorello et al., 2020). The vertical error bars represent the uncertainty range (see Section 2.4.3) of the annual average of GPP_{EC} for the corresponding years. The site ID, PFT, and Köppen-Geiger climate class (KG) of the site are provided on top of the figure in bold.

parameterization (median NNSE: 0.82), and DBF and MF for global parameterization (median NNSE: 0.81). We found similar results also for climate–vegetation types (Section 2.2), where a more detailed parameterization strategy achieved higher model performance than a generalized parameterization strategy (Text S5 and Figure S9 of Supporting Information S1).

Specifically, we found the model performance significantly differed between per–site–year parameterization and global model parameterization for most PFTs and both models (Figure 10). Model performance was also similar between a pair of detailed parameterization strategies (per–site–year and per–site parameterization) and general parameterization strategies (per-PFT and global parameterization) for most PFTs. For PFTs with very few sites, such as CSH, DNF, SNO, and WSA, statistical significance testing showed that the model performance was similar among parameterization strategies. However, statistical significance tests can be unreliable for a few samples. The model performance between P^{W}_{hr} model and the Bao_{hr} model for a specific parameterization strategy was similar for most PFTs (Table S6 of Supporting Information S1). Similarly, model performance between both models for a specific parameterization strategy was also identical for most PFTs (Table S7 of Supporting Information S1).

3.8. Correlation Between Annual Model Performance and Model Performance in Simulating Diurnal GPP Peaks

One of the crucial reasons behind poor annual model performance (Figure 2 and Table D1) can be the inability of both the P^{W}_{hr} model and the Bao_{hr} model to capture the peaks of GPP_{EC} (Figure S10 of Supporting

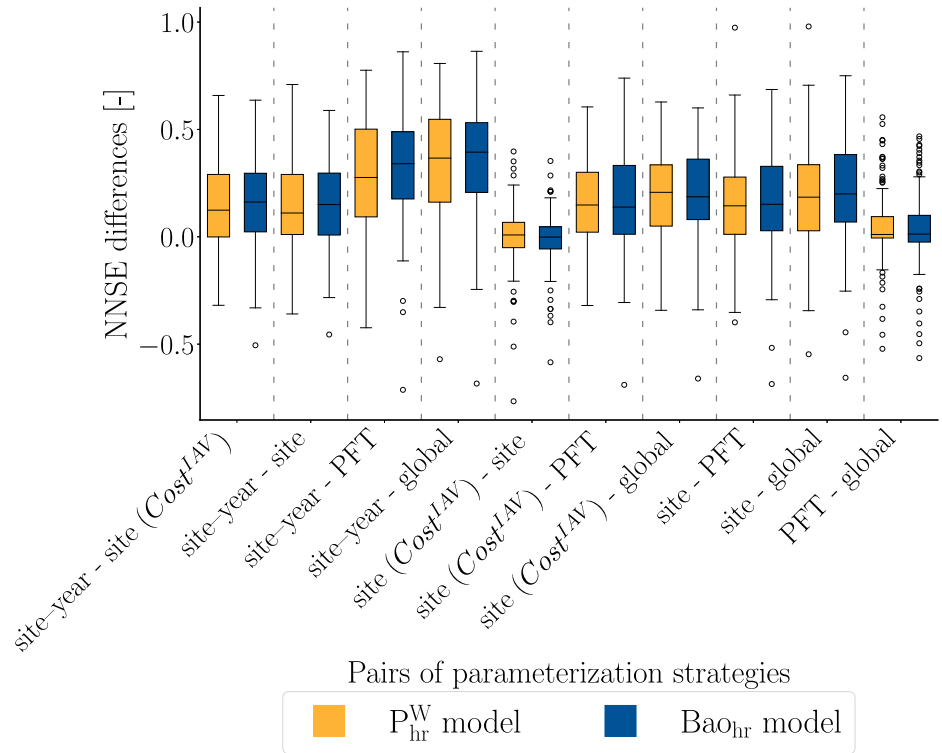

Figure 9. Distributions of the differences between model performance measures (normalized Nash-Sutcliffe efficiency, viz. NNSE) calculated at annual scale, from various pairs of model parameterization experiments conducted for the P-model of Mengoli et al. (2022) with drought stress, parameterized with hourly data (P_{hr}^{W} model) and the light use efficiency model of Bao, Wutzler, et al. (2022), parameterized with hourly data (Bao_{hr} model). $Cost^{IAV}$ in parentheses denotes the usage of an additional constraint on annual gross primary production flux during per–site parameterization. The boxes are spanned between the first and third quartiles of the differences, and the line in the middle represents the median. The whiskers show the farthest data point from the box within 1.5× of the interquartile range. The circles represent the outliers that go beyond the limits of the whiskers. The vertical dotted gray lines separate each pair of model parameterization strategies.

Information S1). Specifically, $P90_{GPP_{EC}}$ was highly underestimated in the case of global parameterization. The median of the ratio of $P90_{GPP_{sim}}$ to $P90_{GPP_{EC}}$ were 0.77 and 0.84 for the P_{hr}^{W} model and the Bao_{hr} model, respectively, during global parameterization. The underestimation generally decreased with more detailed parameterization strategies, with little difference between the models. The median values of the ratio of $P90_{GPP_{sim}}$ to $P90_{GPP_{EC}}$ were 0.95 and 0.93 for the site–year parameterization of the P_{hr}^{W} model and the Bao_{hr} model, respectively. Moreover, the lower values of the interquartile range (IQR) of these ratios signify the importance of site–year parameterization compared to per PFT or global parameterization to reliably capture the peak GPP_{EC} in diurnal cycles for most of the sites and to attain better model performance at the sub-daily scale. The values of IQR were 0.1 for both the P_{hr}^{W} model and the Bao_{hr} model in the case of site–year parameterization, 0.44 and 0.37 for the P_{hr}^{W} model and the Bao_{hr} model, respectively in the case of PFT-specific parameterization, and 0.44 and 0.49 for the P_{hr}^{W} model and the Bao_{hr} model, respectively in the case of global parameterization.

We further found that if a certain parameterization strategy better simulated the $P90_{GPP_{EC}}$ for each site–year, it corresponded to a comparatively better annual model performance for a site which is demonstrated by the positive values of Pearson correlation coefficients (Figure 11). Here also, a detailed parameterization strategy, such as site–year parameterization resulted in a better simulation of $P90_{GPP_{EC}}$, and thus better annual model performance for most of the sites compared to a generalized parameterization strategy, such as global parameterization. In this case when $j1$ was site–year parameterization and $j2$ was global parameterization, 91% and 89% sites had higher $NNSE_{P90}^{j1}$ than $NNSE_{P90}^{j2}$ and corresponding $NNSE_{y}^{j1}$ than $NNSE_{y}^{j2}$ for the P_{hr}^{W} model and the Bao_{hr} model, respectively. When $j1$ was parameterization per site using $Cost^{IAV}$ and $j2$ was parameterization per site, respectively, only 34% and 37% had positive values of $\Delta NNSE_{P90}$ (i.e., $NNSE_{P90}^{j1} > NNSE_{P90}^{j2}$) and corresponding

Table 3
Akaike's Information Criterion (AIC) or Corrected AIC (AIC_c) Values for Modeling Experiments of Various Complexities

Temporal scale/ aggregation	Models	Parameterization strategies				
		Per site–year	Per site using $Cost^{IAV}$	Per site	Per PFT	Global
Hourly scale (AIC)	P^{W}_{hr}	1.72×10^{7}	1.84×10^{7}	1.86×10^{7}	2.16×10^{7}	2.25×10^{7}
	Bao_{hr}	1.58×10^{7}	1.70×10^{7}	1.68×10^{7}	2.10×10^{7}	2.16×10^{7}
Daily scale/ aggregation (AIC)	P^{W}_{hr}	4.58×10^{5}	5.05×10^{5}	5.11×10^{5}	6.88×10^{5}	7.42×10^{5}
	Bao_{hr}	3.99×10^{5}	4.28×10^{5}	4.24×10^{5}	6.65×10^{5}	6.92×10^{5}
	Bao_{dd}	2.68×10^{5}	3.12×10^{5}	3.18×10^{5}	4.98×10^{5}	5.58×10^{5}
Monthly aggregation (AIC_c)	P^{W}_{hr}	1.30×10^{6}	1.63×10^{4}	1.63×10^{4}	2.04×10^{4}	2.25×10^{4}
	Bao_{hr}	-4.55×10^{4}	1.79×10^{4}	1.79×10^{4}	1.97×10^{4}	2.02×10^{4}
	Bao_{dd}	-3.40×10^{4}	1.67×10^{4}	1.70×10^{4}	1.52×10^{4}	1.73×10^{4}
Annual aggregation (AIC_c)	P^{W}_{hr}	-3.56×10^{3}	-5.22×10^{3}	-5.57×10^{3}	9.09×10^{2}	9.28×10^{2}
	Bao_{hr}	-3.19×10^{3}	-3.84×10^{3}	-3.72×10^{3}	1.42×10^{3}	9.26×10^{2}
	Bao_{dd}	-3.66×10^{3}	-3.45×10^{3}	-3.39×10^{3}	1.12×10^{3}	7.49×10^{2}

$\Delta NNSE_y$ (i.e., $NNSE_y^{j1} > NNSE_y^{j2}$) for the P^{W}_{hr} model and the Bao_{hr} model, respectively. This signified that using an additional constraint related to the IAV of GPP in the cost function during model parameterization did not improve the prediction of peak GPP values for most of the sites.

4. Discussion

4.1. Uncertainties in Modeling Experiments

Any model–data–integration study is prone to uncertainties related to both data and the model. The EC data set used in our study has a couple of well-known uncertainties. For example, the NEE measurements using the eddy covariance technique can have uncertainties due to the accumulation of atmospheric CO_2 under the canopy at night (storage) and a sudden turbulent mixing during the morning when the stable night-time boundary layer breaks up, or because of advection of atmospheric CO_2 out of the control volume sampled by the eddy covariance system (Aubinet, 2008; D. Baldocchi et al., 2000; Jocher et al., 2018). The GPP fluxes that we used were derived from NEE measurements by extrapolating the night-time respiration of the ecosystem (Reichstein et al., 2005) to daytime. Moreover, GPP can be estimated based on another well-known algorithm, the daytime partitioning method (Lasslop et al., 2010). We preferred night-time partitioning as only respiration is modeled in this method. In daytime partitioning, both GPP and respiration are modeled, resulting in higher prediction errors. The uncertainties in our modeling results due to the choice of partitioning algorithm should be small as quantified in a previous study by Desai, et al. (2008). Papale et al. (2006) proposed a standardized set of flux correction techniques for the above-described issues related to EC methods and removing random spikes in EC measurements. Many of these correction techniques were adapted to the standardized ONEFlux pipeline for the production of the FLUXNET2015 data set (Pastorello et al., 2020). Papale et al. (2006) also found that the uncertainties associated with annual NEE, and fluxes derived from NEE, such as GPP and TER have an inherent uncertainty well below 100 $gC \cdot m^{-2} \cdot year^{-1}$. In our study, we found that annual GPP_{Sim} produced by experiments related to detailed parameterization strategies were mostly within the range of uncertainty of GPP_{EC} on the choice of different variables produced by the data processing pipeline. However, quantifying full uncertainty in GPP_{EC} related to measurement errors, random noises, data gaps and gap-filling methods, flux correction methods, and flux partitioning methods as well as propagating all the uncertainties to various temporal scales is a very challenging task and beyond the scope of this study. Similarly, GPP_{Sim} can also have various uncertainties related to model structure and simplified representation of ecosystem functions (such as stomatal conductance, photosynthesis, leaf energy balance etc.), forcing data, and parameters (Schaefer et al., 2012; Zheng et al., 2018). For example, the Bao model used in our study is based on the big leaf assumption. In contrast, differentiating between sunlit and shaded leaves (two big-leaf assumption) in a similar model can lead to higher performance under certain conditions, such as under hot and dry conditions at daily and weekly scales (Bao, Ibrom, et al., 2022). However, the two big-leaf model was also equally poor at explaining IAV. In this study, we aimed to address some of these

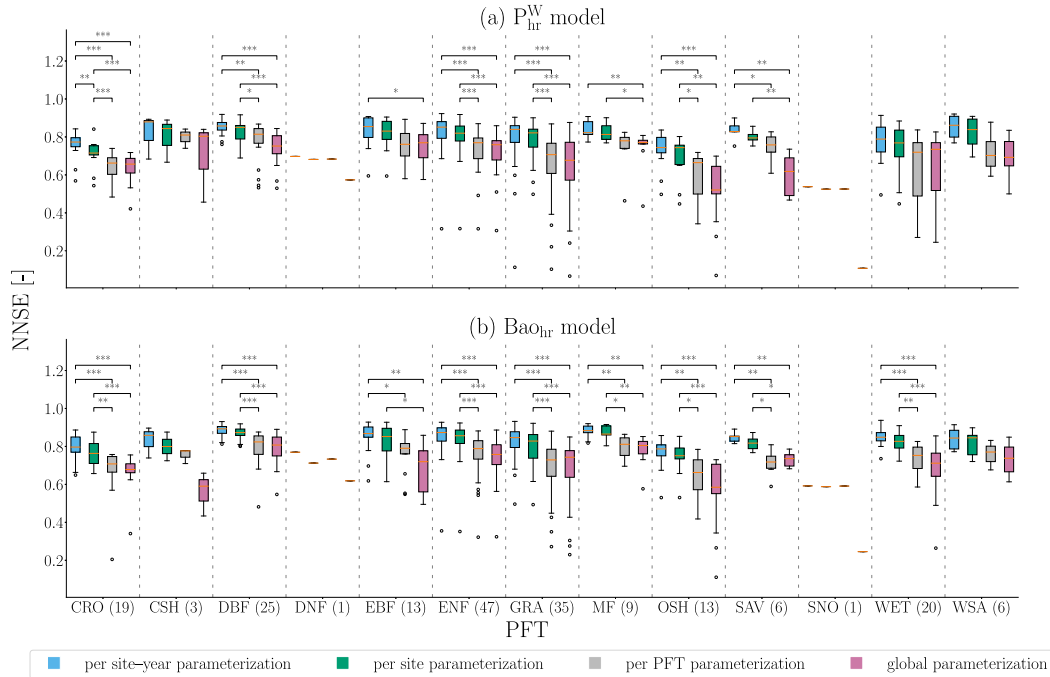

Figure 10. Box-plots showing the range of the hourly model performance metric (normalized Nash-Sutcliffe efficiency, viz. NNSE), for the sites in different plant–functional types (PFT), and different parameterization experiments. The subplots show the model performance for (a) P-model of Mengoli et al. (2022) with drought stress function, parameterized with hourly data (P^{W}_{hr} model), and (b) the light use efficiency model of Bao, Wutzler, et al. (2022) parameterized with hourly data (Bao_{hr} model). The numbers in parentheses beside the name of each PFT on the *x*-axis are the number of sites present in a specific PFT. The boxes are spanned between the first and third quartiles of NNSE values, and the line in the middle represents the median. The whiskers show the farthest data point from the box within 1.5× of the interquartile range. The circles represent the outliers that go beyond the limits of the whiskers. The results of statistical significance testing using a two-sample Kolmogorov-Smirnov test (Hodges, 1958) between a pair of model parameterization strategies (connecting bars over boxplots) are shown as * ($0.05 > p$-value ≥ 0.01), ** ($0.01 > p$-value ≥ 0.001), *** (p-value < 0.001) if the distributions of model performances were not identical. No bars and star symbols over a pair of boxplots signify that the distributions of model performances from a pair of parameterization strategies were identical and the null hypothesis could not be rejected (p-value ≥ 0.05). For, deciduous needle-leaf forests (DNF), and areas covered by snow (SNO) only the median value could be shown as these PFTs have only one site. The vertical dotted gray lines separate each PFT.

uncertainties in GPP_{Sim} by adopting majorly two different model structures and various parameterization schemes.

We also used ET in the cost function which is equivalent to latent heat flux. The mismatch between the summation of latent, sensible, and ground heat fluxes with net radiation calculated using incoming and outgoing radiation, the so-called lack of energy–balance closure, remains a long-standing challenge with EC measurements (Foken, 2008; Mauder et al., 2020; Zhang et al., 2024). Quality control of millions of data points at an hourly scale was also challenging, especially when we merged data from various sources, such as in-situ measurements, modeled re-analysis data, and remote sensing-based estimates. Another major uncertainty arises from the mismatch between the footprint of EC towers and the grid of remote sensing data which were used to calculate vegetation indices (Chu et al., 2021). The PFT classification of sites based on a simple PFT classification method may not accurately represent the vegetation of some of the sites. For example, a site at Alice Springs (AU-ASM) in central Australia was classified as a savanna in FLUXNET2015 (Pastorello et al., 2020). In fact, this site is dominated by a discontinuous canopy of Mulga (*Acacia aneura*) that has needle leaves and a seasonal understory grassy layer (Cleverly et al., 2013). This site can be classified as a woody savanna as well. An arctic site in Bayelva (SJ-Blv) has a combination of snow, wet grounds, and specific tundra vegetation (Boike et al., 2018) which were not well represented by the snow classification of FLUXNET2015 (Pastorello et al., 2020). Another limitation of the data set is that sites are mostly clustered in European and North American countries and, hence do

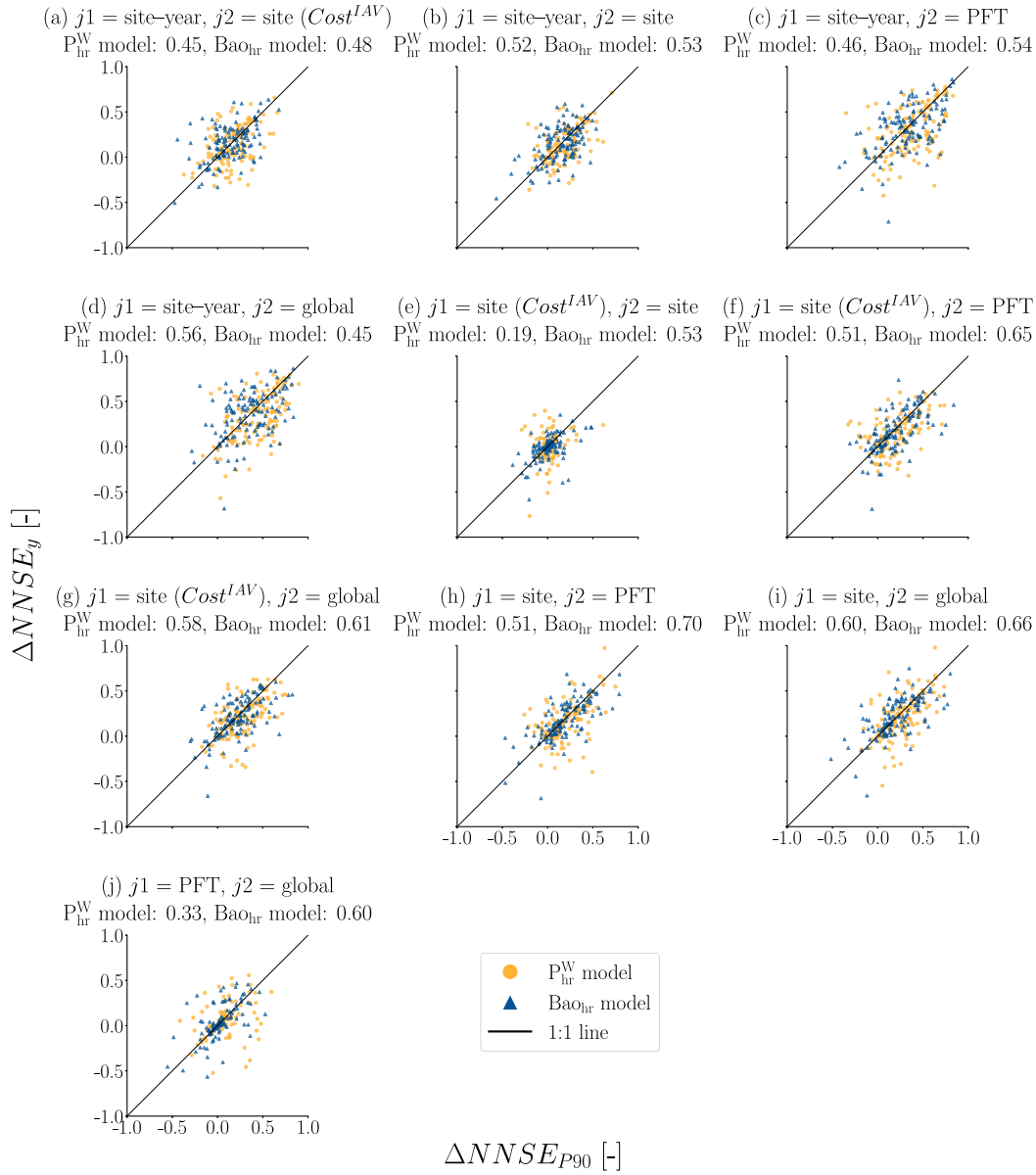

Figure 11. Scatter between differences in model performance in simulating peak gross primary production, viz. GPP ($\Delta NNSE_{P90}$) and annual average of GPP ($\Delta NNSE_y$). $j1$ and $j2$ are a pair of parameterization strategies for which differences are calculated in each subplot from (a to j). Each dot in the scatter represents a site. The P^{W}_{hr} model and Bao_{hr} model are P-model of Mengoli et al. (2022) with drought stress function and the light use efficiency model of Bao, Wutzler, et al. (2022), both were parameterized with hourly data. The values on top of each subplot indicate the Pearson correlation coefficient (Kirch, 2008) for respective models.

not necessarily represent global ecosystem functioning particularly well due to sampling bias (Papale et al., 2015). Similarly, some PFTs are represented by very few sites, which makes PFT-specific parameterization challenging.

4.2. General Performance of Models in Simulating GPP

Mengoli et al. (2022) evaluated the P_{hr} model across 10 sites consisting of boreal forest, temperate deciduous broadleaf forest, mixed forest, tropical forest, and temperate grassland. They found reasonable performance of P_{hr} model for these sites. In this study, we extended the evaluation of optimality-based P^{W}_{hr} and P_{hr} models across a wide range of sites, representing various vegetation and climate types. We uncovered poor model performance of the P_{hr} model at many sites, especially at arid sites. Calculating *WAI* using a simple hydrological model and

inducing a moisture stress function, that is, the introduction of the P_{hr}^{W} model substantially improved model performance to simulate the annual average of GPP fluxes across many sites, including both water–limited and energy–limited sites. Inclusion of the moisture stress function in the P_{hr} model improved not only the annual model performance but also the model performance across all the temporal scales or aggregation levels. This highlights the importance of representing soil moisture conditions in modeling approaches, which aim to accurately represent ecosystem functioning and vegetation response. Our findings also support another study by Schaefer et al. (2012) which found mostly poor performance of 26 models in simulating GPP under dry conditions across EC sites in North America. Even though the drought stress function used in this study does not explicitly account for long legacy effects, our results still confirmed the substantial effect of drought stress on GPP as found by numerous other studies (Anderegg et al., 2015; Müller & Bahn, 2022; Z. Yu et al., 2017; X. Yu et al., 2022). However, the coupling of the hydrological model raised the need to calibrate nine more parameters, which counters the vision of developing a parameter–sparse approach using theories that demand a lower site or site–year specific fine–tuning of model parameters (Prentice et al., 2015). Further experimentation is needed to find a balance between the number of key model parameters, which require calibration, and an accurate representation of ecosystem processes.

Coming to the differences in model structure, we found that semi-empirical models (Bao_{hr} and Bao_{dd} models) performed statistically better, that is, had a lower value of AIC compared to optimality-based model (P_{hr}^{W} model) at hourly and daily scale or aggregations for most of the parameterization experiments even though the semi-empirical modeling experiments needed more parameters to be parameterized. At the monthly aggregation level, the seasonal cycles were also significantly better captured by the parameter–heavy semi-empirical model parameterized with daily data (Bao_{dd} model) for most of the parameterization experiments. However, at the annual aggregation level, the optimality-based model, that is, the P_{hr}^{W} model was comparatively better in most cases and a more flexible semi-empirical model with a higher number of parameters did not have a substantial improvement in annual model performance. In an earlier study, Sims et al. (2005) found that midday gross CO_2 flux is highly correlated with daily and 8-day average of gross CO_2 flux and the midday values can be used to estimate fluxes at higher timescales, that is, at daily and 8-day. In this study, we also found that both hourly and daily GPP estimates from the Bao_{hr} model, Bao_{dd} model, respectively can be used to estimate fluxes at weekly and monthly scales reliably. However, both models poorly estimated the annual average GPP flux per site.

Though the partial sensitivity functions of environmental variables used in the Bao_{hr} model and the Bao_{dd} model were found to be applicable for most of the sites, they can be of many different types and may vary across site conditions (Bao, Wutzler, et al., 2022). The EC sites were also affected by human management, such as irrigation, harvesting, and mowing as well as natural disturbances, such as fire, and pest attacks. These factors can affect the IAV of GPP flux which was estimated from EC measurements. Models used in this study may not be able to account for all of these factors due to structural limitations. For example, in the hydrological model, we only used precipitation and ET to calculate the mass balance of water. However, human management (such as irrigation and drainage) can play an important role, and the *WAI* estimates in managed sites, such as at an irrigated maize site (US-Ne1) may not be accurate.

4.3. The Importance of the Parameterization Approach on Estimating IAV of GPP

We also performed inter–comparison between five different parameterization approaches for both an optimality-based model and a semi-empirical model, and also for a large number of sites. We did these extensive evaluations to emphasize the importance of model parameterization in capturing the IAV of GPP and gain higher confidence in our conclusions. Model parameterization largely determined model performances and calibrated parameters captured the individual characteristics of sites or climatic events of the site–years (J. Wu et al., 2012). Earlier studies (Groenendijk et al., 2011; Huang et al., 2021) found higher variability of model parameters across sites within a PFT and detailed parameterization was necessary to better simulate carbon fluxes as there can be variations in vegetation functioning and climatic conditions between sites and a simple PFT classification may not be enough to account for these variations. Similarly, we also found detailed model parameterization strategies, such as parameterization specific to site–years or sites comparatively better predicted the annual average of GPP fluxes and year-specific parameters explained some parts of the IAV of GPP flux. At hourly and daily scales, we found slightly better model performance in the case of site–year parameterization compared to site-specific parameterization. This can mainly be due to variations in hydrological conditions, such as drought or excess rainfall

between years in a site and site–year–specific parameters may be able to better capture these events. However, in the annual scale model performance was similar between site–year and site-specific parameterization, even though we assumed parametrizing models using data from each site–year would be advantageous to capture IAV of GPP. Changes in parameters between years could reflect structural model issues, such as changes in state variables not represented correctly in the model (e.g., soil moisture) or absent in the model, but with a possible role on IAV (e.g., reserve or enzymatic pools, other biogeochemical cycles, such as nitrogen, or biotic factors promoting, e.g. herbivory). Changes in parameters could also reflect observation artifacts, such as biases, or changes in instrumentation. We would argue that the difference from site to site–year would reflect possible enhancements in performance via improvements in model structure, or via statistically learning temporal dynamics of parameters, which would add an inference component from the influence of environmental forcing on the responses from missing processes. Moreover, as the fast rate of change in climatic characteristics has become more frequent in recent years, developing a generalized model structure to simulate carbon fluxes between years and/or between sites of similar vegetation types has become even more challenging (Knauer et al., 2023).

The generalized model parameterization strategy, that is, global parameterization was also dominated by PFTs, such as ENF and GRA which were represented by many sites, and certain PFTs, such as DNF was represented by only one site in the FLUXNET2015 data set (Pastorello et al., 2020). This may imply that global parameterization or parameter up-scaling experiments using the FLUXNET2015 data set (Pastorello et al., 2020) may result in biased parameter sets that cannot be generalized to the global scale or a weighted site representation may be necessary in this case. Besides model parameterization, a recent study by Zou et al. (2024) highlighted that the importance of each independent driver, and their relative contributions vary over time and ecosystem type. The relative importance of forcing variables may also be another factor besides model parameterization. We also found both the P^{W}_{hr} model and the Bao_{hr} model showed the highest model performance at the sub-daily scale mostly for forest sites compared to savannas or grasslands, this in turn led to the poor simulation of IAV at many sites which are not forests. In most cases, we found that parameterization strategy played an important role in the variability of model performance across PFTs. For most PFTs, model performance between per–site–year and global parameterization were statistically different. However, there was no significant difference between model performance across PFTs between P^{W}_{hr} model and Bao_{hr} model.

Though we have demonstrated the capability of the P^{W}_{hr} model that included drought stress and the Bao_{hr} model to simulate the hourly fluxes of GPP, accurate estimation of IAV of GPP fluxes at the site level with these models requires further developments. Particularly, both models failed to capture the peak GPP in diurnal cycles at many sites even after model parameterization at a sub-daily scale and using an additional constraint on the IAV of GPP in the cost function. These underestimations at an hourly scale may have accumulated to a larger error when the fluxes were aggregated at an annual scale to study the IAV. We also showed that comparatively better model performances were achieved when the GPP peaks per site–year were better simulated. These results are similar to another study by Lin et al. (2023), directed at evaluating terrestrial ecosystem models' capability in explaining the IAV of GPP which also found an underestimation of GPP. Though the occurrences of peak GPP in a diurnal cycle can be comparatively smaller, an earlier study by Zscheischler et al. (2016) found that high GPP values during ideal weather conditions majorly contributed to the IAV of GPP flux. While the study of Zscheischler et al. (2016) was performed for temperate forests, we found a similar pattern for sites representing diverse climate–vegetation types in our study. Paschalis et al. (2015) also found that short-term variability of meteorological forcing can affect carbon and water fluxes from hourly to annual or even at longer scales, especially if they affect soil water availability and similar slow processes. Another study by Fatichi and Ivanov (2014) which involved synthetic data analysis also concluded that random occurrences of favorable weather conditions and subsequent higher carbon assimilation explain IAV of aboveground NPP better than average weather conditions of a year or growing season. Unlike some of the previous studies mentioned above which were mainly focused on finding correlations between GPP peaks and annual GPP from either only observed data or synthetic data, here, we found a direct correlation between model performance in simulating GPP peaks and model performance in simulating IAV of GPP. It is also true that some of the peak values found in EC-derived diurnal GPP can also be outliers, which are artifacts of data processing algorithms such as the gap-filling algorithm. It can be hard to distinguish these outliers from the true peaks of GPP. However, the bias introduced by the gap-filling algorithm is relatively low (Moffat et al., 2007). Therefore, it is unlikely that the reasoning behind the general underestimation of GPP peaks by models is due to the bias introduced during gap-filling.

The poor representation of IAV of GPP can be attributed to either limitations of models or model parameterization strategies. It is important to discover which seasonal phases of the GPP dynamics for particular vegetation types or climatic zones are not well represented in models simulating the IAV of GPP. In our study, we accounted for biophysical forcings, such as meteorological variables in our models, and used fAPAR to represent phenological dynamics. However, if there is a decoupling between the phenological and GPP dynamics, the length since GPP onset and senescence can be another factor behind IAV, especially during climate extremes, or large meteorological time shifts. Previous studies such as Wolf, et al. (2016) showed that the net effect of climate extremes, that is, the 2012 summer drought on carbon uptake was compensated by warmer springs, and increased soil moisture consumption during warmer springs led to the drought conditions in summer. Similar findings were also reported by van der Woude et al. (2023) for European forests where the effect of the 2018 drought was offset by prolonged carbon uptake during warm autumn. Bastos et al. (2020) and Smith et al. (2020) reported a similar finding that the increased vegetation growth during warm spring was responsible for soil moisture depletion and inflation of the 2018 drought effect in Europe. It is particularly important to focus on the meteorological sensitivity of GPP during periods of high productivity where improvements in the prediction of high fluxes would tend to improve the description of IAV. Another aspect could also be to decompose the metric (Gupta et al., 2009) used in the cost function or develop a more detailed model evaluation to understand which other parts of the time series were not well constrained during model parameterization.

5. Conclusions

We have demonstrated the capability of an improved version of an optimality-based model (P_{hr}^{W} model) and a semi-empirical LUE model (Bao_{hr} and Bao_{dd} models) to simulate sub-daily or daily GPP fluxes across 198 EC sites, representing 13 different vegetation types including forests, grasslands, savannas, croplands, and tundra. We also performed various model parameterization strategies to systematically evaluate the factors affecting the IAV of GPP. The main conclusions from our study are:

1. We found that the semi-empirical model mostly produced better results at hourly, daily, and monthly scales compared to the optimality-based model. At an annual scale, the improvement in the performance of the semi-empirical model was not significant even though more parameters were parameterized to flexibly capture the ecosystem dynamics. Both optimality-based and semi-empirical models performed better on hourly, daily, weekly, and monthly scales compared to annual scale.
2. Model structure was an important factor behind variability in both hourly and annual model performances when drought stress was not explicitly accounted for in the optimality-based model. However, differences in climate classes and parameterization strategies became important factors behind variability in hourly and annual model performances, respectively, when the previous version of the optimality-based model (without drought stress) was not considered in the analysis.
3. Explicit accounting of drought stress in the optimality-based ecosystem model is a necessity as it proved to be an important factor in controlling GPP fluxes at all temporal scales including at annual aggregation. The explicit representation of drought stress not only improved the performance of the optimality-based model at arid sites but also at energy–limited sites.
4. Both models performed better mostly at forest sites compared to grasslands or savannas which may also lead to poor estimation of IAV of GPP at many sites globally.
5. While these models generally performed well in simulating hourly GPP dynamics, the small errors at the sub-daily scale, particularly related to the estimation of GPP peaks, accumulated to bigger errors at the annual scale and led to poor performance of models in explaining the IAV of GPP. We found that comparatively better annual model performance could be achieved when the peaks of GPP were better simulated.

Our results further suggest the need to focus on sub-daily GPP dynamics during the various seasonal phases, especially highly productive ones, toward an improved constraint on GPP sensitivities. Hence, better annual model performance with a detailed parameterization strategy, such as site–year parameterization, signifies that temporally varying model parameters are necessary to better capture the variations of annual average GPP and indicate that ecosystem functioning is not stable between years. These new understandings can guide us toward developing models and parameterization strategies for simulating the inter–annual variations in ecosystem GPP more successfully, and improve our understanding of the global carbon cycle response to changing climatic conditions.

Appendix A: Data Description

Table A1
Description of Forcing and Model Parameterization Data

Abbreviation	Definition	Unit	Variable name in data set/remarks	Reference
GPP_{EC}[a]	GPP derived from EC based net ecosystem exchange (NEE) using night-time partitioning* method. Used for model calibration and evaluation.	$\mu molCO_2 \cdot m^{-2} \cdot s^{-1}$	GPP_NT_VUT_USTAR50	Pastorello et al. (2020); Reichstein et al. (2005)
GPP_NT_VUT_05	GPP derived from percentile 5 of 40 different estimates of NEE using night-time partitioning method. Used to quantify uncertainty in GPP_{EC}.	$\mu molCO_2 \cdot m^{-2} \cdot s^{-1}$	GPP_NT_VUT_05	Pastorello et al. (2020); Reichstein et al. (2005)
GPP_NT_VUT_95	GPP derived from percentile 95 of 40 different estimates of NEE using night-time partitioning method. Used to quantify uncertainty in GPP_{EC}.	$\mu molCO_2 \cdot m^{-2} \cdot s^{-1}$	GPP_NT_VUT_95	Pastorello et al. (2020); Reichstein et al. (2005)
GPP_DT_VUT_05	GPP derived from percentile 5 of 40 different estimates of NEE using daytime partitioning method. Used to quantify uncertainty in GPP_{EC}.	$\mu molCO_2 \cdot m^{-2} \cdot s^{-1}$	GPP_DT_VUT_05	Pastorello et al. (2020); Lasslop et al. (2010)
GPP_DT_VUT_95	GPP derived from percentile 95 of 40 different estimates of NEE using daytime partitioning method. Used to quantify uncertainty in GPP_{EC}.	$\mu molCO_2 \cdot m^{-2} \cdot s^{-1}$	GPP_DT_VUT_95	Pastorello et al. (2020); Lasslop et al. (2010)
σ_{NEE}	Random uncertainty for NEE	$\mu molCO_2 \cdot m^{-2} \cdot s^{-1}$	NEE_VUT_USTAR50_RANDUNC	Pastorello et al. (2020)
LE	Latent heat flux	$W \cdot m^{-2}$	LE_F_MDS	Pastorello et al. (2020)
σ_{LE}	Random uncertainty for latent heat flux	$W \cdot m^{-2}$	LE_RANDUNC	Pastorello et al. (2020)
SW_IN[b]	Incoming shortwave radiation	$W \cdot m^{-2}$	SW_IN_F	Pastorello et al. (2020)
$NETRAD$[b, c]	Net radiation	$W \cdot m^{-2}$	NETRAD	Pastorello et al. (2020)
SW_IN_POT	Potential incoming shortwave radiation	$W \cdot m^{-2}$	SW_IN_POT	Pastorello et al. (2020)
$PPFD\_IN$[a]	Incoming photosynthetic photon flux density	$\mu mol\ photons \cdot m^{-2} \cdot s^{-1}$	*PPFD_IN* gap-filled with 2.04 × *SW_IN*	Pastorello et al. (2020); see Section 3.4.2 of Stocker et al. (2020) for the gap-filling equation
T[b]	Air temperature	°C	TA_F_MDS	Pastorello et al. (2020)
VPD[b]	Vapor pressure deficit	Pa	VPD_F_MDS	Pastorello et al. (2020)
P[b,d]	Precipitation	$mm \cdot h^{-1}$ or $mm \cdot d^{-1}$	P	Pastorello et al. (2020)
CO_2	Atmospheric CO_2 concentration dry air mole fractions from quasi-continuous measurements at Mauna Loa	ppm	CO_2_mlo_surface-insitu_1_ccgg_DailyData (interpolated linearly to hourly scale). The measurements from Mauna Loa were used for all sites as the CO_2 concentration measurements at EC sites are often noisy and discontinuous.	Thoning et al. (2021)
$elev$	Site elevation	m a.s.l.	Collected from literature	Bao, Wutzler, et al. (2022)
ET_{LE}[a]	Evapotranspiration derived from *LE* flux	$mm \cdot h^{-1}$ or $mm \cdot d^{-1}$	Calculated from *LE* with a dependency on *T*	Henderson-Sellers (1984)

Table A1
Continued

Abbreviation	Definition	Unit	Variable name in data set/remarks	Reference
σ_{ET}	Random uncertainty for *ET_LE*	$mm \cdot h^{-1}$ or $mm \cdot d^{-1}$	Calculated from *LE_RANDUNC* with a dependency on *T*	Henderson-Sellers (1984)
PET	Potential evapotranspiration	$mm \cdot h^{-1}$ or $mm \cdot d^{-1}$	Calculated from *T*, *NETRAD* and *elev* using the method of Priestley and Taylor	Priestley and Taylor (1972)
CI	Cloudiness index	–	Calculated as $1 - \left(\frac{SW\_IN}{SW\_IN\_POT}\right)$	Bao, Wutzler, et al. (2022); Fu and Rich (1999); Turner et al. (2006)
WAI	Water availability indicator	mm	Described in Text S1 of Supporting Information S1	Bao, Wutzler, et al. (2022); Tramontana et al. (2016); Trautmann et al. (2018)
W	Soil water supply	$mm \cdot mm^{-1}$	Calculated as $\frac{WAI}{AWC}$ (*AWC* is defined in Table 1)	Bao, Wutzler, et al. (2022)
NDVI	Normalized difference vegetation index	–	Daily *NDVI* from FluxnetEO v2 (MODIS) was linearly interpolated to hourly	Walther et al. (2022, 2023)
fAPAR	Fraction of incident photosynthetic photon flux that is absorbed by vegetation	–	Linear relationship between *NDVI* and *fAPAR* was assumed. $\begin{cases} NDVI, & \text{if } NDVI > 0 \\ 0, & \text{if } NDVI \le 0 \end{cases}$	Bao, Wutzler, et al. (2022); Myneni et al. (1997)
QC[a]	Data quality flags	–	1.0 (good quality), 0.5 (medium quality), and 0.0 (bad quality) in the case of hourly data, which is the fraction of good quality measured or gap-filled data from two half-hours. In the case of daily, *QC* can have any values between 0.0 and 1.0, which is a fraction representing the percentage of good quality measured or gap-filled data in a day. The daily data with $QC > 0.8$ was considered good.	Pastorello et al. (2020); Nelson et al. (2024)

Note. *We preferred the night-time partitioning (Reichstein et al., 2005) over daytime partitioning (Lasslop et al., 2010) as only respiration is modeled in this case and GPP is derived as the difference between measured NEE and respiration. Whereas, in the daytime partitioning method, GPP is modeled as well and can have prediction errors due to uncertain model parameters. [a]For GPP_{EC}, the QC flags of *NEE*, and for ET_{LE} the QC flags of *LE* were used, as they were derived from the respective variables. *QC* flags of *SW_IN* were used to determine bad and medium quality data of *PPFD_IN*, which were replaced with a gap-filling procedure. [b]Bad, medium quality (value of *QC* is 0 and 0.5) data and gaps were filled with downscaled (Besnard et al., 2019) ERA5 (Hersbach et al., 2023) or ERA-Interim v2.0 data (Berrisford et al., 2011). [c]We have collected good quality *SW_IN* and *NETRAD* values from all the sites and fitted a linear regression model using the RANdom SAmple Consensus (RANSAC) algorithm (Fischler & Bolles, 1981) to determine the relation between them. The fitted equation ($NETRAD = 0.7066 \times SW\_IN - 0.1345$) was used to fill gaps in *NETRAD* using *SW_IN*. The gap-filling with regression was only applied for a few sites at hourly scale. [d]At hourly scale, the data gaps or bad quality data in *P* were filled by distributing the daily downscaled *P* (Besnard et al., 2019) from ERA-Interim v2.0 (Berrisford et al., 2011) for a certain day to the hourly timesteps, based on hourly *P* from gridded ERA5 data (Hersbach et al., 2023).

Appendix B: Data Screening for Model Parameterization

We used only good–quality data to calibrate model parameters. At hourly scale, we selected GPP_{EC} and ET_{LE} as good quality data when the values of their respective QC flag were 1 (Table A1). At the daily scale, we considered a GPP_{EC} and ET_{LE} data point as good when the value of the QC flag was greater than 0.8. We also removed any data gaps from observed and simulated data, σ_{NEE}, and σ_{LE} (Table A1). There were certain negative values in our GPP_{EC} data, as it was calculated using night-time based partitioning method (Reichstein et al., 2005). In this case, if a negative GPP_{EC} value occurred, when the *SW_IN* (Table A1) is zero that is, during night hours, we replaced

those data points with 0 and used them in the cost function. If the negative GPP_{EC} occurred during day hours, we excluded them.

Appendix C: Data Screening for Evaluation of Model Performance

The good quality data at an hourly scale were selected using the same criteria described in Appendix B. The data screening at a daily scale was also similar to Appendix B, when the LUE model was parameterized using daily data. For all other cases, we assigned a flag (0 = not considered, 1 = considered) to identify which data points were considered during model parameterization. We aggregated this flag to daily, weekly, monthly, and annual scales by taking averages. Then this flag indicated the fraction of good quality data used to calculate a data point in a certain temporal resolution. We only used data points at certain temporal resolutions which were calculated using more than 50% (flag value > 0.5) good quality data points from hourly/daily resolution. We calculated monthly, and annual model performance metrics for a certain site if at least three data points were present. We couldn't calculate annual metrics for 76 and 85 sites due to low numbers of good quality site–years when the annual data was aggregated from hourly, and daily data, respectively. The monthly metrics were not calculated for the three sites due to the same reason when they were aggregated from daily data.

Appendix D: Median Values of Model Performance

The median values of the model performance metric, that is, NNSE which are plotted in Figure 2 are summarized in Table D1.

Table D1
Median NNSE Obtained at Each Modeling Experiment at Hourly/Daily Scale and Annual Aggregations

		Parameterization strategies				
Temporal scale/ aggregation	Models	Per site–year	Per site using $Cost^{IAV}$	Per site	Per PFT	Global
Hourly/ daily scale	P^{W}_{hr}	0.827	0.799	0.805	0.738	0.712
	P_{hr}	0.478	0.470	0.469	0.461	0.490
	Bao_{hr}	0.855	0.837	0.838	0.758	0.730
	Bao_{dd}	0.837	0.796	0.796	0.686	0.642
Annual aggregation	P^{W}_{hr}	0.543	0.405	0.373	0.201	0.143
	P_{hr}	0.018	0.019	0.018	0.018	0.019
	Bao_{hr}	0.628	0.460	0.460	0.187	0.189
	Bao_{dd}	0.704	0.449	0.475	0.233	0.151

Appendix E: Mean Values of Fraction of Site–Years per Site for Which Simulated GPP Was Within Uncertainty Range

The mean values of fractions of site–years per site for which the annual average of GPP_{sim} was within the uncertainty range of GPP_{EC} are plotted in Figure 3 and are summarized in Table E1.

Table E1
Mean Values of Fractions of Site–Years per Site for Which Annual Average of Simulated Gross Primary Production (GPP_{sim}) Was Within the Uncertainty Range of Eddy-Covariance Derived GPP (GPP_{EC})

	Parameterization strategies				
Models	Per site–year	Per site using $Cost^{IAV}$	Per site	Per PFT	Global
P^{W}_{hr}	0.869	0.757	0.773	0.481	0.409
P_{hr}	0.123	0.128	0.131	0.129	0.131
Bao_{hr}	0.931	0.831	0.840	0.531	0.430
Bao_{dd}	0.942	0.835	0.838	0.507	0.389

Acknowledgments
We would like to express our gratitude to the FLUXNET community, including regional networks: AmeriFlux, AfriFlux, AsiaFlux, CarboAfrica, CarboEuropeIP, CarboItaly, CarboMont, ChinaFlux, FluxnetCanada, GreenGrass, ICOS, KoFlux, LBA, NECC, OzFlux-TERN, TCOSSiberia, and USCCC for their contributions in developing the eddy covariance based FLUXNET2015 data set, which was invaluable to our study. We also thank all the site investigators for generously sharing their data with the respective networks. The FLUXNET eddy covariance data processing and harmonization was carried out by the ICOS Ecosystem Thematic Center, AmeriFlux Management Project, and Fluxdata project of FLUXNET, with the support of CDIAC, and the OzFlux, ChinaFlux and AsiaFlux offices. We acknowledge suggestions received from Jacob Nelson regarding the FLUXNET2015 data set, suggestions received from Sophia Walther regarding the FluxnetEO data set, assistance received from Ulrich Weber in some of the data processing steps, FLUXCOM team for preparing hourly aggregates of FLUXNET2015 data set, assistance received from Giulia Mengoli with P-model codes, assistance received from Nikolaus Hansen regarding the usage of pycma, and members of the Model–Data Integration group at Max Planck Institute for Biogeochemistry for sharing constructive feedback. We thank Olaf Kolle, J. Rose Cleverly, and Shirley Papuga for providing clarifications and further information on site characteristics. We thank Donatella Zona, J. Rose Cleverly, Pasi Kolari, Julia Boike, Iris Feigenwinter, Donatella Spano, Javier Houspanossian, and Wang Yi for providing feedback on an earlier version of the manuscript. RD acknowledges the funding from the International Max Planck Research School for Global Biogeochemical Cycles (IMPRS-gBGC) for carrying out his doctoral research. TT considers this a contribution to the Swedish National Space Agency projects (SNSA Dnr, 2021-00144; 2021-00111) and also acknowledges funding from FORMAS (Dnr 2021-00644; 2023–02436). LŠ acknowledges support from the Ministry of Education, Youth and Sports of the Czech Republic within the CzeCOS program (Grant LM2023048) and the AdAgriF project (CZ.02.01.01/00/22_008/0004635). LH acknowledges funding from the SNF funded projects ICOS-CH Phase 1, 2, and 3 (20FI21_148992, 20FI20_173691, and 20F120_198227). SS acknowledges Horizon Europe funding (Open-Earth-Monitor Cyberinfrastructure project, 101059548). M. Roland and BG acknowledge the support of the Research Foundation Flanders (FWO) for the support to ICOS Research Infrastructure. LM acknowledges the funding from the Forest Services, Autonomous Province of

Data Availability Statement

The codes that were used to perform all the necessary analyses and plot all the figures in this study are available at https://doi.org/10.5281/zenodo.13729514 (De, 2025). The data from eddy covariance sites are available through FLUXNET at https://fluxnet.org/data/fluxnet2015-dataset/, and the Digital Object Identifier (DOI) of the data set for each site are listed in the Table S8 of Supporting Information S1 (Pastorello et al., 2020; FLUXNET.org, 2024a). The FluxnetEO MODIS version 2 data set is available at https://doi.org/10.18160/0KWD-3RRW (Walther et al., 2022, 2023). The ERA5 data set is available at https://doi.org/10.24381/cds.adbb2d47 Hersbach et al. (2023). The ERA-Interim v2.0 data set has been currently archived by ECMWF; however, it can be accessed following these instructions (Berrisford et al., 2011). Atmospheric CO_2 measurements at Mauna Loa observatory are available at https://doi.org/10.15138/yaf1-bk21 (Thoning et al., 2021).

References

Amos, B., Arkebauer, T. J., & Doran, J. W. (2005). Soil surface fluxes of greenhouse gases in an irrigated maize-based agroecosystem. *Soil Science Society of America Journal*, *69*(2), 387–395. https://doi.org/10.2136/sssaj2005.0387

Anav, A., Friedlingstein, P., Beer, C., Ciais, P., Harper, A., Jones, C., et al. (2015). Spatiotemporal patterns of terrestrial gross primary production: A review. *Reviews of Geophysics*, *53*(3), 785–818. https://doi.org/10.1002/2015RG000483

Anderegg, W. R. L., Schwalm, C., Biondi, F., Camarero, J. J., Koch, G., Litvak, M., et al. (2015). Pervasive drought legacies in forest ecosystems and their implications for carbon cycle models. *Science*, *349*(6247), 528–532. https://doi.org/10.1126/science.aab1833

Assal, T. J., Anderson, P. J., & Sibold, J. (2016). Spatial and temporal trends of drought effects in a heterogeneous semi-arid forest ecosystem. *Forest Ecology and Management*, *365*, 137–151. https://doi.org/10.1016/j.foreco.2016.01.017

Aubinet, M. (2008). Eddy covariance CO_2 flux measurements in nocturnal conditions: An analysis of the problem. *Ecological Applications*, *18*(6), 1368–1378. https://doi.org/10.1890/06-1336.1

Aubinet, M., Feigenwinter, C., Heinesch, B., Bernhofer, C., Canepa, E., Lindroth, A., et al. (2010). Direct advection measurements do not help to solve the night-time CO_2 closure problem: Evidence from three different forests. *Agricultural and Forest Meteorology*, *150*(5), 655–664. https://doi.org/10.1016/j.agrformet.2010.01.016

Baldocchi, D., Chu, H., & Reichstein, M. (2018). Inter-annual variability of net and gross ecosystem carbon fluxes: A review. *Agricultural and Forest Meteorology*, *249*, 520–533. https://doi.org/10.1016/j.agrformet.2017.05.015

Baldocchi, D., Finnigan, J., Wilson, K., Paw U, K., & Falge, E. (2000). On measuring net ecosystem carbon exchange over tall vegetation on complex terrain. *Boundary-Layer Meteorology*, *96*(1–2), 257–291. https://doi.org/10.1023/A:1002497616547

Baldocchi, D. D. (2003). Assessing the eddy covariance technique for evaluating carbon dioxide exchange rates of ecosystems: Past, present and future. *Global Change Biology*, *9*(4), 479–492. https://doi.org/10.1046/j.1365-2486.2003.00629.x

Bao, S., Alonso, L., Wang, S., Gensheimer, J., De, R., & Carvalhais, N. (2023). Toward robust parameterizations in ecosystem-level photosynthesis models. *Journal of Advances in Modeling Earth Systems*, *15*(8), e2022MS003464. https://doi.org/10.1029/2022MS003464

Bao, S., Ibrom, A., Wohlfahrt, G., Koirala, S., Migliavacca, M., Zhang, Q., & Carvalhais, N. (2022). Narrow but robust advantages in two-big-leaf light use efficiency models over big-leaf light use efficiency models at ecosystem level. *Agricultural and Forest Meteorology*, *326*, 109185. https://doi.org/10.1016/j.agrformet.2022.109185

Bao, S., Wutzler, T., Koirala, S., Cuntz, M., Ibrom, A., Besnard, S., et al. (2022). Environment-sensitivity functions for gross primary productivity in light use efficiency models. *Agricultural and Forest Meteorology*, *312*, 108708. https://doi.org/10.1016/j.agrformet.2021.108708

Bastos, A., Ciais, P., Friedlingstein, P., Sitch, S., Pongratz, J., Fan, L., et al. (2020). Direct and seasonal legacy effects of the 2018 heat wave and drought on European ecosystem productivity. *Science Advances*, *6*(24). https://doi.org/10.1126/sciadv.aba2724

Beck, H. E., Zimmermann, N. E., McVicar, T. R., Vergopolan, N., Berg, A., & Wood, E. F. (2018). Present and future Köppen-Geiger climate classification maps at 1-km resolution. *Scientific Data*, *5*(1), 180214. https://doi.org/10.1038/sdata.2018.214

Berrisford, P., Dee, D., Poli, P., Brugge, R., Fielding, M., Fuentes, M., et al. (2011). *The ERA-Interim archive version 2.0 (Computer Software Manual No. 1)*. ECMWF. https://www.ecmwf.int/en/elibrary/73682-era-interim-archive-version-20

Besnard, S., Carvalhais, N., Arain, M. A., Black, A., Brede, B., Buchmann, N., et al. (2019). Memory effects of climate and vegetation affecting net ecosystem CO_2 fluxes in global forests. *PLOS ONE*, *14*(2), e0211510. https://doi.org/10.1371/journal.pone.0211510

BioRender. De, R. (2024). Retrieved from https://BioRender.com/i01x768

Boese, S., Jung, M., Carvalhais, N., Teuling, A. J., & Reichstein, M. (2019). Carbon–water flux coupling under progressive drought. *Biogeosciences*, *16*(13), 2557–2572. https://doi.org/10.5194/bg-16-2557-2019

Boike, J., Juszak, I., Lange, S., Chadburn, S., Burke, E., Overduin, P. P., et al. (2018). A 20-year record (1998–2017) of permafrost, active layer and meteorological conditions at a high arctic permafrost research site (Bayelva, Spitsbergen). *Earth System Science Data*, *10*(1), 355–390. https://doi.org/10.5194/essd-10-355-2018

Bultan, S., Nabel, J. E., Hartung, K., Ganzenmüller, R., Xu, L., Saatchi, S., & Pongratz, J. (2022). Tracking 21st century anthropogenic and natural carbon fluxes through model-data integration. *Nature Communications*, *13*(1), 5516. https://doi.org/10.1038/s41467-022-32456-0

Burnham, K. P., & Anderson, D. R. (2004). Multimodel inference: Understanding AIC and BIC in model selection. *Sociological methods & research*, *33*(2), 261–304. https://doi.org/10.1177/0049124104268644

Burton, C. A., Renzullo, L. J., Rifai, S. W., & Van Dijk, A. I. J. M. (2023). Empirical upscaling of OzFlux eddy covariance for high-resolution monitoring of terrestrial carbon uptake in Australia. *Biogeosciences*, *20*(19), 4109–4134. https://doi.org/10.5194/bg-20-4109-2023

Chai, T., & Draxler, R. R. (2014). Root mean square error (RMSE) or mean absolute error (MAE)? – Arguments against avoiding RMSE in the literature. *Geoscientific Model Development*, *7*(3), 1247–1250. https://doi.org/10.5194/gmd-7-1247-2014

Chen, J. (2021). *Biophysical models and applications in ecosystem analysis*. Michigan State University Press. Retrieved from https://muse.jhu.edu/book/82816

Chen, J.-L., Reynolds, J. F., Harley, P. C., & Tenhunen, J. D. (1993). Coordination theory of leaf nitrogen distribution in a canopy. *Oecologia*, *93*(1), 63–69. https://doi.org/10.1007/BF00321192

Chu, H., Luo, X., Ouyang, Z., Chan, W. S., Dengel, S., Biraud, S. C., et al. (2021). Representativeness of eddy-covariance flux footprints for areas surrounding ameriflux sites. *Agricultural and Forest Meteorology*, *301–302*, 108350. https://doi.org/10.1016/j.agrformet.2021.108350

Bozen. GW acknowledges financial support from the Autonomous Province of Bozen via the CarboST project. Large language models (LLM), that is, ChatGPT (version GPT-4-1106-vision-preview API) and GitHub Copilot (v1.172.0) were used to generate certain code snippets to perform some of the analyses in this study, and to generate code documentation, followed by careful evaluations by authors. However, no texts in this research paper were written with the aid of LLM. We thank the three anonymous reviewers, and handling editor, Natasha MacBean for their constructive feedback that contributed to the improvement of this research article. Open Access funding enabled and organized by DEAL Konsortium.

Ciais, P., Reichstein, M., Viovy, N., Granier, A., Ogée, J., Allard, V., et al. (2005). Europe-wide reduction in primary productivity caused by the heat and drought in 2003. *Nature*, *437*(7058), 529–533. https://doi.org/10.1038/nature03972

Cleverly, J., Boulain, N., Villalobos-Vega, R., Grant, N., Faux, R., Wood, C., et al. (2013). Dynamics of component carbon fluxes in a semi-arid Acacia woodland, central Australia. *Journal of Geophysical Research: Biogeosciences*, *118*(3), 1168–1185. https://doi.org/10.1002/jgrg.20101

Dannenberg, M. P., Barnes, M. L., Smith, W. K., Johnston, M. R., Meerdink, S. K., Wang, X., et al. (2023). Upscaling dryland carbon and water fluxes with artificial neural networks of optical, thermal, and microwave satellite remote sensing. *Biogeosciences*, *20*(2), 383–404. https://doi.org/10.5194/bg-20-383-2023

De, R. (2025). Scripts for analyses presented in "Addressing challenges in simulating inter–annual variability of gross primary production" (v1.3-published). *Zenodo*. https://doi.org/10.5281/zenodo.13729514

De, R., Brenning, A., Reichstein, M., Šigut, L., Ruiz Reverter, B., Korkiakoski, M., et al. (2025). Inter–annual variability of hydrological parameters improves simulation of annual gross primary production. *ESS Open Archive*. https://doi.org/10.22541/essoar.174349993.30198378/v1

Desai, A. R. (2010). Climatic and phenological controls on coherent regional interannual variability of carbon dioxide flux in a heterogeneous landscape. *Journal of Geophysical Research: Biogeosciences*, *115*(G3). https://doi.org/10.1029/2010JG001423

Desai, A. R., Richardson, A. D., Moffat, A. M., Kattge, J., Hollinger, D. Y., Barr, A., et al. (2008). Cross-site evaluation of eddy covariance GPP and RE decomposition techniques. *Agricultural and Forest Meteorology*, *148*(6), 821–838. https://doi.org/10.1016/j.agrformet.2007.11.012

Farquhar, G. D., von Caemmerer, S. V., & Berry, J. A. (1980). A biochemical model of photosynthetic CO_2 assimilation in leaves of C3 species. *planta*, *149*(1), 78–90. https://doi.org/10.1007/BF00386231

Fatichi, S., & Ivanov, V. Y. (2014). Interannual variability of evapotranspiration and vegetation productivity. *Water Resources Research*, *50*(4), 3275–3294. https://doi.org/10.1002/2013WR015044

Fischler, M. A., & Bolles, R. C. (1981). Random sample consensus: A paradigm for model fitting with applications to image analysis and automated cartography. *Communication ACM*, *24*(6), 381–395. https://doi.org/10.1145/358669.358692

FLUXNET.org. (2024a). FLUXNET2015 dataset. Retrieved from https://fluxnet.org/data/fluxnet2015-dataset/

FLUXNET.org. (2024b). IGBP classification. Retrieved from https://fluxnet.org/data/badm-data-templates/igbp-classification/

FLUXNET.org. (2024c). Köppen climate classification. Retrieved from https://fluxnet.org/data/badm-data-templates/koppen-climate-classification/

Foken, T. (2008). The energy balance closure problem: An overview. *Ecological Applications*, *18*(6), 1351–1367. https://doi.org/10.1890/06-0922.1

Foken, T., Aubinet, M., & Leuning, R. (2011). The eddy covariance method. In *Eddy covariance* (pp. 1–19). Springer. https://doi.org/10.1007/978-94-007-2351-1_1

Fu, P., & Rich, P. M. (1999). Design and implementation of the solar analyst: An ArcView extension for modeling solar radiation at landscape scales. In *Proceedings of the nineteenth annual ESRI user conference* (Vol. 1, pp. 1–31). https://proceedings.esri.com/library/userconf/proc99/proceed/papers/pap867/p867.htm

Groenendijk, M., Dolman, A., van der Molen, M., Leuning, R., Arneth, A., Delpierre, N., et al. (2011). Assessing parameter variability in a photosynthesis model within and between plant functional types using global fluxnet eddy covariance data. *Agricultural and Forest Meteorology*, *151*(1), 22–38. https://doi.org/10.1016/j.agrformet.2010.08.013

Gupta, H. V., Kling, H., Yilmaz, K. K., & Martinez, G. F. (2009). Decomposition of the mean squared error and NSE performance criteria: Implications for improving hydrological modelling. *Journal of Hydrology*, *377*(1), 80–91. https://doi.org/10.1016/j.jhydrol.2009.08.003

Hansen, N., Akimoto, Y., & Baudis, P. (2019). CMA-ES/pycma on Github. *Zenodo*. https://doi.org/10.5281/zenodo.2559634

Hansen, N., & Kern, S. (2004). Evaluating the CMA Evolution strategy on multimodal test functions. In X. Yao, E. K. Burke, J. A. Lozano, J. Smith, J. J. Merelo-Guervós, J. A. Bullinaria, et al. (Eds.), *Parallel problem solving from nature - PPSN VIII* (pp. 282–291). Springer. https://doi.org/10.1007/978-3-540-30217-9_29

Henderson-Sellers, B. (1984). A new formula for latent heat of vaporization of water as a function of temperature. *Quarterly Journal of the Royal Meteorological Society*, *110*(466), 1186–1190. https://doi.org/10.1002/qj.49711046626

Hersbach, H., Bell, B., Berrisford, P., Biavati, G., Horányi, A., Muñoz Sabater, J., et al. (2023). ERA5 hourly data on single levels from 1940 to present. *Copernicus Climate Change Service (C3S) Climate Data Store (CDS)*. https://doi.org/10.24381/cds.adbb2d47

Hodges, J. L. (1958). The significance probability of the smirnov two-sample test. *Arkiv för Matematik*, *3*(5), 469–486. https://doi.org/10.1007/bf02589501

Hollinger, D. Y., & Richardson, A. D. (2005). Uncertainty in eddy covariance measurements and its application to physiological models. *Tree Physiology*, *25*(7), 873–885. https://doi.org/10.1093/treephys/25.7.873

Horn, J. E., & Schulz, K. (2011). Identification of a general light use efficiency model for gross primary production. *Biogeosciences*, *8*(4), 999–1021. https://doi.org/10.5194/bg-8-999-2011

Huang, X., Xiao, J., Wang, X., & Ma, M. (2021). Improving the global MODIS GPP model by optimizing parameters with FLUXNET data. *Agricultural and Forest Meteorology*, *300*, 108314. https://doi.org/10.1016/j.agrformet.2020.108314

Hundecha, Y., & Merz, B. (2012). Exploring the relationship between changes in climate and floods using a model-based analysis. *Water Resources Research*, *48*(4). https://doi.org/10.1029/2011WR010527

Jez, J. M., Topp, C. N., Siebers, M. H., Gomez-Casanovas, N., Fu, P., Meacham-Hensold, K., & Bernacchi, C. J. (2021). Emerging approaches to measure photosynthesis from the leaf to the ecosystem. *Emerging Topics in Life Sciences*, *5*(2), 261–274. https://doi.org/10.1042/ETLS20200292

Jocher, G., Marshall, J., Nilsson, M. B., Linder, S., De Simon, G., Hörnlund, T., et al. (2018). Impact of canopy decoupling and subcanopy advection on the annual carbon balance of a boreal Scots pine forest as derived from eddy covariance. *Journal of Geophysical Research: Biogeosciences*, *123*(2), 303–325. https://doi.org/10.1002/2017JG003988

Jung, M., Reichstein, M., Margolis, H. A., Cescatti, A., Richardson, A. D., Arain, M. A., et al. (2011). Global patterns of land-atmosphere fluxes of carbon dioxide, latent heat, and sensible heat derived from eddy covariance, satellite, and meteorological observations. *Journal of Geophysical Research: Biogeosciences*, *116*(G3), G00J07. https://doi.org/10.1029/2010JG001566

Jung, M., Schwalm, C., Migliavacca, M., Walther, S., Camps-Valls, G., Koirala, S., et al. (2020). Scaling carbon fluxes from eddy covariance sites to globe: Synthesis and evaluation of the fluxcom approach. *Biogeosciences*, *17*(5), 1343–1365. https://doi.org/10.5194/bg-17-1343-2020

Kannenberg, S. A., Novick, K. A., Alexander, M. R., Maxwell, J. T., Moore, D. J. P., Phillips, R. P., & Anderegg, W. R. L. (2019). Linking drought legacy effects across scales: From leaves to tree rings to ecosystems. *Global Change Biology*, *25*(9), 2978–2992. https://doi.org/10.1111/gcb.14710

Kaufmann, J., & Schering, A. (2014). Analysis of variance ANOVA. In *Wiley statsref: Statistics reference online*. John Wiley & Sons, Ltd. https://doi.org/10.1002/9781118445112.stat06938

Kirch, W. (2008). Pearson's correlation coefficient. In W. Kirch (Ed.), *Encyclopedia of public health* (pp. 1090–1091). Springer Netherlands. https://doi.org/10.1007/978-1-4020-5614-7_2569

Knauer, J., Cuntz, M., Smith, B., Canadell, J. G., Medlyn, B. E., Bennett, A. C., et al. (2023). Higher global gross primary productivity under future climate with more advanced representations of photosynthesis. *Science Advances*, *9*(46), eadh9444. https://doi.org/10.1126/sciadv.adh9444

Knohl, A., Schulze, E.-D., Kolle, O., & Buchmann, N. (2003). Large carbon uptake by an unmanaged 250-year-old deciduous forest in central Germany. *Agricultural and Forest Meteorology*, *118*(3), 151–167. https://doi.org/10.1016/S0168-1923(03)00115-1

Krause, P., Boyle, D. P., & Bäse, F. (2005). Comparison of different efficiency criteria for hydrological model assessment. *Advances in Geosciences*, *5*, 89–97. https://doi.org/10.5194/adgeo-5-89-2005

Lasslop, G., Reichstein, M., Papale, D., Richardson, A. D., Arneth, A., Barr, A., et al. (2010). Separation of net ecosystem exchange into assimilation and respiration using a light response curve approach: Critical issues and global evaluation. *Global Change Biology*, *16*(1), 187–208. https://doi.org/10.1111/j.1365-2486.2009.02041.x

Levene, H. (1960). *Contributions to probability and statistics: Essays in honor of Harold Hotelling*. In I. Olkin (Ed.), (pp. 278–292). Stanford University Press. https://doi.org/10.1137/1003016

Lin, S., Hu, Z., Wang, Y., Chen, X., He, B., Song, Z., et al. (2023). Underestimated interannual variability of terrestrial vegetation production by terrestrial ecosystem models. *Global Biogeochemical Cycles*, *37*(4), e2023GB007696. https://doi.org/10.1029/2023GB007696

Maire, V., Martre, P., Kattge, J., Gastal, F., Esser, G., Fontaine, S., & Soussana, J.-F. (2012). The coordination of leaf photosynthesis links C and N fluxes in C3 plant species. *PLOS ONE*, *7*(6), 1–15. https://doi.org/10.1371/journal.pone.0038345

Mäkelä, A., Pulkkinen, M., Kolari, P., Lagergren, F., Berbigier, P., Lindroth, A., et al. (2008). Developing an empirical model of stand GPP with the LUE approach: Analysis of eddy covariance data at five contrasting conifer sites in Europe. *Global Change Biology*, *14*(1), 92–108. https://doi.org/10.1111/j.1365-2486.2007.01463.x

Mauder, M., Foken, T., & Cuxart, J. (2020). Surface-energy-balance closure over land: A review. *Boundary-Layer Meteorology*, *177*(2–3), 395–426. https://doi.org/10.1007/s10546-020-00529-6

McGuire, A. D., Sitch, S., Clein, J. S., Dargaville, R., Esser, G., Foley, J., et al. (2001). Carbon balance of the terrestrial biosphere in the twentieth century: Analyses of CO_2, climate and land use effects with four process-based ecosystem models. *Global Biogeochemical Cycles*, *15*(1), 183–206. https://doi.org/10.1029/2000GB001298

Mengoli, G., Agustí-Panareda, A., Boussetta, S., Harrison, S. P., Trotta, C., & Prentice, I. C. (2022). Ecosystem photosynthesis in land-surface models: A first-principles approach incorporating acclimation. *Journal of Advances in Modeling Earth Systems*, *14*(1). https://doi.org/10.1029/2021MS002767

Mengoli, G., Harrison, S. P., & Prentice, I. C. (2023). A global function of climatic aridity accounts for soil moisture stress on carbon assimilation. *EGUsphere*, *2023*, 1–19. https://doi.org/10.5194/egusphere-2023-1261

Moffat, A. M., Papale, D., Reichstein, M., Hollinger, D. Y., Richardson, A. D., Barr, A. G., et al. (2007). Comprehensive comparison of gap-filling techniques for eddy covariance net carbon fluxes. *Agricultural and Forest Meteorology*, *147*(3–4), 209–232. https://doi.org/10.1016/j.agrformet.2007.08.011

Monteith, J. (1972). Solar radiation and productivity in tropical ecosystems. *Journal of Applied Ecology*, *9*(3), 747–766. https://doi.org/10.2307/2401901

Montgomery, R. B. (1948). Vertical eddy flux of heat in the atmosphere. *Journal of Atmospheric Sciences*, *5*(6), 265–274. https://doi.org/10.1175/1520-0469(1948)005<0265:VEFOHI>2.0.CO;2

Müller, L. M., & Bahn, M. (2022). Drought legacies and ecosystem responses to subsequent drought. *Global Change Biology*, *28*(17), 5086–5103. https://doi.org/10.1111/gcb.16270

Myneni, R. B., Ramakrishna, R., Nemani, R., & Running, S. W. (1997). Estimation of global leaf area index and absorbed PAR using radiative transfer models. *IEEE Transactions on Geoscience and Remote Sensing*, *35*(6), 1380–1393. https://doi.org/10.1109/36.649788

Nash, J., & Sutcliffe, J. (1970). River flow forecasting through conceptual models part I — A discussion of principles. *Journal of Hydrology*, *10*(3), 282–290. https://doi.org/10.1016/0022-1694(70)90255-6

Nelson, J. A., Walther, S., Gans, F., Kraft, B., Weber, U., Novick, K., et al. (2024). X-BASE: The first terrestrial carbon and water flux products from an extended data-driven scaling framework, FLUXCOM-X. *Biogeosciences*, *21*(22), 5079–5115. https://doi.org/10.5194/bg-21-5079-2024

Orth, R., Destouni, G., Jung, M., & Reichstein, M. (2020). Large-scale biospheric drought response intensifies linearly with drought duration in arid regions. *Biogeosciences*, *17*(9), 2647–2656. https://doi.org/10.5194/bg-17-2647-2020

Papale, D., Black, T. A., Carvalhais, N., Cescatti, A., Chen, J., Jung, M., et al. (2015). Effect of spatial sampling from European flux towers for estimating carbon and water fluxes with artificial neural networks. *Journal of Geophysical Research: Biogeosciences*, *120*(10), 1941–1957. https://doi.org/10.1002/2015JG002997

Papale, D., Reichstein, M., Aubinet, M., Canfora, E., Bernhofer, C., Kutsch, W., et al. (2006). Towards a standardized processing of net ecosystem exchange measured with eddy covariance technique: Algorithms and uncertainty estimation. *Biogeosciences*, *3*(4), 571–583. https://doi.org/10.5194/bg-3-571-2006

Paschalis, A., Fatichi, S., Katul, G. G., & Ivanov, V. Y. (2015). Cross-scale impact of climate temporal variability on ecosystem water and carbon fluxes. *Journal of Geophysical Research: Biogeosciences*, *120*(9), 1716–1740. https://doi.org/10.1002/2015jg003002

Pastorello, G., Trotta, C., Canfora, E., Chu, H., Christianson, D., Cheah, Y.-W., et al. (2020). The FLUXNET2015 dataset and the ONEFlux processing pipeline for eddy covariance data. *Scientific Data*, *7*(1), 225. https://doi.org/10.1038/s41597-020-0534-3

Plummer, S. (2006). On validation of the MODIS gross primary production product. *IEEE Transactions on Geoscience and Remote Sensing*, *44*(7), 1936–1938. https://doi.org/10.1109/TGRS.2006.872521

Prentice, I. C., Dong, N., Gleason, S. M., Maire, V., & Wright, I. J. (2014). Balancing the costs of carbon gain and water transport: Testing a new theoretical framework for plant functional ecology. *Ecology Letters*, *17*(1), 82–91. https://doi.org/10.1111/ele.12211

Prentice, I. C., Liang, X., Medlyn, B. E., & Wang, Y.-P. (2015). Reliable, robust and realistic: The three R's of next-generation land-surface modelling. *Atmospheric Chemistry and Physics*, *15*(10), 5987–6005. https://doi.org/10.5194/acp-15-5987-2015

Priestley, C. H. B., & Taylor, R. J. (1972). On the assessment of surface heat flux and evaporation using large-scale parameters. *Monthly weather review*, *100*(2), 81–92. https://doi.org/10.1175/1520-0493(1972)100<0081:otaosh>2.3.co;2

Python Core Team. (2021). Python: A dynamic, open source programming language. *Computer Software Manual*. Retrieved from https://www.python.org/

Reichstein, M., Bahn, M., Ciais, P., Frank, D., Mahecha, M. D., Seneviratne, S. I., et al. (2013). Climate extremes and the carbon cycle. *Nature*, *500*(7462), 287–295. https://doi.org/10.1038/nature12350

Reichstein, M., Falge, E., Baldocchi, D., Papale, D., Aubinet, M., Berbigier, P., et al. (2005). On the separation of net ecosystem exchange into assimilation and ecosystem respiration: Review and improved algorithm. *Global Change Biology*, *11*(9), 1424–1439. https://doi.org/10.1111/j.1365-2486.2005.001002.x

Richardson, A. D., Hollinger, D. Y., Aber, J. D., Ollinger, S. V., & Braswell, B. H. (2007). Environmental variation is directly responsible for short- but not long-term variation in forest-atmosphere carbon exchange. *Global Change Biology*, *13*(4), 788–803. https://doi.org/10.1111/j.1365-2486.2007.01330.x

Rubel, F., Brugger, K., Haslinger, K., & Auer, I. (2017). The climate of the European Alps: Shift of very high resolution Köppen-Geiger climate zones 1800–2100. *Meteorologische Zeitschrift*, *26*(2), 115–125. https://doi.org/10.1127/metz/2016/0816

Ruehr, S., Keenan, T. F., Williams, C., Zhou, Y., Lu, X., Bastos, A., et al. (2023). Evidence and attribution of the enhanced land carbon sink. *Nature Reviews Earth & Environment*, *4*(8), 518–534. https://doi.org/10.1038/s43017-023-00456-3

Running, S. W., Thornton, P. E., Nemani, R., & Glassy, J. M. (2000). Global terrestrial gross and net primary productivity from the earth observing system. In O. E. Sala, R. B. Jackson, H. A. Mooney, & R. W. Howarth (Eds.), *Methods in ecosystem science* (pp. 44–57). Springer New York. https://doi.org/10.1007/978-1-4612-1224-9_4

Schaefer, K., Schwalm, C. R., Williams, C., Arain, M. A., Barr, A., Chen, J. M., et al. (2012). A model-data comparison of gross primary productivity: Results from the north american carbon program site synthesis. *Journal of Geophysical Research: Biogeosciences*, *117*(G3). https://doi.org/10.1029/2012JG001960

Schimel, D. (2001). Preface. In E.-D. Schulze, M. Heimann, S. Harrison, E. Holland, J. Lloyd, I. C. Prentice, et al. (Eds.), *Global biogeochemical cycles in the climate system* (pp. xvii–xxi). Academic Press. https://doi.org/10.1016/B978-012631260-7/50002-9

Seabold, S., & Perktold, J. (2010). Statsmodels: Econometric and statistical modeling with python. In *9th python in science conference*.

Seneviratne, S. I., Nicholls, N., Easterling, D., Goodess, C. M., Kanae, S., Kossin, J., et al. (2012). Changes in climate extremes and their impacts on the natural physical environment. In C. B. Field, V. Barros, T. F. Stocker, & Q. Dahe (Eds.), *Managing the risks of extreme events and disasters to advance climate change adaptation: Special report of the intergovernmental panel on climate change* (pp. 109–230). Cambridge University Press. Retrieved from https://www.cambridge.org/core/books/managing-the-risks-of-extreme-events-and-disasters-to-advance-climate-change-adaptation/changes-in-climate-extremes-and-their-impacts-on-the-natural-physical-environment/A4B05D458547ACA9017591A37860DDD3?utm_campaign=shareaholic&utm_medium=copy_link&utm_source=bookmark

Sims, D. A., Rahman, A. F., Cordova, V. D., Baldocchi, D. D., Flanagan, L. B., Goldstein, A. H., et al. (2005). Midday values of gross CO_2 flux and light use efficiency during satellite overpasses can be used to directly estimate eight-day mean flux. *Agricultural and Forest Meteorology*, *131*(1), 1–12. https://doi.org/10.1016/j.agrformet.2005.04.006

Sitch, S., Friedlingstein, P., Gruber, N., Jones, S. D., Murray-Tortarolo, G., Ahlström, A., et al. (2015). Recent trends and drivers of regional sources and sinks of carbon dioxide. *Biogeosciences*, *12*(3), 653–679. https://doi.org/10.5194/bg-12-653-2015

Skillman, J. B. (2008). Quantum yield variation across the three pathways of photosynthesis: Not yet out of the dark. *Journal of Experimental Botany*, *59*(7), 1647–1661. https://doi.org/10.1093/jxb/ern029

Smith, N. E., Kooijmans, L. M. J., Koren, G., van Schaik, E., van der Woude, A. M., Wanders, N., et al. (2020). Spring enhancement and summer reduction in carbon uptake during the 2018 drought in northwestern Europe. *Philosophical Transactions of the Royal Society B: Biological Sciences*, *375*(1810), 20190509. https://doi.org/10.1098/rstb.2019.0509

Stocker, B. D., Wang, H., Smith, N. G., Harrison, S. P., Keenan, T. F., Sandoval, D., et al. (2020). P-Model v1.0: An optimality-based light use efficiency model for simulating ecosystem gross primary production. *Geoscientific Model Development*, *13*(3), 1545–1581. https://doi.org/10.5194/gmd-13-1545-2020

Swinbank, W. C. (1951). The measurement of vertical transfer of heat and water vapor by eddies in the lower atmosphere. *Journal of Atmospheric Sciences*, *8*(3), 135–145. https://doi.org/10.1175/1520-0469(1951)008<0135:TMOVTO>2.0.CO;2

Tamrakar, R., Rayment, M. B., Moyano, F., Mund, M., & Knohl, A. (2018). Implications of structural diversity for seasonal and annual carbon dioxide fluxes in two temperate deciduous forests. *Agricultural and Forest Meteorology*, *263*, 465–476. https://doi.org/10.1016/j.agrformet.2018.08.027

Thoning, K., Crotwell, A., & Mund, J. (2021). Atmospheric carbon dioxide dry air mole fractions from continuous measurements at mauna loa, Hawaii, barrow, Alaska, American Samoa and south pole. In *1973-2020 version 2021-08-09. National Oceanic and Atmospheric Administration (NOAA)*. Global Monitoring Laboratory (GML). https://doi.org/10.15138/yaf1-bk21

Tramontana, G., Jung, M., Schwalm, C. R., Ichii, K., Camps-Valls, G., Ráduly, B., et al. (2016). Predicting carbon dioxide and energy fluxes across global fluxnet sites with regression algorithms. *Biogeosciences*, *13*(14), 4291–4313. https://doi.org/10.5194/bg-13-4291-2016

Trautmann, T., Koirala, S., Carvalhais, N., Eicker, A., Fink, M., Niemann, C., & Jung, M. (2018). Understanding terrestrial water storage variations in northern latitudes across scales. *Hydrology and Earth System Sciences*, *22*(7), 4061–4082. https://doi.org/10.5194/hess-22-4061-2018

Turner, D. P., Ritts, W. D., Styles, J. M., Yang, Z., Cohen, W. B., Law, B. E., & Thornton, P. E. (2006). A diagnostic carbon flux model to monitor the effects of disturbance and interannual variation in climate on regional NEP. *Tellus B: Chemical and Physical Meteorology*, *58*(5), 476–490. https://doi.org/10.1111/j.1600-0889.2006.00221.x

van der Woude, A. M., Peters, W., Joetzjer, E., Lafont, S., Koren, G., Ciais, P., et al. (2023). Temperature extremes of 2022 reduced carbon uptake by forests in Europe. *Nature Communications*, *14*(1), 6218. https://doi.org/10.1038/s41467-023-41851-0

Van Thieu, N. (2023). *Permetrics: A framework of performance metrics for machine learning models*. Zenodo. https://doi.org/10.5281/zenodo.3951205

Van Thieu, N., & Mirjalili, S. (2023). Mealpy: An open-source library for latest meta-heuristic algorithms in python. *Journal of Systems Architecture*, *139*, 102871. https://doi.org/10.1016/j.sysarc.2023.102871

Virtanen, P., Gommers, R., Oliphant, T. E., Haberland, M., Reddy, T., Cournapeau, D., et al. (2020). SciPy 1.0: Fundamental algorithms for scientific computing in python. *Nature Methods*, *17*(3), 261–272. https://doi.org/10.1038/s41592-019-0686-2

Walther, S., Besnard, S., Nelson, J. A., El-Madany, T. S., Migliavacca, M., Weber, U., et al. (2022). Technical note: A view from space on global flux towers by MODIS and landsat: The FluxnetEO data set. *Biogeosciences*, *19*(11), 2805–2840. https://doi.org/10.5194/bg-19-2805-2022

Walther, S., Nelson, J. A., Besnard, S., & Weber, U. (2023). *The FluxnetEO dataset (MODIS)*. ICOS ERIC - Carbon Portal. https://doi.org/10.18160/0KWD-3RRW

Wang, H., Prentice, I. C., Keenan, T. F., Davis, T. W., Wright, I. J., Cornwell, W. K., et al. (2017). Towards a universal model for carbon dioxide uptake by plants. *Nature plants*, *3*(9), 734–741. https://doi.org/10.1038/s41477-017-0006-8

Wohlfahrt, G., & Gu, L. (2015). The many meanings of gross photosynthesis and their implication for photosynthesis research from leaf to globe. *Plant, Cell & Environment*, *38*(12), 2500–2507. https://doi.org/10.1111/pce.12569

Wolf, S., Keenan, T. F., Fisher, J. B., Baldocchi, D. D., Desai, A. R., Richardson, A. D., et al. (2016). Warm spring reduced carbon cycle impact of the 2012 US summer drought. *Proceedings of the National Academy of Sciences*, *113*(21), 5880–5885. https://doi.org/10.1073/pnas.1519620113

Wu, C., & Wang, T. (2022). Evaluating cumulative drought effect on global vegetation photosynthesis using numerous gpp products. *Frontiers in Environmental Science*, *10*. https://doi.org/10.3389/fenvs.2022.908875

Wu, J., van der Linden, L., Lasslop, G., Carvalhais, N., Pilegaard, K., Beier, C., & Ibrom, A. (2012). Effects of climate variability and functional changes on the interannual variation of the carbon balance in a temperate deciduous forest. *Biogeosciences*, *9*(1), 13–28. https://doi.org/10.5194/bg-9-13-2012

Xiao, X., Jin, C., & Dong, J. (2014). Gross primary production of terrestrial vegetation. In J. M. Hanes (Ed.), *Biophysical applications of satellite remote sensing* (pp. 127–148). Springer Berlin Heidelberg. https://doi.org/10.1007/978-3-642-25047-7_5

Yu, X., Orth, R., Reichstein, M., Bahn, M., Klosterhalfen, A., Knohl, A., et al. (2022). Contrasting drought legacy effects on gross primary productivity in a mixed versus pure beech forest. *Biogeosciences*, *19*(17), 4315–4329. https://doi.org/10.5194/bg-19-4315-2022

Yu, Z., Wang, J., Liu, S., Rentch, J. S., Sun, P., & Lu, C. (2017). Global gross primary productivity and water use efficiency changes under drought stress. *Environmental Research Letters*, *12*(1), 014016. https://doi.org/10.1088/1748-9326/aa5258

Yuan, W., Liu, S., Zhou, G., Zhou, G., Tieszen, L. L., Baldocchi, D., et al. (2007). Deriving a light use efficiency model from eddy covariance flux data for predicting daily gross primary production across biomes. *Agricultural and Forest Meteorology*, *143*(3), 189–207. https://doi.org/10.1016/j.agrformet.2006.12.001

Zhang, W., Nelson, J. A., Miralles, D. G., Mauder, M., Migliavacca, M., Poyatos, R., et al. (2024). A new post-hoc method to reduce the energy imbalance in eddy covariance measurements. *Geophysical Research Letters*, *51*(2), e2023GL107084. https://doi.org/10.1029/2023GL107084

Zheng, Y., Zhang, L., Xiao, J., Yuan, W., Yan, M., Li, T., & Zhang, Z. (2018). Sources of uncertainty in gross primary productivity simulated by light use efficiency models: Model structure, parameters, input data, and spatial resolution. *Agricultural and Forest Meteorology*, *263*, 242–257. https://doi.org/10.1016/j.agrformet.2018.08.003

Zomer, R. J., Xu, J., & Trabucco, A. (2022). Version 3 of the global aridity index and potential evapotranspiration database. *Scientific Data*, *9*(1), 409. https://doi.org/10.1038/s41597-022-01493-1

Zou, H., Chen, J., Li, X., Abraha, M., Zhao, X., & Tang, J. (2024). Modeling net ecosystem exchange of CO_2 with gated recurrent unit neural networks. *Agricultural and Forest Meteorology*, *350*, 109985. https://doi.org/10.1016/j.agrformet.2024.109985

Zscheischler, J., Fatichi, S., Wolf, S., Blanken, P. D., Bohrer, G., Clark, K., et al. (2016). Short-term favorable weather conditions are an important control of interannual variability in carbon and water fluxes. *Journal of Geophysical Research: Biogeosciences*, *121*(8), 2186–2198. https://doi.org/10.1002/2016JG003503

References From the Supporting Information

Acosta, M., Pavelka, M., Montagnani, L., Kutsch, W., Lindroth, A., Juszczak, R., & Janouš, D. (2013). Soil surface CO_2 efflux measurements in Norway spruce forests: Comparison between four different sites across Europe – From boreal to alpine forest. *Geoderma*, *192*, 295–303. https://doi.org/10.1016/j.geoderma.2012.08.027

Albert, L. P., Keenan, T. F., Burns, S. P., Huxman, T. E., & Monson, R. K. (2017). Climate controls over ecosystem metabolism: Insights from a fifteen-year inductive artificial neural network synthesis for a subalpine forest. *Oecologia*, *184*(1), 25–41. https://doi.org/10.1007/s00442-017-3853-0

Allison, V. J., Miller, R. M., Jastrow, J. D., Matamala, R., & Zak, D. R. (2005). Changes in soil microbial community structure in a tallgrass prairie chronosequence. *Soil Science Society of America Journal*, *69*(5), 1412–1421. https://doi.org/10.2136/sssaj2004.0252

Amiro, B. (2009). Measuring boreal forest evapotranspiration using the energy balance residual. *Journal of Hydrology*, *366*(1–4), 112–118. https://doi.org/10.1016/j.jhydrol.2008.12.021

Amiro, B. (2016a). *FLUXNET2015 CA-SF1 Saskatchewan - Western Boreal, forest burned in 1977*. FluxNet; University of Manitoba. https://doi.org/10.18140/FLX/1440046

Amiro, B. (2016b). *FLUXNET2015 CA-SF2 Saskatchewan - Western Boreal, forest burned in 1989*. FluxNet; University of Manitoba. https://doi.org/10.18140/FLX/1440047

Amiro, B. (2016c). *FLUXNET2015 CA-SF3 Saskatchewan - Western Boreal, forest burned in 1998*. FluxNet; University of Manitoba; Canadian Forest Service. https://doi.org/10.18140/FLX/1440048

Ammann, C. (2016). *FLUXNET2015 CH-Oe1 Oensingen grassland*. FluxNet; Agroscope Zuerich. https://doi.org/10.18140/FLX/1440135

Ammann, C., Spirig, C., Leifeld, J., & Neftel, A. (2009). Assessment of the nitrogen and carbon budget of two managed temperate grassland fields. *Agriculture, Ecosystems & Environment*, *133*(3–4), 150–162. https://doi.org/10.1016/j.agee.2009.05.006

Anthoni, P. M., Knohl, A., Rebmann, C., Freibauer, A., Mund, M., Ziegler, W., et al. (2004). Forest and agricultural land-use-dependent CO_2 exchange in Thuringia, Germany. *Global Change Biology*, *10*(12), 2005–2019. https://doi.org/10.1111/j.1365-2486.2004.00863.x

Anthoni, P. M., Law, B. E., & Unsworth, M. H. (1999). Carbon and water vapor exchange of an open-canopied ponderosa pine ecosystem. *Agricultural and Forest Meteorology*, *95*(3), 151–168. https://doi.org/10.1016/s0168-1923(99)00029-5

Anthoni, P. M., Unsworth, M. H., Law, B. E., Irvine, J., Baldocchi, D. D., Tuyl, S. V., & Moore, D. (2002). Seasonal differences in carbon and water vapor exchange in young and old-growth ponderosa pine ecosystems. *Agricultural and Forest Meteorology*, *111*(3), 203–222. https://doi.org/10.1016/s0168-1923(02)00021-7

Antonarakis, A. S., Siqueira, P., & Munger, J. W. (2017). Using multi-source data from lidar, radar, imaging spectroscopy, and national forest inventories to simulate forest carbon fluxes. *International Journal of Remote Sensing*, *38*(19), 5464–5486. https://doi.org/10.1080/01431161.2017.1341666

Arain, M. A. (2016a). *FLUXNET2015 CA-TP1 Ontario - Turkey Point 2002 Plantation White Pine*. FluxNet; McMaster University. https://doi.org/10.18140/FLX/1440050

Arain, M. A. (2016b). *FLUXNET2015 CA-TP2 Ontario - Turkey Point 1989 Plantation White Pine*. FluxNet; McMaster University. https://doi.org/10.18140/FLX/1440051

Arain, M. A. (2016c). *FLUXNET2015 CA-TP3 Ontario - Turkey Point 1974 Plantation White Pine*. FluxNet; McMaster University. https://doi.org/10.18140/FLX/1440052

Arain, M. A. (2016d). *FLUXNET2015 CA-TP4 Ontario - Turkey Point 1939 Plantation White Pine*. FluxNet; McMaster University. https://doi.org/10.18140/FLX/1440053

Arain, M. A. (2016e). *FLUXNET2015 CA-TPD Ontario - Turkey Point Mature Deciduous*. FluxNet; McMaster University. https://doi.org/10.18140/FLX/1440112

Arain, M. A., & Restrepo-Coupe, N. (2005). Net ecosystem production in a temperate pine plantation in southeastern Canada. *Agricultural and Forest Meteorology*, *128*(3–4), 223–241. https://doi.org/10.1016/j.agrformet.2004.10.003

Archibald, S. A., Kirton, A., van der Merwe, M. R., Scholes, R. J., Williams, C. A., & Hanan, N. (2009). Drivers of inter-annual variability in Net Ecosystem Exchange in a semi-arid savanna ecosystem, South Africa. *Biogeosciences*, *6*(2), 251–266. https://doi.org/10.5194/bg-6-251-2009

Ardö, J., El Tahir, B. A., & El Khidir, H. A. M. (2016). *FLUXNET2015 SD-Dem Demokeya*. FluxNet; LUND UNIVERSITY. https://doi.org/10.18140/FLX/1440186

Ardö, J., Mölder, M., El-Tahir, B. A., & Elkhidir, H. A. M. (2008). Seasonal variation of carbon fluxes in a sparse savanna in semi arid Sudan. *Carbon Balance and Management*, *3*(1), 7. https://doi.org/10.1186/1750-0680-3-7

Arndt, S., Hinko-Najera, N., & Griebel, A. (2016). *FLUXNET2015 AU-Wom Wombat*. FluxNet; University of Melbourne, School of Ecosystem and Forest Sciences. https://doi.org/10.18140/FLX/1440207

Aron, P. G., Poulsen, C. J., Fiorella, R. P., & Matheny, A. M. (2019). Stable water isotopes reveal effects of intermediate disturbance and canopy structure on forest water cycling. *Journal of Geophysical Research: Biogeosciences*, *124*(10), 2958–2975. https://doi.org/10.1029/2019jg005118

Asner, G. P., Keller, M., Pereira, R., Jr., Zweede, J. C., & Silva, J. N. M. (2004). Canopy damage and recovery after selective logging in Amazonia: Field and satellite studies. *Ecological Applications*, *14*(sp4), 280–298. https://doi.org/10.1890/01-6019

Atkins, J. W., Bohrer, G., Fahey, R. T., Hardiman, B. S., Morin, T. H., Stovall, A. E. L., et al. (2018). Quantifying vegetation and canopy structural complexity from terrestrial LiDAR data using the forestr r package. *Methods in Ecology and Evolution*, *9*(10), 2057–2066. https://doi.org/10.1111/2041-210x.13061

Aubinet, M., Chermanne, B., Vandenhaute, M., Longdoz, B., Yernaux, M., & Laitat, E. (2001). Long term carbon dioxide exchange above a mixed forest in the Belgian Ardennes. *Agricultural and Forest Meteorology*, *108*(4), 293–315. https://doi.org/10.1016/s0168-1923(01)00244-1

Aurela, M., Laurila, T., Hatakka, J., Tuovinen, J.-P., & Rainne, J. (2016). *FLUXNET2015 RU-Tks Tiksi*. FluxNet; Finnish Meteorological Institute. https://doi.org/10.18140/FLX/1440244

Aurela, M., Lohila, A., Tuovinen, J.-P., Hatakka, J., Penttila, T., & Laurila, T. (2015). Carbon dioxide and energy flux measurements in four northern-boreal ecosystems at Pallas. *Boreal Environment Research*, *20*(4), 455–473. Retrieved from https://helda.helsinki.fi/bitstreams/4cfcb066-087c-4586-8933-6b16c4a266c2/download

Aurela, M., Lohila, A., Tuovinen, J.-P., Hatakka, J., Rainne, J., Mäkelä, T., & Lauria, T. (2016). *FLUXNET2015 FI-Lom Lompolojankka*. FluxNet; Finnish Meteorological Institute. https://doi.org/10.18140/FLX/1440228

Aurela, M., Tuovinen, J.-P., Hatakka, J., Lohila, A., Mäkelä, T., Rainne, J., & Lauria, T. (2016). *FLUXNET2015 FI-Sod Sodankyla*. FluxNet; Finnish Meteorological Institute. https://doi.org/10.18140/FLX/1440160

Bagley, J. E., Kueppers, L. M., Billesbach, D. P., Williams, I. N., Biraud, S. C., & Torn, M. S. (2017). The influence of land cover on surface energy partitioning and evaporative fraction regimes in the U.S. Southern Great Plains. *Journal of Geophysical Research: Atmospheres*, *122*(11), 5793–5807. https://doi.org/10.1002/2017jd026740

Baker, B., Guenther, A., Greenberg, J., Goldstein, A., & Fall, R. (1999). Canopy fluxes of 2-methyl-3-buten-2-ol over a ponderosa pine forest by relaxed eddy accumulation: Field data and model comparison. *Journal of Geophysical Research: Atmospheres*, *104*(D21), 26107–26114. https://doi.org/10.1029/1999jd900749

Baker, I., Denning, A. S., Hanan, N., Prihodko, L., Uliasz, M., Vidale, P., et al. (2003). Simulated and observed fluxes of sensible and latent heat and CO_2 at the WLEF-TV tower using SiB2.5. *Global Change Biology*, *9*(9), 1262–1277. https://doi.org/10.1046/j.1365-2486.2003.00671.x

Baker, T. R., Phillips, O. L., Malhi, Y., Almeida, S., Arroyo, L., Di Fiore, A., et al. (2004). Variation in wood density determines spatial patterns inAmazonian forest biomass. *Global Change Biology*, *10*(5), 545–562. https://doi.org/10.1111/j.1365-2486.2004.00751.x

Baldocchi, D. (2016a). *FLUXNET2015 US-Tw2 Twitchell Corn*. FluxNet; University of California. https://doi.org/10.18140/FLX/1440109

Baldocchi, D. (2016b). *FLUXNET2015 US-Twt Twitchell Island*. FluxNet; University of California. https://doi.org/10.18140/FLX/1440106

Baldocchi, D., & Ma, S. (2016). *FLUXNET2015 US-Ton Tonzi Ranch*. FluxNet; University of California, Berkeley. https://doi.org/10.18140/FLX/1440092

Baldocchi, D., Ma, S., & Xu, L. (2016). *FLUXNET2015 US-Var Vaira Ranch- Ione*. FluxNet; University of California, Berkeley. https://doi.org/10.18140/FLX/1440094

Baldocchi, D., & Penuelas, J. (2019). The physics and ecology of mining carbon dioxide from the atmosphere by ecosystems. *Global Change Biology*, *25*(4), 1191–1197. https://doi.org/10.1111/gcb.14559

Baldocchi, D. D., Black, T. A., Curtis, P. S., Falge, E., Fuentes, J. D., Granier, A., et al. (2005). Predicting the onset of net carbon uptake by deciduous forests with soil temperature and climate data: A synthesis of FLUXNET data. *International Journal of Biometeorology*, *49*(6), 377–387. https://doi.org/10.1007/s00484-005-0256-4

Baldocchi, D. D., Ma, S., Rambal, S., Misson, L., Ourcival, J.-M., Limousin, J.-M., et al. (2010). On the differential advantages of evergreenness and deciduousness in mediterranean oak woodlands: A flux perspective. *Ecological Applications*, *20*(6), 1583–1597. https://doi.org/10.1890/08-2047.1

Baldocchi, D. D., Xu, L., & Kiang, N. (2004). How plant functional-type, weather, seasonal drought, and soil physical properties alter water and energy fluxes of an oak–grass savanna and an annual grassland. *Agricultural and Forest Meteorology*, *123*(1–2), 13–39. https://doi.org/10.1016/j.agrformet.2003.11.006

Barr, A., Richardson, A., Hollinger, D., Papale, D., Arain, M., Black, T., et al. (2013). Use of change-point detection for friction–velocity threshold evaluation in eddy-covariance studies. *Agricultural and Forest Meteorology*, *171–172*, 31–45. https://doi.org/10.1016/j.agrformet.2012.11.023

Barr, A. G., Black, T., Hogg, E., Kljun, N., Morgenstern, K., & Nesic, Z. (2004). Inter-annual variability in the leaf area index of a boreal aspen-hazelnut forest in relation to net ecosystem production. *Agricultural and Forest Meteorology*, *126*(3–4), 237–255. https://doi.org/10.1016/j.agrformet.2004.06.011

Barron-Gafford, G. A., Scott, R. L., Jenerette, G. D., Hamerlynck, E. P., & Huxman, T. E. (2013). Landscape and environmental controls over leaf and ecosystem carbon dioxide fluxes under woody plant expansion. *Journal of Ecology*, *101*(6), 1471–1483. https://doi.org/10.1111/1365-2745.12161

Bazot, S., Barthes, L., Blanot, D., & Fresneau, C. (2013). Distribution of non-structural nitrogen and carbohydrate compounds in mature oak trees in a temperate forest at four key phenological stages. *Trees*, *27*(4), 1023–1034. https://doi.org/10.1007/s00468-013-0853-5

Belelli, L., Papale, D., & Valentini, R. (2016). *FLUXNET2015 RU-Ha1 Hakasia steppe*. FluxNet; University of Tuscia - Vietrbo. https://doi.org/10.18140/FLX/1440184

Belelli Marchesini, L., Papale, D., Reichstein, M., Vuichard, N., Tchebakova, N., & Valentini, R. (2007). Carbon balance assessment of a natural steppe of southern Siberia by multiple constraint approach. *Biogeosciences*, *4*(4), 581–595. https://doi.org/10.5194/bg-4-581-2007

Berbigier, P., Bonnefond, J.-M., & Mellmann, P. (2001). CO_2 and water vapour fluxes for 2 years above Euroflux forest site. *Agricultural and Forest Meteorology*, *108*(3), 183–197. https://doi.org/10.1016/s0168-1923(01)00240-4
Berbigier, P., & Loustau, D. (2016). *FLUXNET2015 FR-LBr Le Bray*. FluxNet; INRA - UMR ISPA. https://doi.org/10.18140/FLX/1440163
Beringer, J., Cunningham, S., Baker, P., Cavagnaro, T., MacNally, R., Thompson, R., & McHugh, I. (2016). *FLUXNET2015 AU-Whr Whroo*. FluxNet; Monash University. https://doi.org/10.18140/FLX/1440206
Beringer, J., Hacker, J., Hutley, L. B., Leuning, R., Arndt, S. K., Amiri, R., et al. (2011). SPECIAL—Savanna patterns of energy and carbon integrated across the landscape. *Bulletin of the American Meteorological Society*, *92*(11), 1467–1485. https://doi.org/10.1175/2011bams2948.1
Beringer, J., & Hutley, L. (2016a). *FLUXNET2015 AU-Ade Adelaide River*. FluxNet; Monash University; Charles Darwin University. https://doi.org/10.18140/FLX/1440193
Beringer, J., & Hutley, L. (2016b). *FLUXNET2015 AU-DaP Daly River Savanna*. FluxNet; Monash University; Charles Darwin University. https://doi.org/10.18140/FLX/1440123
Beringer, J., & Hutley, L. (2016c). *FLUXNET2015 AU-DaS Daly River Cleared*. FluxNet; University of Western Australia; Charles Darwin University; Monash University. https://doi.org/10.18140/FLX/1440122
Beringer, J., & Hutley, L. (2016d). *FLUXNET2015 AU-Dry Dry River*. FluxNet; Monash University; University of Western Australia; Charles Darwin University. https://doi.org/10.18140/FLX/1440197
Beringer, J., & Hutley, L. (2016e). *FLUXNET2015 AU-Fog Fogg Dam*. FluxNet; Monash University; Charles Darwin University. https://doi.org/10.18140/FLX/1440124
Beringer, J., & Hutley, L. (2016f). *FLUXNET2015 AU-RDF Red Dirt Melon Farm, Northern Territory*. FluxNet; Monash University; Charles Darwin University. https://doi.org/10.18140/FLX/1440201
Beringer, J., Hutley, L., McGuire, D., & U, P. (2016). *FLUXNET2015 AU-Wac Wallaby Creek*. FluxNet; Monash University; University of California Davis; Charles Darwin University; University of Alaska Fairbanks; University of Melbourne. https://doi.org/10.18140/FLX/1440127
Beringer, J., Hutley, L. B., Hacker, J. M., Neininger, B., & Paw U, K. T. (2011). Patterns and processes of carbon, water and energy cycles across northern Australian landscapes: From point to region. *Agricultural and Forest Meteorology*, *151*(11), 1409–1416. https://doi.org/10.1016/j.agrformet.2011.05.003
Beringer, J., Hutley, L. B., McHugh, I., Arndt, S. K., Campbell, D., Cleugh, H. A., et al. (2016). An introduction to the Australian and New Zealand flux tower network – OzFlux. *Biogeosciences*, *13*(21), 5895–5916. https://doi.org/10.5194/bg-13-5895-2016
Beringer, J., Livesley, S. J., Randle, J., & Hutley, L. B. (2013). Carbon dioxide fluxes dominate the greenhouse gas exchanges of a seasonal wetland in the wet–dry tropics of northern Australia. *Agricultural and Forest Meteorology*, *182–183*, 239–247. https://doi.org/10.1016/j.agrformet.2013.06.008
Beringer, J., & Walker, J. (2016). *FLUXNET2015 AU-Ync Jaxa*. FluxNet; University of Western Australia; Monash University. https://doi.org/10.18140/FLX/1440208
Bernhofer, C., Grünwald, T., Moderow, U., Hehn, M., Eichelmann, U., & Prasse, H. (2016a). *FLUXNET2015 DE-Akm Anklam*. FluxNet; TU Dresden. https://doi.org/10.18140/FLX/1440213
Bernhofer, C., Grünwald, T., Moderow, U., Hehn, M., Eichelmann, U., & Prasse, H. (2016b). *FLUXNET2015 DE-Gri Grillenburg*. FluxNet; TU Dresden. https://doi.org/10.18140/FLX/1440147
Bernhofer, C., Grünwald, T., Moderow, U., Hehn, M., Eichelmann, U., & Prasse, H. (2016c). *FLUXNET2015 DE-Kli Klingenberg*. FluxNet; TU Dresden. https://doi.org/10.18140/FLX/1440149
Bernhofer, C., Grünwald, T., Moderow, U., Hehn, M., Eichelmann, U., & Prasse, H. (2016d). *FLUXNET2015 DE-Obe Oberbärenburg*. FluxNet; TU Dresden. https://doi.org/10.18140/FLX/1440151
Bernhofer, C., Grünwald, T., Moderow, U., Hehn, M., Eichelmann, U., & Prasse, H. (2016e). *FLUXNET2015 DE-Spw Spreewald*. FluxNet; TU Dresden. https://doi.org/10.18140/FLX/1440220
Bernhofer, C., Grünwald, T., Moderow, U., Hehn, M., Eichelmann, U., & Prasse, H. (2016f). *FLUXNET2015 DE-Tha Tharandt*. FluxNet; TU Dresden. https://doi.org/10.18140/FLX/1440152
Berveiller, D., Delpierre, N., Dufrêne, E., Pontailler, J.-Y., Vanbostal, L., Janvier, B., et al. (2016). *FLUXNET2015 FR-Fon Fontainebleau-Barbeau*. FluxNet; CNRS. https://doi.org/10.18140/FLX/1440161
Biederman, J. A., Scott, R. L., Bell, T. W., Bowling, D. R., Dore, S., Garatuza-Payan, J., et al. (2017). CO_2 exchange and evapotranspiration across dryland ecosystems of southwestern North America. *Global Change Biology*, *23*(10), 4204–4221. https://doi.org/10.1111/gcb.13686
Billesbach, D., Bradford, J., & Torn, M. (2016a). *FLUXNET2015 US-AR1 ARM USDA UNL OSU Woodward Switchgrass 1*. FluxNet; Lawerence Berkeley National Lab; U.S. Department of Agriculture; University of Nebraska. https://doi.org/10.18140/FLX/1440103
Billesbach, D., Bradford, J., & Torn, M. (2016b). *FLUXNET2015 US-AR2 ARM USDA UNL OSU Woodward Switchgrass 2*. FluxNet; Lawrence Berkeley National Lab; U.S. Department of Agriculture; University of Nebraska. https://doi.org/10.18140/FLX/1440104
Biraud, S., Fischer, M., Chan, S., & Torn, M. (2016). *FLUXNET2015 US-ARM ARM Southern Great Plains site- Lamont*. FluxNet; Lawrence Berkeley National Laboratory. https://doi.org/10.18140/FLX/1440066
Black, T. A. (2016a). *FLUXNET2015 CA-Oas Saskatchewan - Western Boreal, Mature Aspen*. FluxNet; The University of British Columbia. https://doi.org/10.18140/FLX/1440043
Black, T. A. (2016b). *FLUXNET2015 CA-Obs Saskatchewan - Western Boreal, Mature black Spruce*. FluxNet; The University of British Columbia. https://doi.org/10.18140/FLX/1440044
Blanken, P. D., Monson, R. K., Burns, S. P., Bowling, D. R., & Turnipseed, A. A. (2016). *FLUXNET2015 US-NR1 Niwot Ridge Forest (LTER NWT1)*. FluxNet; University of Colorado. https://doi.org/10.18140/FLX/1440087
Bohrer, G. (2016). *FLUXNET2015 US-ORv Olentangy River Wetland Research Park*. FluxNet; The Ohio State University. https://doi.org/10.18140/FLX/1440102
Boike, J., Kattenstroth, B., Abramova, K., Bornemann, N., Chetverova, A., Fedorova, I., et al. (2013). Baseline characteristics of climate, permafrost and land cover from a new permafrost observatory in the Lena River Delta, Siberia (1998–2011). *Biogeosciences*, *10*(3), 2105–2128. https://doi.org/10.5194/bg-10-2105-2013
Boike, J., Westermann, S., Lüers, J., Langer, M., & Piel, K. (2016). *FLUXNET2015 SJ-Blv Bayelva, Spitsbergen*. FluxNet; University of Oslo, Department of Geosciences, 0316 OSLO, Norway; Universität Bayreuth, Department of Earth Sciences, 95440 Bayreuth, Germany; Alfred Wegener Institute, Helmholtz Centre for Polar and Marine Research, Periglacial Research Unit, 14473 Potsdam, Germany. https://doi.org/10.18140/FLX/1440242
Bonal, D., Bosc, A., Ponton, S., Goret, J., Burban, B., Gross, P., et al. (2008). Impact of severe dry season on net ecosystem exchange in the Neotropical rainforest of French Guiana. *Global Change Biology*, *14*(8), 1917–1933. https://doi.org/10.1111/j.1365-2486.2008.01610.x
Bonal, D., & Burban, B. (2016). *FLUXNET2015 GF-Guy Guyaflux (French Guiana)*. FluxNet; INRA. https://doi.org/10.18140/FLX/1440165

Bowling, D. (2016). *FLUXNET2015 US-Cop Corral Pocket*. FluxNet; University of Utah. https://doi.org/10.18140/FLX/1440100
Bracho, R., Powell, T. L., Dore, S., Li, J., Hinkle, C. R., & Drake, B. G. (2008). Environmental and biological controls on water and energy exchange in Florida scrub oak and pine flatwoods ecosystems. *Journal of Geophysical Research: Biogeosciences*, *113*(G2). https://doi.org/10.1029/2007jg000469
Bristow, M., Hutley, L. B., Beringer, J., Livesley, S. J., Edwards, A. C., & Arndt, S. K. (2016). Quantifying the relative importance of greenhouse gas emissions from current and future savanna land use change across northern Australia. *Biogeosciences*, *13*(22), 6285–6303. https://doi.org/10.5194/bg-13-6285-2016
Brooker, M. R., Bohrer, G., & Mouser, P. J. (2014). Variations in potential CH_4 flux and CO_2 respiration from freshwater wetland sediments that differ by microsite location, depth and temperature. *Ecological Engineering*, *72*, 84–94. https://doi.org/10.1016/j.ecoleng.2014.05.028
Brümmer, C., Lucas-Moffat, A. M., Herbst, M., & Kolle, O. (2016). *FLUXNET2015 DE-Geb Gebesee*. FluxNet; Thünen Institute of Climate-Smart Agriculture, Braunschweig. https://doi.org/10.18140/FLX/1440146
Buysse, P., Durand, B., Gueudet, J.-C., Mascher, N., Larmanou, E., Cellier, P., & Loubet, B. (2016). *FLUXNET2015 FR-Gri Grignon*. FluxNet; French National Institute for Agricultural Research. https://doi.org/10.18140/FLX/1440162
Campbell, J. L., Sun, O. J., & Law, B. E. (2004). Disturbance and net ecosystem production across three climatically distinct forest landscapes. *Global Biogeochemical Cycles*, *18*(4). https://doi.org/10.1029/2004gb002236
Carrara, A., Janssens, I. A., Curiel Yuste, J., & Ceulemans, R. (2004). Seasonal changes in photosynthesis, respiration and NEE of a mixed temperate forest. *Agricultural and Forest Meteorology*, *126*(1–2), 15–31. https://doi.org/10.1016/j.agrformet.2004.05.002
Cañete, E. P. S., Ortiz, P. S., Jiménez, M. R. M., Poveda, F. D., Priego, O. P., Ballesteros, A. L., & Kowalski, A. S. (2016). *FLUXNET2015 ES-LJu Llano de los Juanes*. FluxNet; University of Granada. https://doi.org/10.18140/FLX/1440157
Cernusak, L. A., Hutley, L. B., Beringer, J., Holtum, J. A., & Turner, B. L. (2011). Photosynthetic physiology of eucalypts along a sub-continental rainfall gradient in northern Australia. *Agricultural and Forest Meteorology*, *151*(11), 1462–1470. https://doi.org/10.1016/j.agrformet.2011.01.006
Cescatti, A., Marcolla, B., Zorer, R., & Gianelle, D. (2016). *FLUXNET2015 IT-La2 Lavarone2*. FluxNet; Centro di Ecologia Alpina. https://doi.org/10.18140/FLX/1440235
Chamberlain, S. D., Verfaillie, J., Eichelmann, E., Hemes, K. S., & Baldocchi, D. D. (2017). Evaluation of density corrections to methane fluxes measured by open-path eddy covariance over contrasting landscapes. *Boundary-Layer Meteorology*, *165*(2), 197–210. https://doi.org/10.1007/s10546-017-0275-9
Chen, J. (2016a). *FLUXNET2015 US-Wi0 Young red pine (YRP)*. FluxNet; Michigan State University. https://doi.org/10.18140/FLX/1440055
Chen, J. (2016b). *FLUXNET2015 US-Wi1 Intermediate hardwood (IHW)*. FluxNet; Michigan State University. https://doi.org/10.18140/FLX/1440054
Chen, J. (2016c). *FLUXNET2015 US-Wi2 Intermediate red pine (IRP)*. FluxNet; Michigan State University. https://doi.org/10.18140/FLX/1440056
Chen, J. (2016d). *FLUXNET2015 US-Wi3 Mature hardwood (MHW)*. FluxNet; Michigan State University. https://doi.org/10.18140/FLX/1440057
Chen, J. (2016e). *FLUXNET2015 US-Wi4 Mature red pine (MRP)*. FluxNet; Michigan State University. https://doi.org/10.18140/FLX/1440058
Chen, J. (2016f). *FLUXNET2015 US-Wi5 Mixed young jack pine (MYJP)*. FluxNet; Michigan State University. https://doi.org/10.18140/FLX/1440059
Chen, J. (2016g). *FLUXNET2015 US-Wi6 Pine barrens #1 (PB1)*. FluxNet; Michigan State University. https://doi.org/10.18140/FLX/1440060
Chen, J. (2016h). *FLUXNET2015 US-Wi7 Red pine clearcut (RPCC)*. FluxNet; Michigan State University. https://doi.org/10.18140/FLX/1440061
Chen, J. (2016i). *FLUXNET2015 US-Wi8 Young hardwood clearcut (YHW)*. FluxNet; Michigan State University. https://doi.org/10.18140/FLX/1440062
Chen, J. (2016j). *FLUXNET2015 US-Wi9 Young Jack pine (YJP)*. FluxNet; Michigan State University. https://doi.org/10.18140/FLX/1440063
Chen, J., & Chu, H. (2016a). *FLUXNET2015 US-CRT Curtice Walter-Berger cropland*. FluxNet; University of Toledo / Michigan State University. https://doi.org/10.18140/FLX/1440117
Chen, J., & Chu, H. (2016b). *FLUXNET2015 US-WPT Winous Point North Marsh*. FluxNet; University of Toledo / Michigan State University. https://doi.org/10.18140/FLX/1440116
Chen, J., Chu, H., & Noormets, A. (2016). *FLUXNET2015 US-Oho Oak Openings*. FluxNet; University of Toledo / Michigan State University. https://doi.org/10.18140/FLX/1440088
Chen, S. (2016). *FLUXNET2015 CN-Du2 Duolun grassland (D01)*. FluxNet; Institute of Botany, Chinese Academy of Sciences. https://doi.org/10.18140/FLX/1440140
Chen, S., Chen, J., Lin, G., Zhang, W., Miao, H., Wei, L., et al. (2009). Energy balance and partition in Inner Mongolia steppe ecosystems with different land use types. *Agricultural and Forest Meteorology*, *149*(11), 1800–1809. https://doi.org/10.1016/j.agrformet.2009.06.009
Chiesi, M., Maselli, F., Bindi, M., Fibbi, L., Cherubini, P., Arlotta, E., et al. (2005). Modelling carbon budget of Mediterranean forests using ground and remote sensing measurements. *Agricultural and Forest Meteorology*, *135*(1–4), 22–34. https://doi.org/10.1016/j.agrformet.2005.09.011
Christensen, T. (2016). *FLUXNET2015 SJ-Adv Adventdalen*. FluxNet; NATEKO; Lund University. https://doi.org/10.18140/FLX/1440241
Chu, H., Baldocchi, D. D., Poindexter, C., Abraha, M., Desai, A. R., Bohrer, G., et al. (2018). Temporal dynamics of aerodynamic canopy height derived from eddy covariance momentum flux data across North American flux networks. *Geophysical Research Letters*, *45*(17), 9275–9287. https://doi.org/10.1029/2018gl079306
Chu, H., Chen, J., Gottgens, J. F., Desai, A. R., Ouyang, Z., & Qian, S. S. (2016). Response and biophysical regulation of carbon dioxide fluxes to climate variability and anomaly in contrasting ecosystems in northwestern Ohio, USA. *Agricultural and Forest Meteorology*, *220*, 50–68. https://doi.org/10.1016/j.agrformet.2016.01.008
Cleverly, J., & Eamus, D. (2016a). *FLUXNET2015 AU-ASM Alice Springs*. FluxNet; University of Technology Sydney. https://doi.org/10.18140/FLX/1440194
Cleverly, J., & Eamus, D. (2016b). *FLUXNET2015 AU-TTE Ti Tree East*. FluxNet; University of Technology Sydney. https://doi.org/10.18140/FLX/1440205
Cremonese, E., Galvagno, M., Di Cella, U. M., & Migliavacca, M. (2016). *FLUXNET2015 IT-Tor Torgnon*. FluxNet; Environmental Protection Agency of Aosta Valley. https://doi.org/10.18140/FLX/1440237
De Ligne, A., Manise, T., Heinesch, B., Aubinet, M., & Vincke, C. (2016). *FLUXNET2015 BE-Vie Vielsalm*. FluxNet; University of Liege - Gembloux Agro-Bio Tech; University catholic of Louvain-la-Neuve. https://doi.org/10.18140/FLX/1440130

De Ligne, A., Manise, T., Moureaux, C., Aubinet, M., & Heinesch, B. (2016). *FLUXNET2015 BE-Lon Lonzee*. FluxNet; University of Liege - Gembloux Agro-Bio Tech. https://doi.org/10.18140/FLX/1440129
Desai, A. (2016a). *FLUXNET2015 US-Los Lost Creek*. FluxNet; University of Wisconsin. https://doi.org/10.18140/FLX/1440076
Desai, A. (2016b). *FLUXNET2015 US-PFa Park Falls/WLEF*. FluxNet; University of Wisconsin. https://doi.org/10.18140/FLX/1440089
Desai, A. (2016c). *FLUXNET2015 US-Syv Sylvania Wilderness area*. FluxNet; University of Wisconsin. https://doi.org/10.18140/FLX/1440091
Desai, A. (2016d). *FLUXNET2015 US-WCr Willow Creek*. FluxNet; University of Wisconsin. https://doi.org/10.18140/FLX/1440095
Desai, A. R., Noormets, A., Bolstad, P. V., Chen, J., Cook, B. D., Davis, K. J., et al. (2008). Influence of vegetation and seasonal forcing on carbon dioxide fluxes across the Upper Midwest, USA: Implications for regional scaling. *Agricultural and Forest Meteorology*, *148*(2), 288–308. https://doi.org/10.1016/j.agrformet.2007.08.001
Dietiker, D., Buchmann, N., & Eugster, W. (2010). Testing the ability of the DNDC model to predict CO_2 and water vapour fluxes of a Swiss cropland site. *Agriculture, Ecosystems & Environment*, *139*(3), 396–401. https://doi.org/10.1016/j.agee.2010.09.002
Dolman, H., Hendriks, D., Parmentier, F.-J., Marchesini, L. B., Dean, J., & Van Huissteden, K. (2016). *FLUXNET2015 NL-Hor Horstermeer*. FluxNet; Vrije Universiteit Amsterdam. https://doi.org/10.18140/FLX/1440177
Dolman, H., Van Der Molen, M., Parmentier, F.-J., Marchesini, L. B., Dean, J., Van Huissteden, K., & Maximov, T. (2016). *FLUXNET2015 RU-Cok Chokurdakh*. FluxNet; Vrije Universiteit Amsterdam. https://doi.org/10.18140/FLX/1440182
Dong, G. (2016). *FLUXNET2015 CN-Cng Changling*. FluxNet; Shanxi University. https://doi.org/10.18140/FLX/1440209
Drake, B., & Hinkle, R. (2016a). *FLUXNET2015 US-KS1 Kennedy space center (slash pine)*. FluxNet; Smithsonian Environmental Research Center; University of Central Florida. https://doi.org/10.18140/FLX/1440074
Drake, B., & Hinkle, R. (2016b). *FLUXNET2015 US-KS2 Kennedy Space Center (scrub oak)*. FluxNet; Smithsonian Environmental Research Center; University of Central Florida. https://doi.org/10.18140/FLX/1440075
Dušek, J., Janouš, D., & Pavelka, M. (2016). *FLUXNET2015 CZ-Wet Trebon (CZECHWET)*. FluxNet; Global Change Research Institute CAS. https://doi.org/10.18140/FLX/1440145
Dušek, J., Čížková, H., Stellner, S., Czerný, R., & Květ, J. (2012). Fluctuating water table affects gross ecosystem production and gross radiation use efficiency in a sedge-grass marsh. *Hydrobiologia*, *692*(1), 57–66. https://doi.org/10.1007/s10750-012-0998-z
Elson, P., de Andrade, E. S., Lucas, G., May, R., Hattersley, R., Campbell, E., et al. (2023). *SciTools/cartopy v0.22.0 on Github*. Zenodo. https://doi.org/10.5281/zenodo.1182735
Etzold, S., Ruehr, N. K., Zweifel, R., Dobbertin, M., Zingg, A., Pluess, P., et al. (2011). The carbon balance of two contrasting mountain forest ecosystems in Switzerland: Similar annual trends, but seasonal differences. *Ecosystems*, *14*(8), 1289–1309. https://doi.org/10.1007/s10021-011-9481-3
Ewers, B., & Pendall, E. (2016). *FLUXNET2015 US-Sta Saratoga*. FluxNet; University of Wyoming. https://doi.org/10.18140/FLX/1440115
Fares, S. (2016). *FLUXNET2015 US-Lin Lindcove Orange Orchard*. FluxNet; Entecra. https://doi.org/10.18140/FLX/1440107
Fares, S., Savi, F., & Conte, A. (2016). *FLUXNET2015 IT-Cp2 Castelporziano 2*. FluxNet; Council for Agricultural Research and Economics. https://doi.org/10.18140/FLX/1440233
Fares, S., Savi, F., Muller, J., Matteucci, G., & Paoletti, E. (2014). Simultaneous measurements of above and below canopy ozone fluxes help partitioning ozone deposition between its various sinks in a Mediterranean Oak Forest. *Agricultural and Forest Meteorology*, *198–199*, 181–191. https://doi.org/10.1016/j.agrformet.2014.08.014
Fares, S., Vargas, R., Detto, M., Goldstein, A. H., Karlik, J., Paoletti, E., & Vitale, M. (2013). Tropospheric ozone reduces carbon assimilation in trees: Estimates from analysis of continuous flux measurements. *Global Change Biology*, *19*(8), 2427–2443. https://doi.org/10.1111/gcb.12222
Ferréa, C., Zenone, T., Comolli, R., & Seufert, G. (2012). Estimating heterotrophic and autotrophic soil respiration in a semi-natural forest of Lombardy, Italy. *Pedobiologia*, *55*(6), 285–294. https://doi.org/10.1016/j.pedobi.2012.05.001
Fischer, M. L., Torn, M. S., Billesbach, D. P., Doyle, G., Northup, B., & Biraud, S. C. (2012). Carbon, water, and heat flux responses to experimental burning and drought in a tallgrass prairie. *Agricultural and Forest Meteorology*, *166–167*, 169–174. https://doi.org/10.1016/j.agrformet.2012.07.011
Friborg, T., Biasi, C., & Shurpali, N. J. (2016). *FLUXNET2015 RU-Vrk Seida/Vorkuta*. FluxNet; University of Copenhagen. https://doi.org/10.18140/FLX/1440245
Friborg, T., Jammet, M., & Crill, P. (2016). *FLUXNET2015 SE-St1 Stordalen grassland*. FluxNet; University of Copenhagen. https://doi.org/10.18140/FLX/1440187
Galvagno, M., Wohlfahrt, G., Cremonese, E., Rossini, M., Colombo, R., Filippa, G., et al. (2013). Phenology and carbon dioxide source/sink strength of a subalpine grassland in response to an exceptionally short snow season. *Environmental Research Letters*, *8*(2), 025008. https://doi.org/10.1088/1748-9326/8/2/025008
Garbulsky, M. F., Peñuelas, J., Papale, D., & Filella, I. (2008). Remote estimation of carbon dioxide uptake by a Mediterranean forest. *Global Change Biology*, *14*(12), 2860–2867. https://doi.org/10.1111/j.1365-2486.2008.01684.x
Garcia, A., Di Bella, C., Houspanossian, J., Magliano, P., Jobbágy, E., Posse, G., et al. (2016). *FLUXNET2015 AR-SLu San Luis*. FluxNet; Instituto Nacional de Tecnología Agropecuaria (INTA). https://doi.org/10.18140/FLX/1440191
Gianelle, D., Cavagna, M., Zampedri, R., & Marcolla, B. (2016). *FLUXNET2015 IT-MBo Monte Bondone*. FluxNet; Edmund Mach Foundation. https://doi.org/10.18140/FLX/1440170
Gianelle, D., Zampedri, R., Cavagna, M., & Sottocornola, M. (2016). *FLUXNET2015 IT-Lav Lavarone*. FluxNet; Edmund Mach Foundation. https://doi.org/10.18140/FLX/1440169
Goldstein, A. (2016). *FLUXNET2015 US-Blo Blodgett Forest*. FluxNet; University of California. https://doi.org/10.18140/FLX/1440068
Gough, C., Bohrer, G., & Curtis, P. (2016a). *FLUXNET2015 US-UMB Univ. Of Mich. Biological station*. FluxNet; Ohio State University; Virginia Commonwealth University. https://doi.org/10.18140/FLX/1440093
Gough, C., Bohrer, G., & Curtis, P. (2016b). *FLUXNET2015 US-UMd UMBS disturbance*. FluxNet; Ohio State University; Virginia Commonwealth University. https://doi.org/10.18140/FLX/1440101
Goulden, M. (2016a). *FLUXNET2015 BR-Sa3 Santarem-Km83-Logged Forest*. FluxNet; University of California - Irvine. https://doi.org/10.18140/FLX/1440033
Goulden, M. (2016b). *FLUXNET2015 CA-NS2 UCI-1930 burn site*. FluxNet; University of California - Irvine. https://doi.org/10.18140/FLX/1440037
Goulden, M. (2016c). *FLUXNET2015 CA-NS3 UCI-1964 burn site*. FluxNet; University of California - Irvine. https://doi.org/10.18140/FLX/1440038
Goulden, M. (2016d). *FLUXNET2015 CA-NS4 UCI-1964 burn site wet*. FluxNet; University of California - Irvine. https://doi.org/10.18140/FLX/1440039

Goulden, M. (2016e). *FLUXNET2015 CA-NS5 UCI-1981 burn site*. FluxNet; University of California - Irvine. https://doi.org/10.18140/FLX/1440040
Goulden, M. (2016f). *FLUXNET2015 CA-NS6 UCI-1989 burn site*. FluxNet; University of California - Irvine. https://doi.org/10.18140/FLX/1440041
Goulden, M. (2016g). *FLUXNET2015 CA-NS7 UCI-1998 burn site*. FluxNet; University of California - Irvine. https://doi.org/10.18140/FLX/1440042
Gruening, C., Goded, I., Cescatti, A., Manca, G., & Seufert, G. (2016). *FLUXNET2015 IT-SRo San Rossore*. FluxNet; European Commission - Joint Research Centre. https://doi.org/10.18140/FLX/1440176
Gruening, C., Goded, I., Cescatti, A., & Pokorska, O. (2016a). *FLUXNET2015 IT-Isp Ispra ABC-IS*. FluxNet; European Commission - Joint Research Centre. https://doi.org/10.18140/FLX/1440234
Gruening, C., Goded, I., Cescatti, A., & Pokorska, O. (2016b). *FLUXNET2015 IT-SR2 San Rossore 2*. FluxNet; European Commission - Joint Research Centre. https://doi.org/10.18140/FLX/1440236
Grünwald, T., & Bernhofer, C. (2007). A decade of carbon, water and energy flux measurements of an old spruce forest at the Anchor Station Tharandt. *Tellus B*, *59*(3). https://doi.org/10.3402/tellusb.v59i3.17000
Guan, D.-X., Wu, J.-B., Zhao, X.-S., Han, S.-J., Yu, G.-R., Sun, X.-M., & Jin, C.-J. (2006). CO_2 fluxes over an old, temperate mixed forest in northeastern China. *Agricultural and Forest Meteorology*, *137*(3–4), 138–149. https://doi.org/10.1016/j.agrformet.2006.02.003
Hansen, B. U. (2016). *FLUXNET2015 GL-NuF Nuuk Fen*. FluxNet; University of Copenhagen; University of Aarhus; Asiaq - Greenland Survey. https://doi.org/10.18140/FLX/1440222
Hommeltenberg, J., Schmid, H. P., Drösler, M., & Werle, P. (2014). Can a bog drained for forestry be a stronger carbon sink than a natural bog forest? *Biogeosciences*, *11*(13), 3477–3493. https://doi.org/10.5194/bg-11-3477-2014
Hutley, L. B., Beringer, J., Isaac, P. R., Hacker, J. M., & Cernusak, L. A. (2011). A sub-continental scale living laboratory: Spatial patterns of savanna vegetation over a rainfall gradient in northern Australia. *Agricultural and Forest Meteorology*, *151*(11), 1417–1428. https://doi.org/10.1016/j.agrformet.2011.03.002
Hörtnagl, L., Eugster, W., Buchmann, N., Paul-Limoges, E., Etzold, S., & Haeni, M. (2016a). *FLUXNET2015 CH-Lae Laegern*. FluxNet; ETH Zurich. https://doi.org/10.18140/FLX/1440134
Hörtnagl, L., Eugster, W., Merbold, L., Buchmann, N., Gharun, M., Etzold, S., et al. (2016b). *FLUXNET2015 CH-Dav Davos*. FluxNet; ETH Zurich. https://doi.org/10.18140/FLX/1440132
Hörtnagl, L., Feigenwinter, I., Fuchs, K., Merbold, L., Buchmann, N., Eugster, W., & Zeeman, M. (2016c). *FLUXNET2015 CH-Cha Chamau*. FluxNet; ETH Zurich. https://doi.org/10.18140/FLX/1440131
Hörtnagl, L., Feigenwinter, I., Fuchs, K., Merbold, L., Buchmann, N., Eugster, W., & Zeeman, M. (2016d). *FLUXNET2015 CH-Fru Früebüel*. FluxNet; ETH Zurich. https://doi.org/10.18140/FLX/1440133
Hörtnagl, L., Maier, R., Eugster, W., Buchmann, N., & Emmel, C. (2016e). *FLUXNET2015 CH-Oe2 Oensingen crop*. FluxNet; ETH Zurich. https://doi.org/10.18140/FLX/1440136
Ibrom, A., & Pilegaard, K. (2016). *FLUXNET2015 DK-Sor Soroe*. FluxNet; Technical University of Denmark (DTU). https://doi.org/10.18140/FLX/1440155
Ikawa, H., Nakai, T., Busey, R. C., Kim, Y., Kobayashi, H., Nagai, S., et al. (2015). Understory CO_2, sensible heat, and latent heat fluxes in a black spruce forest in interior Alaska. *Agricultural and Forest Meteorology*, *214–215*, 80–90. https://doi.org/10.1016/j.agrformet.2015.08.247
Imer, D., Merbold, L., Eugster, W., & Buchmann, N. (2013). Temporal and spatial variations of soil CO_2, CH_4 and N_2O fluxes at three differently managed grasslands. *Biogeosciences*, *10*(9), 5931–5945. https://doi.org/10.5194/bg-10-5931-2013
Jacobs, C. M. J., Jacobs, A. F. G., Bosveld, F. C., Hendriks, D. M. D., Hensen, A., Kroon, P. S., et al. (2007). Variability of annual CO_2 exchange from Dutch grasslands. *Biogeosciences*, *4*(5), 803–816. https://doi.org/10.5194/bg-4-803-2007
Jammet, M., Crill, P., Dengel, S., & Friborg, T. (2015). Large methane emissions from a subarctic lake during spring thaw: Mechanisms and landscape significance. *Journal of Geophysical Research: Biogeosciences*, *120*(11), 2289–2305. https://doi.org/10.1002/2015jg003137
Kato, T., Tang, Y., Gu, S., Hirota, M., Du, M., Li, Y., & Zhao, X. (2006). Temperature and biomass influences on interannual changes in CO_2 exchange in an alpine meadow on the Qinghai-Tibetan Plateau. *Global Change Biology*, *12*(7), 1285–1298. https://doi.org/10.1111/j.1365-2486.2006.01153.x
Keppel-Aleks, G., Wennberg, P. O., Washenfelder, R. A., Wunch, D., Schneider, T., Toon, G. C., et al. (2012). The imprint of surface fluxes and transport on variations in total column carbon dioxide. *Biogeosciences*, *9*(3), 875–891. https://doi.org/10.5194/bg-9-875-2012
Kilinc, M., Beringer, J., Hutley, L. B., Tapper, N. J., & McGuire, D. A. (2013). Carbon and water exchange of the world's tallest angiosperm forest. *Agricultural and Forest Meteorology*, *182–183*, 215–224. https://doi.org/10.1016/j.agrformet.2013.07.003
Klatt, J., Schmid, H. P., Mauder, M., & Steinbrecher, R. (2016). *FLUXNET2015 DE-SfN Schechenfilz Nord*. FluxNet; Karlsruhe Institute of Technology, IMK-IFU. https://doi.org/10.18140/FLX/1440219
Knohl, A., Tiedemann, F., Kolle, O., Schulze, E.-D., Anthoni, P., Kutsch, W., et al. (2016). *FLUXNET2015 DE-Lnf Leinefelde*. FluxNet; University of Goettingen, Bioclimatology. https://doi.org/10.18140/FLX/1440150
Knohl, A., Tiedemann, F., Kolle, O., Schulze, E.-D., Kutsch, W., Herbst, M., & Siebicke, L. (2016). *FLUXNET2015 DE-Hai Hainich*. FluxNet; University of Goettingen, Bioclimatology. https://doi.org/10.18140/FLX/1440148
Kobayashi, H., & Suzuki, R. (2016). *FLUXNET2015 US-Prr Poker Flat Research Range Black Spruce Forest*. FluxNet; Japan Agency for Marine-Earth Science and Technology. https://doi.org/10.18140/FLX/1440113
Korkiakoski, M., Tuovinen, J.-P., Aurela, M., Koskinen, M., Minkkinen, K., Ojanen, P., et al. (2017). Methane exchange at the peatland forest floor – Automatic chamber system exposes the dynamics of small fluxes. *Biogeosciences*, *14*(7), 1947–1967. https://doi.org/10.5194/bg-14-1947-2017
Kotani, A. (2016a). *FLUXNET2015 JP-MBF Moshiri Birch Forest Site*. FluxNet; Nagoya University. https://doi.org/10.18140/FLX/1440238
Kotani, A. (2016b). *FLUXNET2015 JP-SMF Seto Mixed Forest Site*. FluxNet; Nagoya University. https://doi.org/10.18140/FLX/1440239
Kurbatova, J., Li, C., Varlagin, A., Xiao, X., & Vygodskaya, N. (2008). Modeling carbon dynamics in two adjacent spruce forests with different soil conditions in Russia. *Biogeosciences*, *5*(4), 969–980. https://doi.org/10.5194/bg-5-969-2008
Kurc, S. (2016). *FLUXNET2015 US-SRC Santa Rita Creosote*. FluxNet; University of Arizona. https://doi.org/10.18140/FLX/1440098
Kutsch, W. L., Merbold, L., & Kolle, O. (2016). *FLUXNET2015 ZM-Mon Mongu*. FluxNet; Max-Planck Institute for Biogeochemistry. https://doi.org/10.18140/FLX/1440189
Kutzbach, L., Sachs, T., Boike, J., Wille, C., Schreiber, P., Langer, M., & Pfeiffer, E.-M. (2016). *FLUXNET2015 RU-Sam Samoylov*. Helmholtz Centre for Polar and Marine Research, Periglacial Research Unit, 14473 Potsdam, Germany; Institute of Soil Science, Center for Earth System Research and Sustainability (CEN), Universität Hamburg, 20146 Hamburg, Germany; GFZ German Research Centre for Geosciences, 14473 Potsdam, Germany. FluxNet; Alfred Wegener Institute. https://doi.org/10.18140/FLX/1440185

Kwon, H., Oechel, W. C., Zulueta, R. C., & Hastings, S. J. (2006). Effects of climate variability on carbon sequestration among adjacent wet sedge tundra and moist tussock tundra ecosystems. *Journal of Geophysical Research: Biogeosciences*, *111*(G3). https://doi.org/10.1029/2005jg000036

Law, B. (2016a). *FLUXNET2015 US-Me1 Metolius - Eyerly burn*. FluxNet; Oregon State University. https://doi.org/10.18140/FLX/1440078

Law, B. (2016b). *FLUXNET2015 US-Me2 Metolius mature ponderosa pine*. FluxNet; Oregon State University. https://doi.org/10.18140/FLX/1440079

Law, B. (2016c). *FLUXNET2015 US-Me3 Metolius-second young aged pine*. FluxNet; Oregon State University. https://doi.org/10.18140/FLX/1440080

Law, B. (2016d). *FLUXNET2015 US-Me4 Metolius-old aged ponderosa pine*. FluxNet; Oregon State University. https://doi.org/10.18140/FLX/1440081

Law, B. (2016e). *FLUXNET2015 US-Me5 Metolius-first young aged pine*. FluxNet; Oregon State University. https://doi.org/10.18140/FLX/1440082

Law, B. (2016f). *FLUXNET2015 US-Me6 Metolius Young Pine Burn*. FluxNet; Oregon State University. https://doi.org/10.18140/FLX/1440099

Leuning, R., Cleugh, H. A., Zegelin, S. J., & Hughes, D. (2005). Carbon and water fluxes over a temperate Eucalyptus forest and a tropical wet/dry savanna in Australia: Measurements and comparison with MODIS remote sensing estimates. *Agricultural and Forest Meteorology*, *129*(3–4), 151–173. https://doi.org/10.1016/j.agrformet.2004.12.004

Liddell, M. J. (2016). *FLUXNET2015 AU-Rob Robson Creek, Queensland, Australia*. FluxNet; James Cook University. https://doi.org/10.18140/FLX/1440203

Lindauer, M., Schmid, H., Grote, R., Mauder, M., Steinbrecher, R., & Wolpert, B. (2014). Net ecosystem exchange over a non-cleared wind-throw-disturbed upland spruce forest—Measurements and simulations. *Agricultural and Forest Meteorology*, *197*, 219–234. https://doi.org/10.1016/j.agrformet.2014.07.005

Lindauer, M., Steinbrecher, R., Wolpert, B., Mauder, M., & Schmid, H. P. (2016). *FLUXNET2015 DE-Lkb Lackenberg*. FluxNet; Karlsruhe Institute of Technology, IMK-IFU. https://doi.org/10.18140/FLX/1440214

Lohila, A., Aurela, M., Tuovinen, J., & Laurila, T. (2004). Annual CO_2 exchange of a peat field growing spring barley or perennial forage grass. *Journal of Geophysical Research: Atmospheres*, *109*(D18). https://doi.org/10.1029/2004jd004715

Lohila, A., Aurela, M., Tuovinen, J.-P., Hatakka, J., & Laurila, T. (2016). *FLUXNET2015 FI-Jok Jokioinen*. FluxNet; Finnish Meteorological Institute. https://doi.org/10.18140/FLX/1440159

Lohila, A., Korkiakoski, M., Tuovinen, J.-P., Hatakka, J., Aurela, M., Rainne, J., et al. (2016). *FLUXNET2015 FI-Let Lettosuo*. FluxNet; Finnish Meteorological Institute. https://doi.org/10.18140/FLX/1440227

Loubet, B., Laville, P., Lehuger, S., Larmanou, E., Fléchard, C., Mascher, N., et al. (2011). Carbon, nitrogen and Greenhouse gases budgets over a four years crop rotation in northern France. *Plant and Soil*, *343*(1–2), 109–137. https://doi.org/10.1007/s11104-011-0751-9

Lund, M., Falk, J. M., Friborg, T., Mbufong, H. N., Sigsgaard, C., Soegaard, H., & Tamstorf, M. P. (2012). Trends in CO_2 exchange in a high Arctic tundra heath, 2000–2010. *Journal of Geophysical Research: Biogeosciences*, *117*(G2). https://doi.org/10.1029/2011jg001901

Lund, M., Jackowicz-Korczyński, M., & Abermann, J. (2016a). *FLUXNET2015 GL-ZaF Zackenberg Fen*. FluxNet; Aarhus University. https://doi.org/10.18140/FLX/1440223

Lund, M., Jackowicz-Korczyński, M., & Abermann, J. (2016b). *FLUXNET2015 GL-ZaH Zackenberg Heath*. FluxNet; Aarhus University. https://doi.org/10.18140/FLX/1440224

López-Ballesteros, A., Serrano-Ortiz, P., Kowalski, A. S., Sánchez-Cañete, E. P., Scott, R. L., & Domingo, F. (2017). Subterranean ventilation of allochthonous CO_2 governs net CO_2 exchange in a semiarid Mediterranean grassland. *Agricultural and Forest Meteorology*, *234–235*, 115–126. https://doi.org/10.1016/j.agrformet.2016.12.021

López-Blanco, E., Lund, M., Williams, M., Tamstorf, M. P., Westergaard-Nielsen, A., Exbrayat, J.-F., et al. (2017). Exchange of CO_2 in Arctic tundra: Impacts of meteorological variations and biological disturbance. *Biogeosciences*, *14*(19), 4467–4483. https://doi.org/10.5194/bg-14-4467-2017

Lüers, J., Westermann, S., Piel, K., & Boike, J. (2014). Annual CO_2 budget and seasonal CO_2 exchange signals at a high Arctic permafrost site on Spitsbergen, Svalbard archipelago. *Biogeosciences*, *11*(22), 6307–6322. https://doi.org/10.5194/bg-11-6307-2014

Macfarlane, C., Lambert, P., Byrne, J., Johnstone, C., & Smart, N. (2016). *FLUXNET2015 AU-Gin Gingin*. FluxNet; Edith Cowan University (Centre for Ecosystem Management). https://doi.org/10.18140/FLX/1440199

Magliulo, V., Di Tommasi, P., Famulari, D., Gasbarra, D., Vitale, L., & Manco, A. (2016). *FLUXNET2015 IT-BCi Borgo Cioffi*. FluxNet; CNR ISAFOM. https://doi.org/10.18140/FLX/1440166

Mammarella, I., Vesala, T., Keronen, P., Kolari, P., Launiainen, S., Pumpanen, J., et al. (2016). *FLUXNET2015 FI-Hyy Hyytiala*. FluxNet; University of Helsinki. https://doi.org/10.18140/FLX/1440158

Manca, G., & Goded, I. (2016). *FLUXNET2015 IT-PT1 Parco Ticino forest*. FluxNet; European Commission - DG Joint Research Centre. https://doi.org/10.18140/FLX/1440172

Marcolla, B., Cescatti, A., Manca, G., Zorer, R., Cavagna, M., Fiora, A., et al. (2011). Climatic controls and ecosystem responses drive the inter-annual variability of the net ecosystem exchange of an alpine meadow. *Agricultural and Forest Meteorology*, *151*(9), 1233–1243. https://doi.org/10.1016/j.agrformet.2011.04.015

Marcolla, B., Pitacco, A., & Cescatti, A. (2003). Canopy architecture and turbulence structure in a Coniferous forest. *Boundary-Layer Meteorology*, *108*(1), 39–59. https://doi.org/10.1023/a:1023027709805

Margolis, H. A. (2016). *FLUXNET2015 CA-Qfo Quebec - Eastern Boreal, Mature Black Spruce*. FluxNet; Université Laval. https://doi.org/10.18140/FLX/1440045

Marras, S., Pyles, R., Sirca, C., Paw U, K., Snyder, R., Duce, P., & Spano, D. (2011). Evaluation of the Advanced Canopy–Atmosphere–Soil Algorithm (ACASA) model performance over mediterranean maquis ecosystem. *Agricultural and Forest Meteorology*, *151*(6), 730–745. https://doi.org/10.1016/j.agrformet.2011.02.004

Massman, B. (2016a). *FLUXNET2015 US-GBT GLEES Brooklyn Tower*. FluxNet; USDA Forest Service. https://doi.org/10.18140/FLX/1440118

Massman, B. (2016b). *FLUXNET2015 US-GLE GLEES*. FluxNet; USDA Forest Service. https://doi.org/10.18140/FLX/1440069

Matamala, R. (2016). *FLUXNET2015 US-IB2 Fermi National Accelerator Laboratory- Batavia (Prairie site)*. FluxNet; Argonne National Laboratory. https://doi.org/10.18140/FLX/1440072

Matsumoto, K., Ohta, T., Nakai, T., Kuwada, T., Daikoku, K., Iida, S., et al. (2008). Energy consumption and evapotranspiration at several boreal and temperate forests in the Far East. *Agricultural and Forest Meteorology*, *148*(12), 1978–1989. https://doi.org/10.1016/j.agrformet.2008.09.008

Matteucci, G. (2016). *FLUXNET2015 IT-Col Collelongo*. FluxNet; Istituto di Ecologia e Idrologia Forestale CNR. https://doi.org/10.18140/FLX/1440167

Maximov, T. (2016). *FLUXNET2015 RU-SkP Yakutsk Spasskaya Pad larch*. FluxNet; IBPC. https://doi.org/10.18140/FLX/1440243
McCaughey, H. (2016). *FLUXNET2015 CA-Gro Ontario - Groundhog river, boreal Mixedwood forest*. FluxNet; Queen's University. https://doi.org/10.18140/FLX/1440034
McEwing, K. R., Fisher, J. P., & Zona, D. (2015). Environmental and vegetation controls on the spatial variability of CH_4 emission from wet-sedge and tussock tundra ecosystems in the Arctic. *Plant and Soil*, *388*(1–2), 37–52. https://doi.org/10.1007/s11104-014-2377-1
McHugh, I. D., Beringer, J., Cunningham, S. C., Baker, P. J., Cavagnaro, T. R., Mac Nally, R., & Thompson, R. M. (2017). Interactions between nocturnal turbulent flux, storage and advection at an "ideal" eucalypt woodland site. *Biogeosciences*, *14*(12), 3027–3050. https://doi.org/10.5194/bg-14-3027-2017
Merbold, L., Ardö, J., Arneth, A., Scholes, R. J., Nouvellon, Y., de Grandcourt, A., et al. (2009). Precipitation as driver of carbon fluxes in 11 African ecosystems. *Biogeosciences*, *6*(6), 1027–1041. https://doi.org/10.5194/bg-6-1027-2009
Merbold, L., Eugster, W., Stieger, J., Zahniser, M., Nelson, D., & Buchmann, N. (2014). Greenhouse gas budget (CO_2, $CH_4$and N_2O) of intensively managed grassland following restoration. *Global Change Biology*, *20*(6), 1913–1928. https://doi.org/10.1111/gcb.12518
Merbold, L., Kutsch, W. L., Corradi, C., Kolle, O., Rebmann, C., Stoy, P. C., et al. (2009). Artificial drainage and associated carbon fluxes (CO_2/CH_4) in a tundra ecosystem. *Global Change Biology*, *15*(11), 2599–2614. https://doi.org/10.1111/j.1365-2486.2009.01962.x
Merbold, L., Rebmann, C., & Corradi, C. (2016). *FLUXNET2015 RU-Che Cherski*. FluxNet; Max-Planck Institute for Biogeochemistry. https://doi.org/10.18140/FLX/1440181
Meyer, W., Cale, P., Koerber, G., Ewenz, C., & Sun, Q. (2016). *FLUXNET2015 AU-Cpr Calperum*. FluxNet; University of Adelaide. https://doi.org/10.18140/FLX/1440195
Meyer, W. S., Kondrlovà, E., & Koerber, G. R. (2015). Evaporation of perennial semi-arid woodland in southeastern Australia is adapted for irregular but common dry periods. *Hydrological Processes*, *29*(17), 3714–3726. https://doi.org/10.1002/hyp.10467
Meyers, T. (2016). *FLUXNET2015 US-Goo Goodwin Creek*. FluxNet; NOAA/ARL. https://doi.org/10.18140/FLX/1440070
Migliavacca, M., Meroni, M., Busetto, L., Colombo, R., Zenone, T., Matteucci, G., et al. (2009). Modeling gross primary production of Agro-forestry ecosystems by assimilation of satellite-derived information in a process-based model. *Sensors*, *9*(2), 922–942. https://doi.org/10.3390/s90200922
Montagnani, L., Manca, G., Canepa, E., Georgieva, E., Acosta, M., Feigenwinter, C., et al. (2009). A new mass conservation approach to the study of CO_2 advection in an alpine forest. *Journal of Geophysical Research: Atmospheres*, *114*(D7). https://doi.org/10.1029/2008jd010650
Montagnani, L., & Minerbi, S. (2016). *FLUXNET2015 IT-Ren Renon*. FluxNet; Autonomous Province of Bolzano, Forest Services. https://doi.org/10.18140/FLX/1440173
Moors, E., & Elbers, J. (2016). *FLUXNET2015 NL-Loo Loobos*. FluxNet; ALTERRA/Wageningen Environmental Research. https://doi.org/10.18140/FLX/1440178
Moors, E. J. (2012). *Water use of forests in The Netherlands* (PhD thesis). Vrije Universiteit Amsterdam. https://edepot.wur.nl/213926
Moureaux, C., Debacq, A., Bodson, B., Heinesch, B., & Aubinet, M. (2006). Annual net ecosystem carbon exchange by a sugar beet crop. *Agricultural and Forest Meteorology*, *139*(1–2), 25–39. https://doi.org/10.1016/j.agrformet.2006.05.009
Munger, J. W. (2016). *FLUXNET2015 US-Ha1 Harvard Forest EMS Tower (HFR1)*. FluxNet; Harvard University. https://doi.org/10.18140/FLX/1440071
Neirynck, J., Verbeeck, H., Carrara, A., Kowalski, A. S., Ceulemans, R., Janssens, I. A., et al. (2016). *FLUXNET2015 BE-Bra Brasschaat*. FluxNet; University of Antwerp. https://doi.org/10.18140/FLX/1440128
Novick, K., & Phillips, R. (2016). *FLUXNET2015 US-MMS Morgan Monroe State Forest*. FluxNet; Indiana University. https://doi.org/10.18140/FLX/1440083
Olesen, J. (2016). *FLUXNET2015 DK-Fou Foulum*. FluxNet; Danish Institute of Agricultural Sciences. https://doi.org/10.18140/FLX/1440154
Ourcival, J.-M. (2016). *FLUXNET2015 FR-Pue Puechabon*. FluxNet; CNRS. https://doi.org/10.18140/FLX/1440164
Papale, D., Tirone, G., Valentini, R., Arriga, N., Belelli, L., Consalvo, C., et al. (2016). *FLUXNET2015 IT-Ro2 Roccarespampani 2*. FluxNet; University of Tuscia - Vietrbo. https://doi.org/10.18140/FLX/1440175
Pendall, E., & Griebel, A. (2016). *FLUXNET2015 AU-Cum Cumberland Plains*. FluxNet; Western Sydney University. https://doi.org/10.18140/FLX/1440196
Pilegaard, K., & Ibrom, A. (2016). *FLUXNET2015 DK-Eng Enghave*. FluxNet; Technical University of Denmark (DTU). https://doi.org/10.18140/FLX/1440153
Pilegaard, K., Ibrom, A., Courtney, M. S., Hummelshøj, P., & Jensen, N. O. (2011). Increasing net CO_2 uptake by a Danish beech forest during the period from 1996 to 2009. *Agricultural and Forest Meteorology*, *151*(7), 934–946. https://doi.org/10.1016/j.agrformet.2011.02.013
Posse, G., Lewczuk, N., Richter, K., & Cristiano, P. (2016a). Carbon and water vapor balance in a subtropical pine plantation. *iForest - Biogeosciences and Forestry*, *9*(5), 736–742. https://doi.org/10.3832/ifor1815-009
Posse, G., Lewczuk, N., Richter, K., & Cristiano, P. (2016b). *FLUXNET2015 AR-Vir Virasoro*. FluxNet; Instituto Nacional de Tecnología Agropecuaria. https://doi.org/10.18140/FLX/1440192
Poveda, F. D., Ballesteros, A. L., Cañete, E. P. S., Ortiz, P. S., Jiménez, M. R. M., Priego, O. P., & Kowalski, A. S. (2016). *FLUXNET2015 ES-Amo Amoladeras*. FluxNet; Estación Experimental de Zona Áridas (EEZA, CSIC). https://doi.org/10.18140/FLX/1440156
Prescher, A.-K., Grünwald, T., & Bernhofer, C. (2010). Land use regulates carbon budgets in eastern Germany: From NEE to NBP. *Agricultural and Forest Meteorology*, *150*(7–8), 1016–1025. https://doi.org/10.1016/j.agrformet.2010.03.008
Rambal, S., Joffre, R., Ourcival, J. M., Cavender-Bares, J., & Rocheteau, A. (2004). The growth respiration component in eddy CO_2 flux from a Quercus ilex mediterranean forest. *Global Change Biology*, *10*(9), 1460–1469. https://doi.org/10.1111/j.1365-2486.2004.00819.x
Reed, D. E., Ewers, B. E., Pendall, E., Naithani, K. J., Kwon, H., & Kelly, R. D. (2018). Biophysical factors and canopy coupling control ecosystem water and carbon fluxes of semiarid Sagebrush ecosystems. *Rangeland Ecology & Management*, *71*(3), 309–317. https://doi.org/10.1016/j.rama.2018.01.003
Reverter, B. R., Perez-Cañete, E. S., & Kowalski, A. S. (2016a). *FLUXNET2015 ES-LgS Laguna Seca*. FluxNet; Universidad de Granada. https://doi.org/10.18140/FLX/1440225
Reverter, B. R., Perez-Cañete, E. S., & Kowalski, A. S. (2016b). *FLUXNET2015 ES-Ln2 Lanjaron-Salvage logging*. Universidad de Granada. https://doi.org/10.18140/FLX/1440226
Reverter, B. R., Sánchez-Cañete, E. P., Resco, V., Serrano-Ortiz, P., Oyonarte, C., & Kowalski, A. S. (2010). Analyzing the major drivers of NEE in a Mediterranean alpine shrubland. *Biogeosciences*, *7*(9), 2601–2611. https://doi.org/10.5194/bg-7-2601-2010
Rey, A., Pegoraro, E., Tedeschi, V., De Parri, I., Jarvis, P. G., & Valentini, R. (2002). Annual variation in soil respiration and its components in a coppice oak forest in Central Italy. *Global Change Biology*, *8*(9), 851–866. https://doi.org/10.1046/j.1365-2486.2002.00521.x
Runkle, B. R. K., Rigby, J. R., Reba, M. L., Anapalli, S. S., Bhattacharjee, J., Krauss, K. W., et al. (2017). Delta-Flux: An eddy covariance network for a climate-smart lower Mississippi basin. *Agricultural & Environmental Letters*, *2*(1). https://doi.org/10.2134/ael2017.01.0003

Sabbatini, S., Arriga, N., Bertolini, T., Castaldi, S., Chiti, T., Consalvo, C., et al. (2016). Greenhouse gas balance of cropland conversion to bioenergy poplar short-rotation coppice. *Biogeosciences*, *13*(1), 95–113. https://doi.org/10.5194/bg-13-95-2016

Sabbatini, S., Arriga, N., Gioli, B., & Papale, D. (2016). *FLUXNET2015 IT-CA2 Castel d'Asso2*. FluxNet; CNR IBIMET; University of Tuscia - Vietrbo. https://doi.org/10.18140/FLX/1440231

Sabbatini, S., Arriga, N., Matteucci, G., & Papale, D. (2016). *FLUXNET2015 IT-CA3 Castel d'Asso 3*. FluxNet; University of Tuscia - Vietrbo; CNR IBAF. https://doi.org/10.18140/FLX/1440232

Sabbatini, S., Arriga, N., & Papale, D. (2016). *FLUXNET2015 IT-CA1 Castel d'Asso1*. FluxNet; University of Tuscia - Vietrbo. https://doi.org/10.18140/FLX/1440230

Sachs, T., Wille, C., Larmanou, E., & Franz, D. (2016). *FLUXNET2015 DE-Zrk Zarnekow*. FluxNet; GFZ German Research Centre for Geosciences. https://doi.org/10.18140/FLX/1440221

Saleska, S. (2016). *FLUXNET2015 BR-Sa1 Santarem-Km67-primary forest*. FluxNet; University of Arizona. https://doi.org/10.18140/FLX/1440032

Sanchez, C. R., Sturtevant, C., Szutu, D., Baldocchi, D., Eichelmann, E., & Knox, S. (2016). *FLUXNET2015 US-Tw4 Twitchell East End Wetland*. FluxNet; University of California. https://doi.org/10.18140/FLX/1440111

Schmidt, M., Reichenau, T., Fiener, P., & Schneider, K. (2012). The carbon budget of a winter wheat field: An eddy covariance analysis of seasonal and inter-annual variability. *Agricultural and Forest Meteorology*, *165*, 114–126. https://doi.org/10.1016/j.agrformet.2012.05.012

Schneider, K., & Schmidt, M. (2016). *FLUXNET2015 DE-Seh Selhausen*. FluxNet; University of Cologne. https://doi.org/10.18140/FLX/1440217

Scholes, B. (2016). *FLUXNET2015 ZA-Kru Skukuza*. FluxNet; University of the Witwatersrand. https://doi.org/10.18140/FLX/1440188

Schroder, I. (2014). Arcturus Emerald OzFlux tower site OzFlux: Australian and New Zealand flux research and monitoring. https://data.ozflux.org.au/portal/pub/viewColDetails.jspx?collection.id=1882850&collection.owner.id=2021502&viewType=anonymous

Schroder, I., Zegelin, S., Palu, T., & Feitz, A. (2016). *FLUXNET2015 AU-Emr Emerald*. FluxNet; CSIRO; Geoscience Australia. https://doi.org/10.18140/FLX/1440198

Scott, R. (2016a). *FLUXNET2015 US-SRG Santa Rita Grassland*. FluxNet; United States Department of Agriculture. https://doi.org/10.18140/FLX/1440114

Scott, R. (2016b). *FLUXNET2015 US-SRM Santa Rita Mesquite*. FluxNet; United States Department of Agriculture. https://doi.org/10.18140/FLX/1440090

Scott, R. (2016c). *FLUXNET2015 US-Whs Walnut Gulch Lucky Hills Shrub*. FluxNet; United States Department of Agriculture. https://doi.org/10.18140/FLX/1440097

Scott, R. (2016d). *FLUXNET2015 US-Wkg Walnut Gulch Kendall grasslands*. FluxNet; United States Department of Agriculture. https://doi.org/10.18140/FLX/1440096

Serrano-Ortiz, P., Domingo, F., Cazorla, A., Were, A., Cuezva, S., Villagarcía, L., et al. (2009). Interannual CO_2 exchange of a sparse Mediterranean shrubland on a carbonaceous substrate. *Journal of Geophysical Research: Biogeosciences*, *114*(G4). https://doi.org/10.1029/2009jg000983

Shao, C. (2016a). *FLUXNET2015 CN-Du3 Duolun Degraded Meadow*. FluxNet. https://doi.org/10.18140/FLX/1440210

Shao, C. (2016b). *FLUXNET2015 CN-Sw2 Siziwang Grazed (SZWG)*. FluxNet. https://doi.org/10.18140/FLX/1440212

Shi, P., Sun, X., Xu, L., Zhang, X., He, Y., Zhang, D., & Yu, G. (2006). Net ecosystem CO_2 exchange and controlling factors in a steppe—Kobresia meadow on the Tibetan Plateau. *Science in China Series D: Earth Sciences*, *49*(S2), 207–218. https://doi.org/10.1007/s11430-006-8207-4

Shi, P., Zhang, X., & He, Y. (2016). *FLUXNET2015 CN-Dan Dangxiong*. FluxNet; IGSNRR Chinese Academy of Sciences. https://doi.org/10.18140/FLX/1440138

Sigut, L., Havrankova, K., Jocher, G., Pavelka, M., & Janouš, D. (2016a). *FLUXNET2015 CZ-BK1 Bily Kriz forest*. FluxNet; Global Change Research Institute CAS. https://doi.org/10.18140/FLX/1440143

Sigut, L., Havrankova, K., Jocher, G., Pavelka, M., & Janouš, D. (2016b). *FLUXNET2015 CZ-BK2 Bily Kriz grassland*. FluxNet; Global Change Research Institute CAS. https://doi.org/10.18140/FLX/1440144

Soegaard, H. (1999). Carbon dioxide exchange in a high-arctic fen estimated by eddy covariance measurements and modelling. *Global Change Biology*, *5*(5), 547. https://doi.org/10.1046/j.1365-2486.1999.00250.x

Spano, D., Duce, P., Marras, S., Sirca, C., Arca, A., Zara, P., & Ventura, A. (2016). *FLUXNET2015 IT-Noe Arca di Noe - Le Prigionette*. FluxNet; University of Sassari; CNR-Ibimet Sassari. https://doi.org/10.18140/FLX/1440171

Stocker, B. D., & Hufkens, K. (2021). *geco-bern/rpmodel on Github*. Zenodo. https://doi.org/10.5281/zenodo.3359706

Sturtevant, C., Szutu, D., Baldocchi, D., Matthes, J. H., Oikawa, P., & Chamberlain, S. D. (2016). *FLUXNET2015 US-Myb Mayberry Wetland*. FluxNet; University of California. https://doi.org/10.18140/FLX/1440105

Sullivan, R. C., Cook, D. R., Ghate, V. P., Kotamarthi, V. R., & Feng, Y. (2019). Improved spatiotemporal representativeness and bias reduction of satellite-based evapotranspiration retrievals via use of in situ meteorology and constrained canopy surface resistance. *Journal of Geophysical Research: Biogeosciences*, *124*(2), 342–352. https://doi.org/10.1029/2018jg004744

Suni, T., Rinne, J., Reissell, A., Altimir, N., Keronen, P., Rannik, U., et al. (2003). Long-term measurements of surface fluxes above a Scots pine forest in hyytiala, southern Finland, 1996-2001. *Boreal Environment Research*, *8*(4), 287–301. Retrieved from https://www.borenv.net/BER/archive/pdfs/ber8/ber8-287.pdf

Suyker, A. (2016a). *FLUXNET2015 US-Ne1 Mead - irrigated continuous maize site*. FluxNet; University of Nebraska - Lincoln. https://doi.org/10.18140/FLX/1440084

Suyker, A. (2016b). *FLUXNET2015 US-Ne2 Mead - irrigated maize-soybean rotation site*. FluxNet; University of Nebraska - Lincoln. https://doi.org/10.18140/FLX/1440085

Suyker, A. (2016c). *FLUXNET2015 US-Ne3 Mead - rainfed maize-soybean rotation site*. FluxNet; University of Nebraska - Lincoln. https://doi.org/10.18140/FLX/1440086

Szutu, D., & Baldocchi, D. (2016). *FLUXNET2015 US-Tw3 Twitchell Alfalfa*. FluxNet; University of California. https://doi.org/10.18140/FLX/1440110

Szutu, D., Baldocchi, D., Eichelmann, E., & Knox, S. (2016). *FLUXNET2015 US-Tw1 Twitchell Wetland West Pond*. FluxNet; University of California. https://doi.org/10.18140/FLX/1440108

Tagesson, T., Ardö, J., & Fensholt, R. (2016). *FLUXNET2015 SN-Dhr Dahra*. FluxNet; Lund University. https://doi.org/10.18140/FLX/1440246

Tagesson, T., Fensholt, R., Guiro, I., Rasmussen, M. O., Huber, S., Mbow, C., et al. (2014). Ecosystem properties of semiarid savanna grassland in West Africa and its relationship with environmental variability. *Global Change Biology*, *21*(1), 250–264. https://doi.org/10.1111/gcb.12734

Tang, Y., Kato, T., & Du, M. (2016). *FLUXNET2015 CN-HaM Haibei Alpine Tibet site*. FluxNet; National Institute for Environmental Studies. https://doi.org/10.18140/FLX/1440190

Tedeschi, V., Rey, A., Manca, G., Valentini, R., Jarvis, P. G., & Borghetti, M. (2005). Soil respiration in a Mediterranean oak forest at different developmental stages after coppicing. *Global Change Biology*, *12*(1), 110–121. https://doi.org/10.1111/j.1365-2486.2005.01081.x

Thum, T., Aalto, T., Laurila, T., Aurela, M., Kolari, P., & Hari, P. (2007). Parametrization of two photosynthesis models at the canopy scale in a northern boreal Scots pine forest. *Tellus B*, *59*(5). https://doi.org/10.3402/tellusb.v59i5.17066

Torn, M. (2016a). *FLUXNET2015 US-ARb ARM Southern Great Plains burn site- Lamont*. FluxNet; Lawrence Berkeley National Laboratory. https://doi.org/10.18140/FLX/1440064

Torn, M. (2016b). *FLUXNET2015 US-ARc ARM Southern Great Plains control site- Lamont*. FluxNet; Lawrence Berkeley National Laboratory. https://doi.org/10.18140/FLX/1440065

Ulke, A. G., Gattinoni, N. N., & Posse, G. (2015). Analysis and modelling of turbulent fluxes in two different ecosystems in Argentina. *International Journal of Environment and Pollution*, *58*(1/2), 52. https://doi.org/10.1504/ijep.2015.076583

Valentini, R., De Angelis, P., Matteucci, G., Monaco, R., Dore, S., & Mucnozza, G. E. S. (1996). Seasonal net carbon dioxide exchange of a beech forest with the atmosphere. *Global Change Biology*, *2*(3), 199–207. https://doi.org/10.1111/j.1365-2486.1996.tb00072.x

Valentini, R., Dore, S., Mazzenga, F., Sabbatini, S., Stefani, P., Tirone, G., & Papale, D. (2016). *FLUXNET2015 IT-Cpz Castelporziano*. FluxNet; University of Tuscia - Vietrbo. https://doi.org/10.18140/FLX/1440168

Valentini, R., Tirone, G., Vitale, D., Papale, D., Arriga, N., Belelli, L., et al. (2016). *FLUXNET2015 IT-Ro1 Roccarespampani 1*. FluxNet; University of Tuscia - Vietrbo. https://doi.org/10.18140/FLX/1440174

Van der Molen, M. K., van Huissteden, J., Parmentier, F. J. W., Petrescu, A. M. R., Dolman, A. J., Maximov, T. C., et al. (2007). The growing season greenhouse gas balance of a continental tundra site in the Indigirka lowlands, NE Siberia. *Biogeosciences*, *4*(6), 985–1003. https://doi.org/10.5194/bg-4-985-2007

Varlagin, A., Kurbatova, J., & Vygodskaya, N. (2016). *FLUXNET2015 RU-Fyo Fyodorovskoye*. FluxNet; A.N. Severtsov Institute of Ecology and Evolution. https://doi.org/10.18140/FLX/1440183

Vitale, L., Di Tommasi, P., D'Urso, G., & Magliulo, V. (2015). The response of ecosystem carbon fluxes to LAI and environmental drivers in a maize crop grown in two contrasting seasons. *International Journal of Biometeorology*, *60*(3), 411–420. https://doi.org/10.1007/s00484-015-1038-2

Wang, H., & Fu, X. (2016). *FLUXNET2015 CN-Qia Qianyanzhou*. FluxNet; IGSNRR Chinese Academy of Sciences. https://doi.org/10.18140/FLX/1440141

Wohlfahrt, G., Hammerle, A., Haslwanter, A., Bahn, M., Tappeiner, U., & Cernusca, A. (2008). Seasonal and inter-annual variability of the net ecosystem CO_2 exchange of a temperate mountain grassland: Effects of weather and management. *Journal of Geophysical Research: Atmospheres*, *113*(D8). https://doi.org/10.1029/2007jd009286

Wohlfahrt, G., Hammerle, A., & Hörtnagl, L. (2016). *FLUXNET2015 AT-Neu Neustift*. FluxNet; University of Innsbruck. https://doi.org/10.18140/FLX/1440121

Wolf, S., Eugster, W., & Buchmann, N. (2016b). *FLUXNET2015 PA-SPn Sardinilla Plantation*. FluxNet; ETH Zurich. https://doi.org/10.18140/FLX/1440180

Wolf, S., Eugster, W., & Buchmann, N. (2016c). *FLUXNET2015 PA-SPs Sardinilla-Pasture*. FluxNet; ETH Zurich. https://doi.org/10.18140/FLX/1440179

Wolf, S., Eugster, W., Potvin, C., Turner, B. L., & Buchmann, N. (2011). Carbon sequestration potential of tropical pasture compared with afforestation in Panama. *Global Change Biology*, *17*(9), 2763–2780. https://doi.org/10.1111/j.1365-2486.2011.02460.x

Woodgate, W., Van Gorsel, E., & Leuning, R. (2016). *FLUXNET2015 AU-Tum Tumbarumba*. FluxNet; CSIRO. https://doi.org/10.18140/FLX/1440126

Yee, M. S., Pauwels, V. R., Daly, E., Beringer, J., Rüdiger, C., McCabe, M. F., & Walker, J. P. (2015). A comparison of optical and microwave scintillometers with eddy covariance derived surface heat fluxes. *Agricultural and Forest Meteorology*, *213*, 226–239. https://doi.org/10.1016/j.agrformet.2015.07.004

Yu, G.-R., Wen, X.-F., Sun, X.-M., Tanner, B. D., Lee, X., & Chen, J.-Y. (2006). Overview of ChinaFLUX and evaluation of its eddy covariance measurement. *Agricultural and Forest Meteorology*, *137*(3–4), 125–137. https://doi.org/10.1016/j.agrformet.2006.02.011

Zak, D., Reuter, H., Augustin, J., Shatwell, T., Barth, M., Gelbrecht, J., & McInnes, R. J. (2015). Changes of the CO_2 and CH_4 production potential of rewetted fens in the perspective of temporal vegetation shifts. *Biogeosciences*, *12*(8), 2455–2468. https://doi.org/10.5194/bg-12-2455-2015

Zhang, J., & Han, S. (2016). *FLUXNET2015 CN-Cha Changbaishan*. FluxNet; IAE Chinese Academy of Sciences. https://doi.org/10.18140/FLX/1440137

Zhou, G., & Yan, J. (2016). *FLUXNET2015 CN-Din Dinghushan*. FluxNet; SCIB Chinese Academy of Sciences. https://doi.org/10.18140/FLX/1440139

Zielis, S., Etzold, S., Zweifel, R., Eugster, W., Haeni, M., & Buchmann, N. (2014). NEP of a Swiss subalpine forest is significantly driven not only by current but also by previous year's weather. *Biogeosciences*, *11*(6), 1627–1635. https://doi.org/10.5194/bg-11-1627-2014

Zona, D., & Oechel, W. (2016a). *FLUXNET2015 US-Atq Atqasuk*. FluxNet; San Diego State University. https://doi.org/10.18140/FLX/1440067

Zona, D., & Oechel, W. (2016b). *FLUXNET2015 US-Ivo Ivotuk*. FluxNet; San Diego State University. https://doi.org/10.18140/FLX/1440073